Information Scrambling in Quantum Many-Body Systems

Thesis by
Yongliang Zhang

In Partial Fulfillment of the Requirements for the
Degree of
Doctor of Philosophy in Theoretical Physics

CALIFORNIA INSTITUTE OF TECHNOLOGY
Pasadena, California

2020
Defended February 20, 2020

Yongliang Zhang
ORCID: 0000-0002-8246-3759

ACKNOWLEDGEMENTS

I am very grateful to my adviser, teachers, colleagues, friends, and family for all their help and support during my years of graduate study. Without their help and support, this thesis would not have been possible.

First and foremost, I would like to express my sincere gratitude to my adviser Prof. Xie Chen for teaching me the most important things in research and for her continuous support and encouragement during my Ph.D. studies. Many thanks to Xie for taking me into the exciting areas of condensed matter theory and quantum information science. Xie always inspires me with her deep insight and great enthusiasm in physics. She helped me find a better way to think and solve challenging problems in research, for which I would be forever grateful. Our discussions and conversations were the most memorable part of my Ph.D. life. Also, I am grateful to my other thesis committee members, Prof. Fernando Brandão, Prof. Jason Alicea, and Prof. Manuel Endres, for offering their valuable insights and expertise. In addition, I would like to thank my collaborators, Dr. Yichen Huang, Prof. Fernando Brandão, and Prof. Vedika Khemani, for sharing their insightful ideas with me and giving me constructive suggestions to attack challenging problems. Without collaborations with them, I could not have moved forward to complete this thesis.

My appreciation to all Caltech faculties, staff and students who made Caltech one of the best places to study and conduct breakthrough research. Many thanks to Prof. Mark Wise for introducing the beautiful quantum field theory, to Prof. Hiroshi Oguri for teaching advanced mathematical methods of physics, and thanks to Prof. Alexei Kitaev and Prof. John Preskill for introducing the fancy foundation and exciting progress of quantum information and quantum computation. In addition, I thank the departments of mathematics and computing + mathematical sciences for offering a lot of fascinating courses in math, statistics, and computer science. All these courses at Caltech consolidated my academic background in physics, mathematics, and computer science. My thanks also go to all my colleagues and friends: Feng Bi, Thomas Bohdanowicz, Baoyi Chen, Yu-An Chen, Tal Einav, Nicholas Hunter-Jones, Joseph Iverson, Shenghan Jiang, Cheng-Ju Lin, Junyu Liu, Xiuqi Ma, Burak Şahinoğlu, Karthik Seetharam, Wilbur Shirley, Kevin Slagle, Paraj Titum, Tian Wang, Christopher White, Ke Ye, Kexin Yi, Nicole Yunger Halpern, and many others. I learned so much from them and enjoyed the conversations and interactions with them.

Last but not least, I would like to thank my family, especially my most beloved person, Yuhan Wang, for their constant support and love, and for always encouraging me to be better. I dedicate this thesis to them.

ABSTRACT

A closed quantum system never forgets its initial state, but the encoded information can get scrambled and become inaccessible without measuring a large fraction of all the system degrees of freedom. This scrambling can be diagnosed by studying the spatial spreading of initially local operators under the Heisenberg time evolution, and the decay of the out-of-time-ordered correlators (OTOC). What insights can OTOCs provide to understand the dynamics of quantum many-body systems? What are the characteristic behaviors of OTOCs during the time evolution? How is information scrambling affected by the dissipation in open quantum many-body systems?

We first study slow scrambling in many-body localized systems via calculating various correlators, two-point retarded correlators and OTOCs. Comparing with retarded correlators, OTOCs provide more information about the dynamics. We find that disorder slows and partially halts the onset of information scrambling. Instead of ballistic spreading, propagation of information forms a logarithmic light cone.

Next, we study the finite-size scaling of OTOCs at late times in generic thermalizing quantum many-body systems. When energy is conserved, the late-time saturation value of the OTOC of generic traceless local operators scales as an inverse polynomial in the system size. This is in contrast to the inverse exponential scaling expected for chaotic dynamics without energy conservation.

We also study information scrambling in open quantum many-body systems. We define a dissipative version of OTOC and study its behaviors in a prototypical chaotic quantum chain with dissipation. We find that dissipation leads to not only the overall decay of the scrambled information due to leaking, but also structural changes so that the information light cone can only reach a finite distance even when the effect of overall decay is removed.

Finally, we construct a family of local Hamiltonians for understanding the asymmetric information scrambling. Our models live on a one-dimensional lattice and exhibit asymmetric butterfly light cone between the left and right spatial directions.

PUBLISHED CONTENT AND CONTRIBUTIONS

The main content of this thesis is adapted from the following papers:

- Yong-Liang Zhang, and Vedika Khemani, "Asymmetric butterfly velocities in2-local Hamiltonians", arXiv: 1909.03988 (2019).
  Y.Z. participated in the concept of the project, and performed analytical and numerical calculations.

- Yong-Liang Zhang, Yichen Huang, and Xie Chen, "Information scrambling in chaotic systems with dissipation", Phys. Rev. B 99, 014303 (2019), DOI: 10.1103/PhysRevB.99.014303.
  Y.Z. participated in the concept of the project, and performed analytical and numerical calculations.

- Yichen Huang, Fernando G. S. L. Brandão, and Yong-Liang Zhang, "Finite-size scaling of out-of-time-ordered correlators at late times", Phys. Rev. Lett. 123, 010601 (2019), DOI: 10.1103/PhysRevLett.123.010601.
  Y.Z. participated in the concept of the project, and performed analytical calculations.

- Yichen Huang, Yong-Liang Zhang, and Xie Chen, "Out-of-time-ordered correlators in many-body localized systems", Ann. Phys. (Berl.) 529, 1600318 (2017), DOI: 10.1002/andp.201600318.
  Y.Z. participated in the concept of the project, and performed analytical and numerical calculations.

TABLE OF CONTENTS

LIST OF ILLUSTRATIONS

LIST OF TABLES

Number *Page*

Chapter 1

INTRODUCTION

Despite the huge success of statistical mechanics in describing the macroscopic thermodynamic behaviors of classical systems, its relation to the underlying microscopic dynamics of quantum many-body systems has persisted as a subject of controversy since the foundations were laid. The past decades have seen a great revival of interest in the foundations of quantum statistical mechanics. Thermalization and information scrambling are the subjects of much recent investigations from the perspective of quantum many-body systems, quantum field theory, black holes, and holography.

What will happen if a quantum system is isolated from the environment and evolves according to the Schrödinger equation? Will the quantum system reach a thermal equilibrium after long-time evolution? The time evolution of isolated quantum systems is unitary and preserves all information about the initial state at any time. However, a generic quantum many-body system contains a macroscopic number of degrees of freedom, but can only be probed through measuring a few of the degrees of freedom, which might be local measurements if the quantum system has spatial locality. Then the meaningful questions become whether the encoded information can get scrambled and become inaccessible without measuring a large fraction of all the system degrees of freedom, and whether local subsystems can reach thermal equilibrium. Information scrambling is a terminology describing the propagation of quantum information in the process of thermalization.

These questions can be formalized by considering the density matrix ρ of the quantum system. The evolution of the density matrix is $\rho(t) = e^{-iHt}\rho_0 e^{iHt}$, where ρ_0 represents the initial state and H is the Hamiltonian. Assume the quantum system is divided into two parts: a subregion A that will be probed, and its complement B. All information can be extracted by local measurements made on A, hence is encoded in the reduced density matrix $\rho_A(t) = \mathrm{tr}_B(\rho(t))$.

At late times, if $\rho_A(t)$ approaches a thermal ensemble density matrix at a temperature, then the quantum system has reached thermalization and no local information about the initial state can be extracted via local measurements. Similar to classical systems, the process of quantum thermalization might be understood in terms

of subsystem B acting as a reservoir for A. In this perspective, the entanglement entropy $S_A(t) = -\mathrm{tr}(\rho_A(t)\log\rho_A(t))$ plays the role of thermal entropy [1–3]. For generic thermalizing quantum many-body systems, they obey the Eigenstate Thermalization Hypothesis (ETH) [4–6] and have volume-law entanglement entropy at any nonzero temperature [7–9], i.e. the entanglement entropy scales with the volume of the subregion A. In these quantum many-body systems with thermalizing dynamics, entanglement entropy grows as a power law in time starting from the low entanglement of the initial state [10].

Not all quantum systems will reach thermal equilibrium after long-time evolution. A well-known example is the Anderson localized single-particle system in the presence of disorder [11]. In Anderson localized systems, diffusion of waves is absent, and conserved quantities, like energy and charge, are localized. Anderson localized systems do not thermalize and therefore cannot be described using statistical mechanics. The phenomenon of localization can also exist in interacting quantum many-body systems. This is called as Many-Body Localization (MBL) [12–24]. MBL systems can remain perfect insulators at non-zero temperature. The energy eigenstates of MBL quantum systems do no obey the ETH, and generically have an area law for entanglement entropy, i.e. the entanglement entropy scales with the surface area of the subregion A. In MBL systems, entanglement entropy grows logarithmically in time starting from the low entanglement of the initial state [25–33]. Many-body localization provides a mechanism for understanding the failure of thermalization in interacting quantum many-body systems with strong disorder.

Recent studies have proposed to quantify thermalization and information scrambling by investigating the spatial spreading of initially local operators under the Heisenberg time evolution, and the decay of the out-of-time-ordered correlators (OTOC) [34–63]. In the Heisenberg picture, the time-evolved operator of an initial local operator A is $A(t) = e^{iHt}Ae^{-iHt}$ which grows in size and becomes nonlocal as time increases. As $A(t)$ grows, it begins to overlap with local operator B at other spatial locations and terminates to commute with them. The effect of information scrambling can be diagnosed via the growth of the norm of the commutator $[A(t), B]$. Correspondingly, it is also manifested as the decay of (the real part of) the OTOC $\langle A^\dagger(t)B^\dagger A(t)B\rangle_\beta$ which is related to the commutator as

$$\Re\,\langle A^\dagger(t)B^\dagger A(t)B\rangle_\beta = 1 - \frac{1}{2}\langle [A(t),B]^\dagger [A(t),B]\rangle_\beta, \tag{1.1}$$

where the local operators A, B are assumed to be unitary for simplicity, $\langle\cdot\rangle_\beta$ denotes

the thermal ensemble average at the inverse temperature $\beta = 1/T$, and $\mathfrak{R}$ represents the real part.

In quantum many-body systems with thermalizing dynamics, the decay of OTOC is usually expected to exhibit the following features.

First, in the long time limit, information initially encoded in $A(t)$ becomes highly nonlocal and cannot be accessed via local measurements. Thus, all OTOCs at infinite temperature $\beta = 0$ decay to zero at late time [40, 43, 49, 51]

$$\lim_{t\to\infty} \mathfrak{R}\, \langle A^\dagger(t) B^\dagger A(t) B\rangle_{\beta=0} = 0, \tag{1.2}$$

where the local operators A and B are traceless.

Secondly, in chaotic zero-dimensional systems with large N degrees of freedom, the OTOC starts to decay at early time in an exponential way [36, 42, 43, 64]

$$\mathfrak{R}\, \langle A^\dagger(t) B^\dagger A(t) B\rangle_{\beta} \sim f_1 - \frac{f_2}{N} e^{\lambda_L t}, \tag{1.3}$$

where the constants f_1, f_2 depend on the choice of local operators A, B in the system. The exponent of the exponential λ_L – the quantum Lyapunov exponent – characterizes how chaotic the quantum dynamics is. Similar to classical systems, λ_L can describe the sensitivity to the initial conditions. Quantum Lyapunov exponent cannot be extracted from the reduced density matrix, entanglement entropy and two-point correlators, thus OTOCs provide more insights for people to understand the chaotic dynamics of thermalizing quantum many-body systems. Recent studies [42–45] show that the Lyapunov exponent is bounded by $\lambda_L \leq \frac{2\pi}{\beta}$ and is expected to be saturated by quantum systems corresponding to black holes. The maximally chaotic systems saturating this bound are called as fastest scramblers [65, 66]. An example of such systems is the SYK model [36, 45, 46, 64]

$$H_{SYK} = \frac{1}{4!} \sum_{i,j,k,l=1}^{N} \chi_i \chi_j \chi_k \chi_l, \tag{1.4}$$

where χ_i are Majorana fermionic operators satisfying $\{\chi_i, \chi_j\} = \delta_{ij}$, and the independent disorders $\{J_{ijkl}\}$ are randomly drawn from the Gaussian distribution with mean zero $\overline{J_{ijkl}} = 0$ and variance $\overline{J_{ijkl}^2} = \frac{3! J^2}{N^3}$ (Fig. 1.1).

Thirdly, in a thermalizing quantum many-body system with spatial locality, quantum information ballistically spreads at the butterfly velocity v_B, leading OTOCs to start to decay after a delay time d_{BA}/v_B, where d_{BA} is the distance between local operators

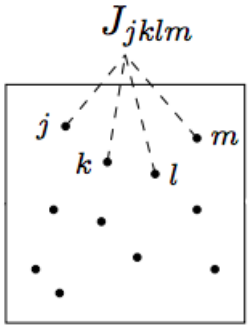

Figure 1.1: SYK model contains $N \gg 1$ Majorana fermions. The couplings are four-fermion interactions.

A and B. OTOCs have the capability to demonstrate a ballistic light, which is called as the butterfly light cone (Fig. 1.3). In the generalized SYK chain model [47], the decay of OTOC is govern by

$$\Re \langle A^\dagger(t) B^\dagger A(t) B \rangle_\beta \sim f_1 - \frac{f_2}{N} e^{\lambda_L (t - \frac{d_{BA}}{v_B})}, \tag{1.5}$$

where N is the number of Majorana fermion per site (Fig. 1.2), and the quantum Lyapunov exponent still can saturate the bound $\lambda_L \leq \frac{2\pi}{\beta}$.

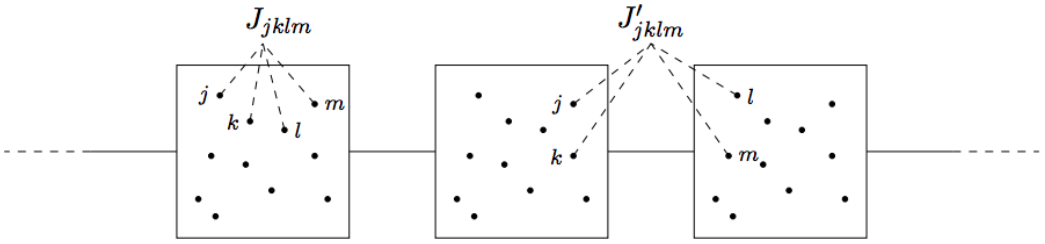

Figure 1.2: Generalized of one dimensional SYK model: each site contains $N \gg 1$ Majorana fermions with SYK four-fermion interactions, and the coupling between nearest neighbor sites are also SYK four-fermion interactions with two from each site.

Inspired by the decay of OTOCs in the generalized SYK model and the Lieb-Robinson bound [67–69], some studies [42, 43] speculate that the early-time behavior of OTOC in generic thermalizing quantum systems can be approximately described by

$$\Re \langle A^\dagger(t) B^\dagger A(t) B \rangle_{\beta=0} \sim f_1' - f_2' e^{\lambda_L (t - d_{BA}/v_B)}, \tag{1.6}$$

where f_1', f_2' are constants depending on the Hamiltonian, thermal ensemble average is discussed at infinite temperature $\beta = 0$, and the quantum system does not have a small parameter, such as $\frac{1}{N}$ in the generalized SYK model.

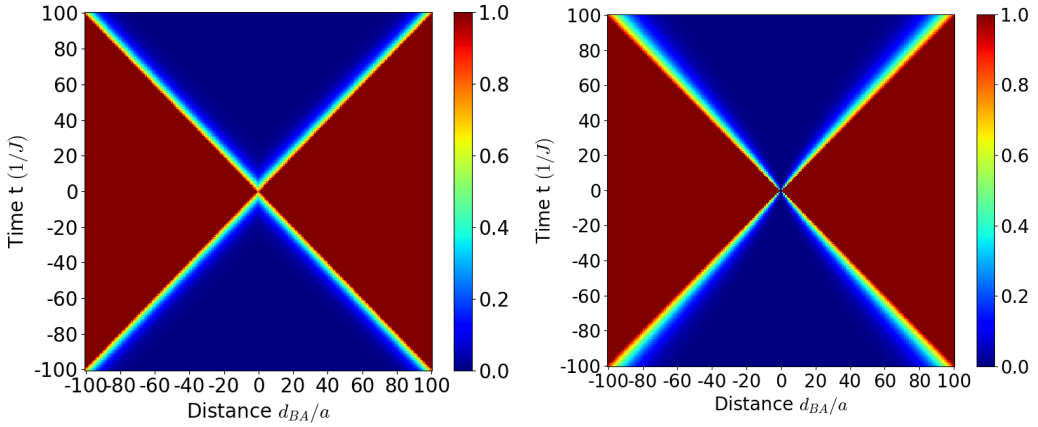

Figure 1.3: Ballistic butterfly light cone in the spacetime, where $1/J$ is the unit of time and a is the unit of distance. Outside the light cone, OTOCs are constant (one if local operators A and B commute with each other); inside the light cone, OTOCs decay to zero. Left panel: it is plotted according to Eq. (1.5) or (1.6) with quantum Lyapunov exponent. The boundary of the wave front is constant. Right panel: it is plotted according to Eq. (1.7) without quantum Lyapunov exponent. The boundary of the wave front is diffusively broadening.

However, in the exactly solvable random circuit model [70–76], the early-time decay of OTOCs is expressed in the following equation

$$\Re \langle A^\dagger(t) B^\dagger A(t) B \rangle_{\beta=0} \sim f_1' - f_2' e^{-\frac{(d_{BA} - v_B t)^2}{4Dt}}, \tag{1.7}$$

where the butterfly velocity is $v_B = \frac{q^2-1}{q^2+1}$, the diffusion constant is $D = \frac{q^2}{(q^2+1)^2}$, and q is the dimension of local Hilbert space at each site (Fig. 1.4). The butterfly light cone revealed by the OTOCs has not only ballistic spreading, but also diffusively broadening boundary of the wave front $\sqrt{Dt}$.

In generic thermalizing quantum spin systems with small local Hilbert space dimensions and short-range interactions, how does OTOC decay? Recently refs. [77, 78] give an in-depth study and conjecture a universal form of the early-time decay of OTOCs

$$\Re \langle A^\dagger(t) B^\dagger A(t) B \rangle_{\beta=0} \sim f_1' - f_2' e^{\lambda (t - \frac{d_{BA}}{v_B})^p / t^{p-1}}, \tag{1.8}$$

where the parameter p controls the broadening of the boundary of the wave front. For example, p is equal to 1 in the generalized SYK model, and 2 in the random

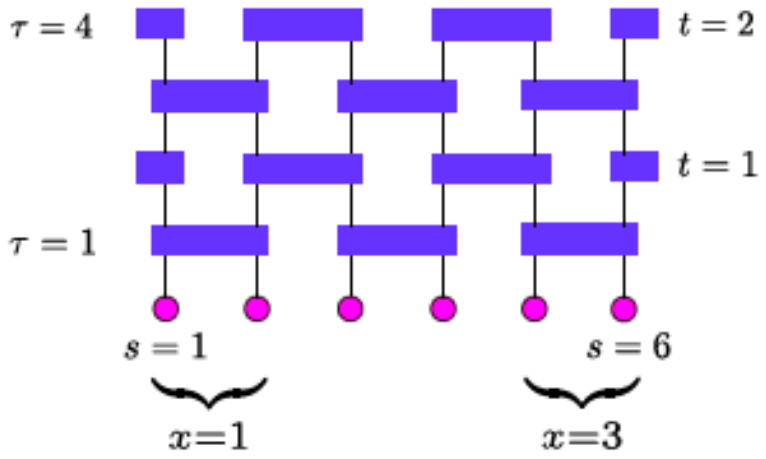

Figure 1.4: Random circuit model on an infinite 1D spin chain: each spin has local Hilbert space dimension q. Its unitary evolution can be described by discrete-time circuit: two-site unitary gates are applied to even bonds on even time steps and odd bonds on odd time steps. Each brick represents a random unitary operator which is independently drawn from the Haar random unitary group $U(q^2)$.

circuit model. When $p \neq 1$, there is no simple quantum Lyapunov exponent, so velocity-dependent Lyapunov exponents are discussed in ref. [78] to characterize the chaotic dynamics in generic thermalizing quantum many-body sytems.

Now let us list the questions we addressed and the results we obtained related to information scrambling in quantum many-body systems.

In Chapter 2, we study the slow information scrambling in many-body localized systems. In MBL systems, local changes in energy or other conserved quantities typically spread only within a finite distance. However, propagation of information forms a light cone that grows logarithmically with time. Information scrambling is slowed down and partially halted. Is it possible to detect the logarithmic light cone generated by a local perturbation from the response of a local operator at a later time? We numerically calculate various correlators in the random-field Heisenberg chain. While the equilibrium retarded correlator $A(t = 0)B(t > 0)$ is not sensitive to the unbounded information propagation, the out-of-time-ordered correlator $A(t = 0)^\dagger B(t > 0)^\dagger A(t = 0)B(t > 0)$ can detect the logarithmic light cone. We relate out-of-time-ordered correlators to the Lieb-Robinson bound in many-body localized systems, and show how to detect the logarithmic light cone with retarded correlators in specially designed states. Furthermore, we study the temperature dependence of the logarithmic light cone using out-of-time-ordered correlators.

In Chapter 3, we investigate the finite-size scaling of OTOCs at late times in generic thermalizing quantum many-body systems. When the system size is finite, out-of-time-ordered correlators do not decay to exact zero at late times. OTOC converges to a small but finite value, which approaches to zero when the system size goes to infinity. It is natural to expect that the residual value can provide useful insights into the thermalizing dynamics. We demonstrate that approximation methods with and without the law of energy conservation make different predictions about OTOCs at late times. For thermalizing quantum systems that the unitary evolution can be described by random matrix ensembles [49, 79–81], the law of energy conservation does not hold, and late-time OTOC scales inverse exponentially with system size. This is consistent with the intuition that the encoded information is scrambled over all degrees of freedom which is exponentially large in the system size. For a given time-independent Hamiltonian with thermalizing dynamics, its total energy is conserved, and the scaling of OTOCs is inverse polynomial in the system size. We provide both analytical arguments and numerical simulations to support these conclusions.

In Chapter 4, we address the following questions: After understanding the characteristic features of early-time decay of OTOCs in closed quantum many-body systems with thermalizing dynamics, what can we expect from the information scrambling in open quantum systems? How is information scrambling affected when the system is coupled to the environment and suffers from dissipation? We address these questions by defining a dissipative version of OTOC and numerically study its behavior in a prototypical chaotic quantum chain in the presence of dissipation. We find that dissipation leads to not only the overall decay of the scrambled information due to leaking, but also structural changes so that the 'information light cone' can only reach a finite distance even when the effect of overall decay is removed. Based on this observation, we conjecture a modified version of the Lieb-Robinson bound in dissipative systems.

In Chapter 5, we try to understand asymmetric information scrambling. In generic thermalizing quantum many-body systems with spatial locality, the butterfly velocity v_B can depend asymmetrically on the direction of information propagation. In one dimensional quantum systems, the asymmetry between the different directions can be quantified by the butterfly velocities v_B^r and v_B^l, where the superscript r (l) denotes propagation direction to the right (left). We construct a family of simple 2-local Hamiltonians for understanding the asymmetric hydrodynamics of operator

spreading. Our models live on a one-dimensional lattice and exhibit asymmetric butterfly velocities between the left and right spatial directions. For integrable Hamiltonians, this asymmetry is transparently understood in terms of quasiparticle velocities. For the constructed non-integrable Hamiltonian with thermalizing dynamics, we employ different methods to estimate the asymmetric butterfly velocities v_B^r and v_B^l. Our methods are developed from a variety of measures including out-of-time-ordered correlations, right/left weight of time-evolved operators, and operator entanglement.

Chapter 2

SLOW SCRAMBLING IN MANY-BODY LOCALIZED SYSTEMS

In the presence of disorder, localization can occur not only in single-particle systems [11], but also in interacting many-body systems [12–22]. The former is known as Anderson localization (AL), and the latter is called many-body localization (MBL). Neither AL nor MBL systems transfer energy, charge, or other local conserved quantities: Changes in energy or charge at position $x = 0$ from equilibrium can spread and lead to changes in the corresponding quantity only within a finite distance $|x| < L_0$, where L_0 is the localization length.

A characteristic feature that distinguishes MBL from AL lies in the dynamics of entanglement after a global quench. Initialized in a random product state at time $t = 0$, the half-chain entanglement entropy remains bounded in AL systems [82], but grows logarithmically with time in MBL systems [25–32]. In sharp contrast to the transport phenomena, the unbounded growth of entanglement in MBL systems suggests that information propagates throughout the system, although very slowly.

The propagation of information can be formulated by adapting the Lieb-Robinson (LR) bound [67, 68, 83] to the present context. In particular, it is manifested as the noncommutativity of a local operator A at $x = 0$ and $t = 0$ with another local operator B at position x and evolved for some time t. In MBL systems, the operator norm of the commutator $[A(0,0), B(x,t)]$ is non-negligible inside a light cone whose radius is given by $|x| \sim \log|t|$, and decays exponentially with distance outside the light cone, i.e. [84],

$$\|[A(0,0), B(x,t)]\| \leq Ce^{-(|x|-v_{LR}\log|t|)/\xi} \tag{2.1}$$

after averaging over disorder. Here, $B(x,t) = e^{iHt}B(x,0)e^{-iHt}$ is the time-evolved operator; $\|\cdot\|$ is the operator norm (the largest singular value); and C, v_{LR}, ξ are positive constants.

Is it possible to detect the logarithmic light cone (LLC) with equilibrium correlators of $A(0,0)$ and $B(x,t)$? Arguably, the most straightforward approach is to measure the commutator in the LR bound (2.1) on equilibrium states, i.e., thermal states or eigenstates, using the Kubo formula in linear response theory:

$$\langle U^\dagger B(x,t)U\rangle - \langle B(x,t)\rangle = \tau\langle i[A(0,0), B(x,t)]\rangle + O(\tau^2), \tag{2.2}$$

where $U = e^{-iA\tau}$ with $\tau \ll 1$ is a local unitary perturbation if A is Hermitian. The first and second terms on the left-hand side of (2.2) are the expectation values of B in the presence and absence of the perturbation U, respectively. The difference is the effect of U observed by measuring B. Note that U and B can be, but do not have to be, chosen as the operators for changing and measuring local conserved quantities, respectively. In this way, the effect of U cannot be detected outside the localization length L_0.

Instead, we consider the out-of-time-ordered (OTO) correlator

$$A(0,0)B(x,t)A(0,0)B(x,t).$$

Proposed long ago in the context of superconductivity [34], OTO correlators have received renewed interest in the study of the AdS/CFT correspondence, black holes, butterfly effect, quantum chaos, and scrambling [35–44]. Recently, several protocols have been proposed for measuring OTO correlators in experiments [85–87]. In MBL systems, we observe that OTO correlators can detect LLC. To understand this, we relate the OTO correlator to the Frobenius norm of $[A(0,0), B(x,t)]$, which is expected to exhibit similar scaling behavior as the operator norm in the LR bound (2.1). Furthermore, we study the temperature dependence of LLC using OTO correlators.

The observation that the expectation value of the commutator $[A(0,0), B(x,t)]$ with respect to thermal states or eigenstates cannot detect LLC described by the LR bound (2.1) raises the question of whether it is possible to saturate the bound (2.1) and thus detect LLC by measuring the commutator on some states using the Kubo formula (2.2). Of course, we can take the eigenstate of the commutator with the largest eigenvalue in magnitude, but such states are arguably not physical. Is it possible to detect LLC by measuring the commutator on physically motivated states? We provide numerical and analytical evidence that this is not the case for eigenstates of the Hamiltonian, any mixture of them, or random product states.

Finally, we compare AL with MBL. In AL systems, propagation of information forms a non-expanding light cone [88]. We show this explicitly using OTO correlators in the random-field XX chain. The distinction between AL and MBL systems, i.e., non-expanding versus LLC, is also manifested in quantum revivals [89], modified spin-echo protocols [90], relaxation of local observables after a quantum quench, growth of connected correlators [30, 91], etc.

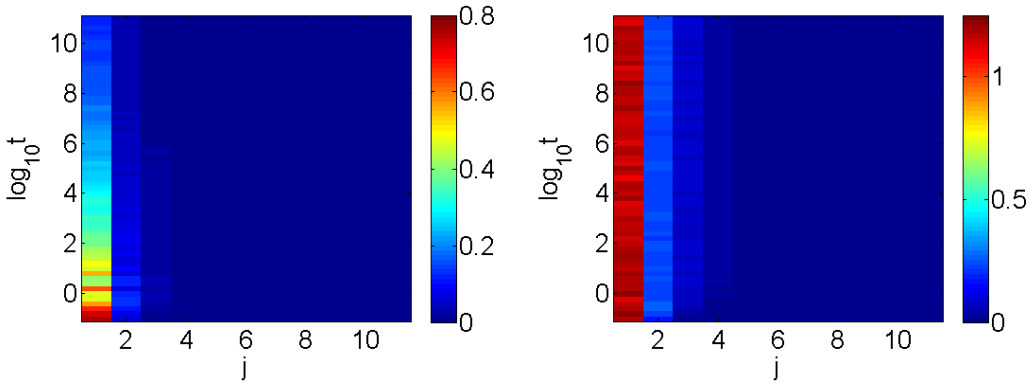

Figure 2.1: Color images of $|\langle i[\sigma_1^x, \sigma_j^x(t)]\rangle_{th}|$ for $\beta = 0.1$ (left) and $|\langle i[\sigma_1^x, \sigma_j^x(t)]\rangle_{eig}|$ (right), averaged over 480 samples. LLC cannot be detected in this way.

2.1 OTO correlators detect logarithmic light cone

As a concrete model of MBL, we consider the spin-1/2 random-field Heisenberg chain and calculate its dynamics using exact diagonalization. The Hamiltonian is

$$H = \sum_{j=1}^{L-1} \left(\sigma_j^x \sigma_{j+1}^x + \sigma_j^y \sigma_{j+1}^y + \sigma_j^z \sigma_{j+1}^z \right) + \sum_{j=1}^{L} h_j \sigma_j^z, \tag{2.3}$$

where $\sigma_j^x, \sigma_j^y, \sigma_j^z$ are the Pauli matrices at the site j, and h_j's are independent and identically distributed (i.i.d.) uniform random variables on the interval $[-h, h]$. This model is known to be in the MBL phase for $h \gtrsim 7$ [92–94]. We take $h = 16$ so that the localization length L_0 is small, and $L = 11$ unless otherwise stated. We perform a finite-size scaling analysis (data not shown for clarity) to ensure that finite-size effects are negligible.

Preparing the system in thermal states or eigenstates, the expectation value of an operator $\hat{O}$ is given by

$$\langle \hat{O} \rangle_{th} = \mathrm{tr}(e^{-\beta H} \hat{O}) / tr(e^{-\beta H}), \quad \langle \hat{O} \rangle_{eig} = \langle \psi | \hat{O} | \psi \rangle, \tag{2.4}$$

where $\beta = 1/T \geq 0$ is the inverse temperature, and $|\psi\rangle$ is a random eigenstate of H.

Figure 2.1 shows the expectation value of the commutator $[\sigma_1^x, \sigma_j^x(t)]$ with respect to thermal states and eigenstates as a function of $j = 1, 2, \ldots, L$ and t. Explained previously using the Kubo formula (2.2), this quantity measures the response at the site j and time t to a perturbation at the first site and $t = 0$. We see that the effect of perturbation spreads only within a small distance. We observe similar behavior (data not shown) for other choices of local operators in the commutator.

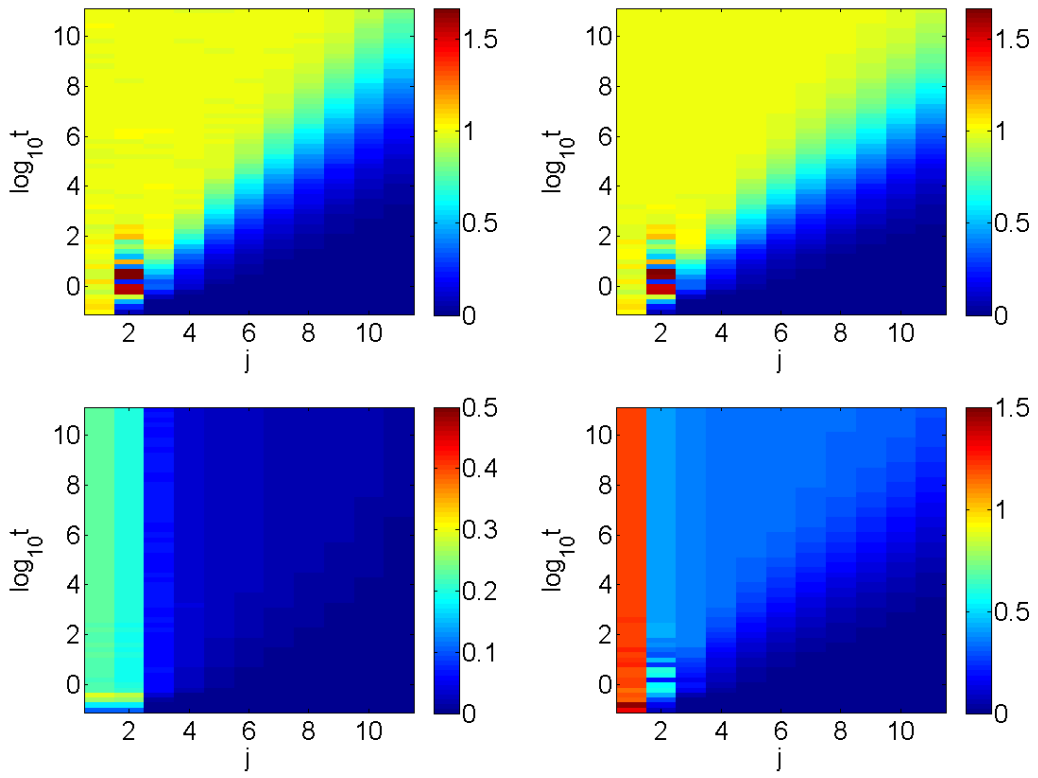

Figure 2.2: Color images of $1 - \mathrm{Re}\langle\sigma_1^x\sigma_j^x(t)\sigma_1^x\sigma_j^x(t)\rangle_{th}$ for $\beta = 0.1$ (top left), $1 - \mathrm{Re}\langle\sigma_1^x\sigma_j^x(t)\sigma_1^x\sigma_j^x(t)\rangle_{eig}$ (top right), $1 - \mathrm{Re}\langle\sigma_1^z\sigma_j^z(t)\sigma_1^z\sigma_j^z(t)\rangle_{eig}$ (bottom left), and $1 - \mathrm{Re}\langle(\sigma_1^x + \sigma_1^z)(\sigma_j^x(t) + \sigma_j^z(t))(\sigma_1^x + \sigma_1^z)(\sigma_j^x(t) + \sigma_j^z(t))\rangle_{eig}/4$ (bottom right), averaged over 480 samples. We see LLC in all but the bottom left panels.

Let us consider the OTO operator $\sigma_1^x\sigma_j^x(t)\sigma_1^x\sigma_j^x(t)$. It is close to the identity operator if $[\sigma_1^x, \sigma_j^x(t)] \approx 0$, i.e., the site j at time t is outside the light cone generated at the first site and $t = 0$; its expectation value may deviate from 1 if the site j is in the light cone. The top panels of Fig. 2.2 show this OTO correlator. We see LLC, in which the OTO correlator decays to zero. The bottom left panel shows the OTO correlator $\sigma_1^z\sigma_j^z(t)\sigma_1^z\sigma_j^z(t)$. We do not see a clear unbounded light cone. The bottom right panel shows $(\sigma_1^x + \sigma_1^z)(\sigma_j^x(t) + \sigma_j^z(t))(\sigma_1^x + \sigma_1^z)(\sigma_j^x(t) + \sigma_j^z(t))$. We see LLC, but in which the OTO correlator does not decay to zero.

The behavior of these OTO correlators can be understood from the local integrals of motion [31, 95] in MBL systems. The operators $\sigma_j^x, \sigma_j^z, \sigma_j^x + \sigma_j^z$ have vanishing, large, moderate overlap with the local integrals of motion. Therefore, the corresponding OTO correlator decays to zero, almost does not decay, or decays to a finite value, respectively.

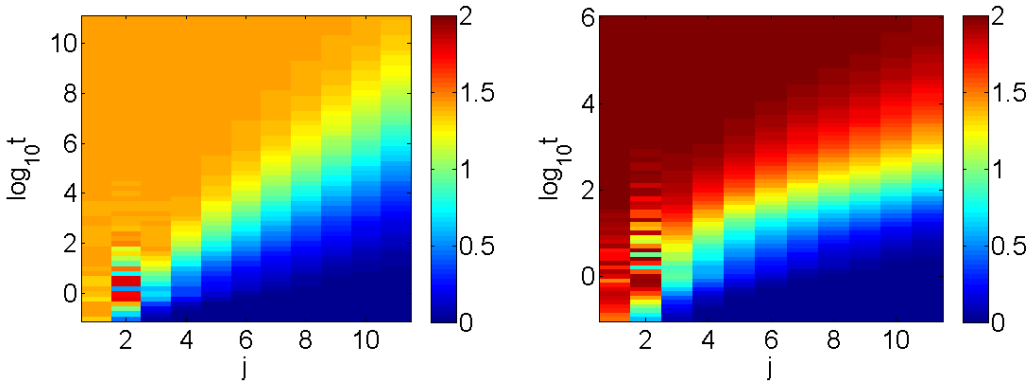

Figure 2.3: Color images of $\|[\sigma_1^x, \sigma_j^x(t)]\|_F/2^{L/2}$ (left) and $\|[\sigma_1^x, \sigma_j^x(t)]\|$ (right), averaged over 480 samples. The left panel is essentially the same (see Eq. 2.5) as the top right panel of Fig. 2.2. The right panel shows that the LR bound (2.1) is tight.

Why do OTO correlators behave differently from normal (i.e., equilibrium retarded) correlators? We have shown that normal correlators measure the response or spread of physical quantities like energy or charge after a perturbation from equilibrium. We now argue that OTO correlators describe the propagation of information.

The OTO correlator can be obtained by expanding the square of the commutator

$$\begin{aligned} -[\sigma_1^x, \sigma_j^x(t)]^2 &= 2 - \sigma_1^x \sigma_j^x(t) \sigma_1^x \sigma_j^x(t) - \sigma_j^x(t) \sigma_1^x \sigma_j^x(t) \sigma_1^x \\ \Rightarrow 1 - \langle \sigma_1^x \sigma_j^x(t) \sigma_1^x \sigma_j^x(t) \rangle_{th} &= \|[\sigma_1^x, \sigma_j^x(t)]\|_F^2 / 2^{L+1}, \end{aligned} \tag{2.5}$$

where $\beta = 0$, and $\|A\|_F = \sqrt{\mathrm{tr}(A^\dagger A)}$ is the Frobenius norm. In comparison, the LR bound (2.1) concerns $\|[\sigma_1^x, \sigma_j^x(t)]\|$. Figure 2.3 shows the Frobenius and operator norms of the commutator. They exhibit similar scaling behavior in the sense of LLC in both panels. Thus, we have related OTO correlators to the LR bound (2.1).

We emphasize the difference between the expectation values of $i[\sigma_1^x, \sigma_j^x(t)]$ and $-[\sigma_1^x, \sigma_j^x(t)]^2$ shown in Figs. 2.1, 2.2, respectively. The observation that the latter detects LLC while the former does not can be understood as follows. The traceless Hermitian operator $i[\sigma_1^x, \sigma_j^x(t)]$ has both positive and negative eigenvalues, which may cancel themselves out upon taking the expectation value (with respect to either thermal states or eigenstates of the Hamiltonian). The eigenvalues of the positive semidefinite operator $-[\sigma_1^x, \sigma_j^x(t)]^2$ are nonnegative and contribute additively when taking the expectation value.

We now study the temperature dependence of LLC using OTO correlators (the temperature dependence of the linear light cone in homogeneous systems has been

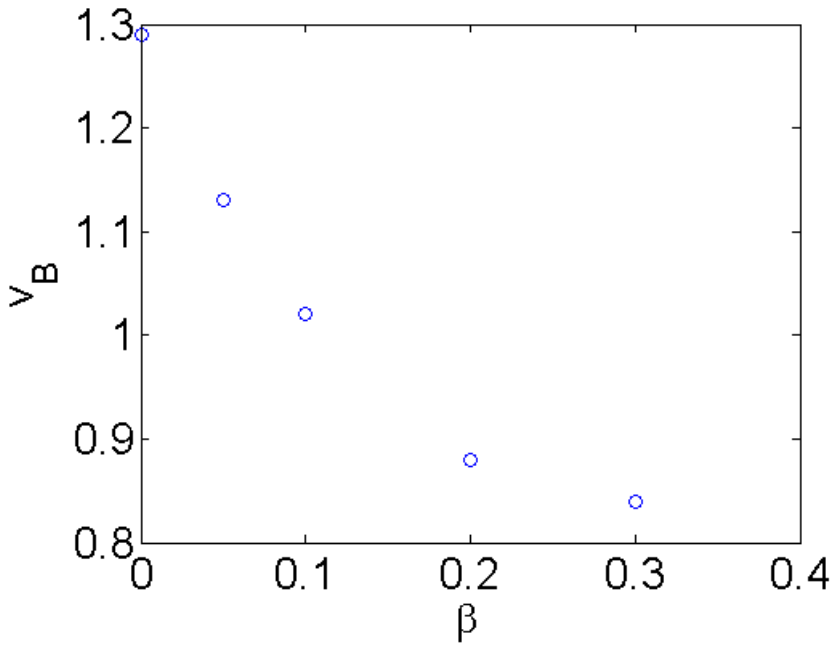

Figure 2.4: LLC boundary $j \sim v_B \log_{10} t$ at various inverse temperatures β. The values of v_B are obtained by solving (3.12) for $\epsilon = 1/2$. The top panels of Fig. 2.2 are the color images for $\beta = 0, 0.1$, and the color images for other values of β are not shown. We see that v_B decreases as β increases.

studied; see, e.g., [42]). To determine the LLC boundary $j \sim v_B \log_{10} t$, we choose a threshold $0 < \epsilon < 1$ and solve the relationship between j and t in the equation

$$1 - \mathrm{Re}\langle \sigma_1^x \sigma_j^x(t) \sigma_1^x \sigma_j^x(t) \rangle_{th} = \epsilon. \tag{2.6}$$

We see from the top panels of Fig. 2.2 that v_B depends on both β and ϵ. For fixed ϵ, Fig. 2.4 shows that v_B decreases as β increases. This trend (faster information propagation at higher temperatures) was also found in some quantum field theories [42].

The model (2.3) for $h \lesssim 7$ has two mobility edges separating delocalized eigenstates in the middle of the energy spectrum from localized ones on the sides [93, 94]. For $h = 16$, (2.3) is deep in the MBL phase, and (almost) all eigenstates are localized. However, eigenstates in the middle of the spectrum might still be less localized than those on the sides. Therefore, we expect that v_B decreases as $|\beta|$ increases. If a many-body localization-delocalization transition has mobility edges separating localized eigenstates in the middle of the spectrum from delocalized ones on the sides, we expect that v_B increases as $|\beta|$ increases on the MBL side of the transition.

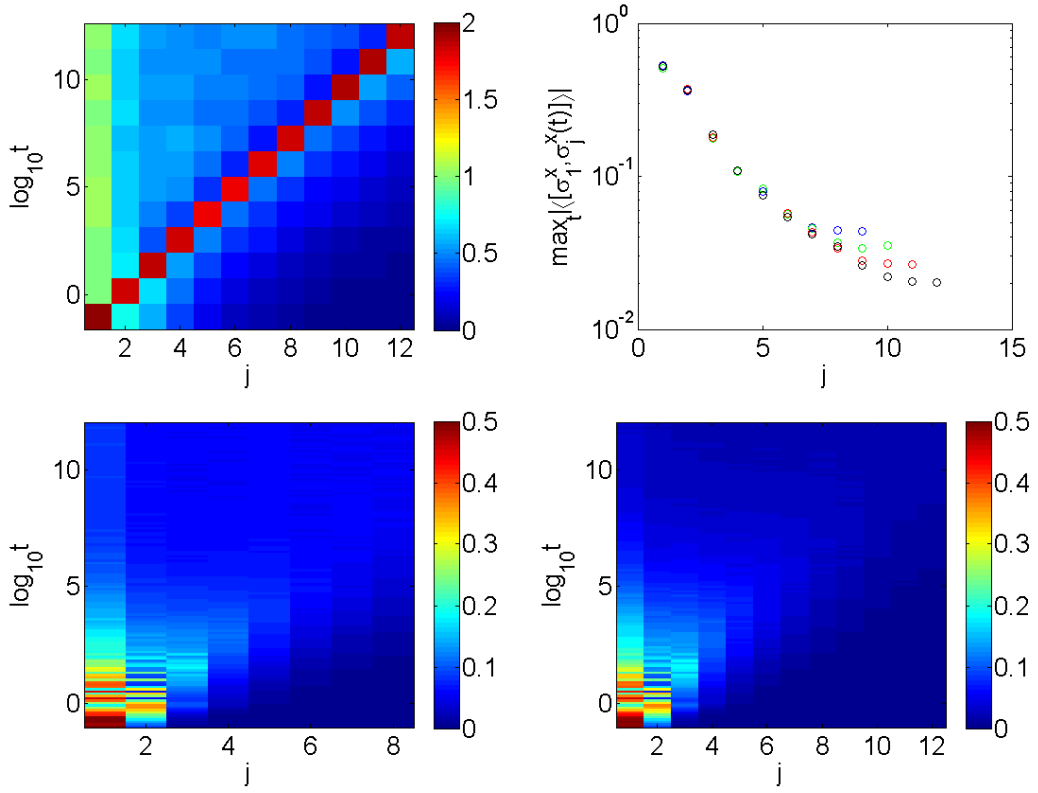

Figure 2.5: (top left) Color image of $|\langle\psi_j|[\sigma_1^x, \sigma_j^x(t)]|\psi_j\rangle|$ for $L = 12$, averaged over 320 samples. Here, $|\psi_j\rangle$ is the eigenstate of $[\sigma_1^x, \sigma_j^x(t = 10^{0.3j+1})]$ with the largest eigenvalue in magnitude. (top right) The quantity $\max_t |\langle[\sigma_1^x, \sigma_j^x(t)]\rangle|$ on random product states for $L = 9$ (blue), 10 (green), 11 (red), 12 (black), averaged over 960 samples. It appears to decay exponentially with distance in the thermodynamic limit. (bottom) Color images of $|\langle[\sigma_1^x, \sigma_j^x(t)]\rangle|$ on random product states for $L = 8$ and $L = 12$.

2.2 How to detect logarithmic light cone with retarded correlators?

Is it possible to saturate the LR bound (2.1) and thus detect LLC by measuring the commutator on some states using the Kubo formula (2.2)? Of course, we can take the eigenstate of the commutator with the largest eigenvalue in magnitude. In the right panel of Fig. 2.3, the LLC boundary is roughly given by $t = 10^{0.3j+1}$. The top left panel of Fig. 2.5 shows $|\langle\psi_j|[\sigma_1^x, \sigma_j^x(t)]|\psi_j\rangle|$, where $|\psi_j\rangle$ is the eigenstate of $[\sigma_1^x, \sigma_j^x(t = 10^{0.3j+1})]$ with the largest eigenvalue in magnitude. Thus, however far the measurement is from the perturbation, there is an initial state such that the effect of the perturbation can eventually be detected. In this sense, we do see LLC.

Since the eigenstates of the commutator are arguably not physical, is it possible to detect LLC by measuring the commutator on physically motivated states? As an

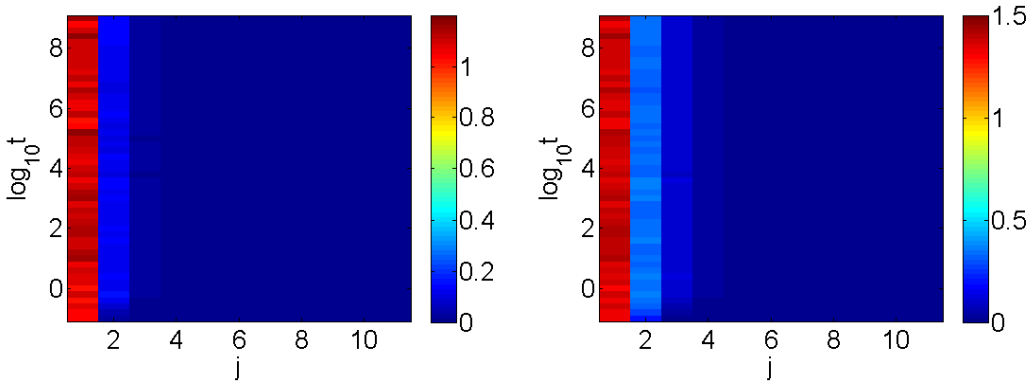

Figure 2.6: Color images of $1 - \mathrm{Re}\langle\sigma_1^x\sigma_j^x(t)\sigma_1^x\sigma_j^x(t)\rangle_{eig}$ (left) and $\|[\sigma_1^x, \sigma_j^x(t)]\|$ (right) in the AL system (2.8), averaged over 320 samples. We see a non-expanding light cone in both panels. This confirms (2.7).

attempt, we consider (random) product states, which are the initial states in most experiments on MBL [96–99]. The lower panels of Fig. 2.5 show the expectation value of the commutator with respect to random product states. We do not see a very clear unbounded light cone, but further analysis is necessary to draw a conclusion.

We consider the quantity $\max_t |\langle[\sigma_1^x, \sigma_j^x(t)]\rangle|$, which is the maximum signal that can ever be detected by measuring σ_j^x (see Eq. 2.2). This quantity is not a function of t, and does not describe how the effect of a perturbation evolves in time. Rather, it detects whether the perturbation has long-range effects. Performing a finite-size scaling analysis, the top right panel of Fig. 2.5 provides evidence that in the thermodynamic limit, $\max_t |\langle[\sigma_1^x, \sigma_j^x(t)]\rangle|$ decays exponentially with j. Thus, a perturbation of random product states has only short-range effects at any time t, and LLC cannot be detected in this way. In the Appendix, we analytically calculate $|\langle[\sigma_1^x, \sigma_j^x(t)]\rangle|$ on some product states in the phenomenological model of MBL [31]. The analytical results agree qualitatively with the numerical results in Fig. 2.5.

2.3 OTO correlators in Anderson localized systems

In AL systems, information propagation forms a non-expanding light cone formulated by a strictly local LR bound [88]

$$\|[A(0,0), B(x,t)]\| \leq Ce^{-|x|/\xi}. \tag{2.7}$$

We now show this explicitly using OTO correlators. Thus, OTO correlators can distinguish AL from MBL.

As a model of AL, we consider the random-field XX chain, which is equivalent to

a model of free fermions hopping in a random potential. The Hamiltonian is

$$H = \sum_{j=1}^{L-1} \left(\sigma_j^x \sigma_{j+1}^x + \sigma_j^y \sigma_{j+1}^y \right) + \sum_{j=1}^{L} h_j \sigma_j^z, \tag{2.8}$$

where h_j's are i.i.d. uniform random variables on the interval $[-h, h]$. This model is in the AL phase for any $h > 0$, and we still take $h = 16$. Figure 2.6 shows the OTO correlator $\sigma_1^x \sigma_j^x(t) \sigma_1^x \sigma_j^x(t)$ and the operator norm of the commutator $[\sigma_1^x, \sigma_j^x(t)]$. We see a non-expanding light cone.

2.4 Discussion and conclusions

We have shown that OTO correlators can detect LLC in MBL systems, and thus distinguish MBL from AL. Furthermore, we have studied the temperature dependence of LLC using OTO correlators. In the random-field Heisenberg chain (2.3), the LLC coefficient v_B decreases as β increases. However, it may be possible to construct models of MBL such that v_B increases as β increases.

In the linear response regime (2.2), we have studied whether a local perturbation of various initial states has long-range effects at a later time and thus can be used to detect LLC. We have shown that this is indeed the case for specially designed states, but may not be the case for thermal states, eigenstates of the Hamiltonian, or random product states. It would be interesting to study whether this is the case for other physically motivated states.

Beyond fully MBL systems, OTO correlators in a microcanonical ensemble can detect mobility edges. When the energy density of the ensemble is in the localized or delocalized region of the spectrum, we expect that OTO correlators demonstrate a logarithmic or power-law light cone, respectively. Furthermore, the linear light cone in diffusive non-integrable systems can be detected by measuring energy after a local perturbation of specially designed states in the linear response regime (2.2). To justify this, we have performed calculations (data now shown) as in the top left panel of Fig. 2.5 for the model in Ref. [10].

Recently, OTO correlators have been used extensively in quantum gravity to study chaos and scrambling of black holes via AdS/CFT duality. This chapter shows that OTO correlators can provide insights into the dynamics of quantum many-body systems without a holographic dual.

Chapter 3

FINITE-SIZE SCALING OF OUT-OF-TIME-ORDERED CORRELATORS AT LATE TIMES

Nonintegrable quantum many-body systems are expected to exhibit chaotic dynamics, which not only leads to thermalization, but also scrambles local information into a nonlocal form. In the Heisenberg picture, the support of $A(t) := e^{iHt}Ae^{-iHt}$ for a local operator A should grow with time under the chaotic dynamics. This growth is reflected in the noncommutativity of $A(t)$ and another local operator B at a different site, which leads to the decay of the out-of-time-ordered correlator (OTOC) $\mathrm{Re}\langle A^\dagger(t)B^\dagger A(t)B\rangle$ [34–36, 38–44, 46, 47, 49, 85, 100]. Assume for simplicity that A and B are unitary. Then,

$$\mathrm{Re}\langle A^\dagger(t)B^\dagger A(t)B\rangle = 1 - \langle [A(t),B]^\dagger [A(t),B]\rangle/2 \tag{3.1}$$

so that when the commutator $[\cdots]$ grows, OTOC decays. The chaotic nature of the dynamics is reflected in the fast decay of OTOC away from 1 in a relatively short time period and the approaching of OTOC to 0 at late times.

Why does chaotic dynamics lead to such decaying behavior of OTOC? While it is not possible to solve exactly the dynamics of nonintegrable systems in general, we might be able to extract some universal features, at least in certain limits. In a large class of chaotic systems without spatial locality (e.g., large-N theories), OTOC at early time t is given by $1 - \epsilon e^{\lambda_L t}$, where ϵ is a small prefactor and λ_L is a constant. Such an exponential deviation from the initial value is reminiscent of the so-called sensitive dependence on initial conditions (i.e., nearby points in phase space separate from each other over time at an exponential rate) in classical chaos. Thus, λ_L may be interpreted as the Lyapunov exponent for quantum systems [35]. In chaotic systems with spatial locality, OTOC of two local operators starts to decay only after a delay that is proportional to the distance between the operators [41–43, 47, 100]. This is a consequence of the Lieb-Robinson bound [67, 68, 83].

In this paper, we study the behavior of OTOC at late times. For simplicity, consider a system of n qubits at infinite temperature so that $\langle\cdots\rangle = \mathrm{tr}(\cdots)/2^n$. In the limit $t \to \infty$, a naive understanding of why OTOC approaches 0 is as follows. We expand

the time-evolved operator in the n-qubit Pauli basis $\{\sigma_0 = I, \sigma_x, \sigma_y, \sigma_z\}^{\otimes n}$:

$$A(t) = \sum_{(k_1,k_2,\ldots,k_n)\in\{0,x,y,z\}^n} a_{k_1k_2\cdots k_n}\sigma_{k_1}\sigma_{k_2}\cdots\sigma_{k_n}. \tag{3.2}$$

The unitarity of $A(t)$ implies

$$\sum_{k_1,k_2,\ldots,k_n} |a_{k_1k_2\cdots k_n}|^2 = 1. \tag{3.3}$$

After undergoing chaotic evolution for a sufficiently long time, the support of $A(t)$ should be the whole system, and one might expect that the coefficients $a_{k_1k_2\cdots k_n}$ behave like random variables due to the chaotic nature of the dynamics. If we choose B to be the Pauli operator σ_x of qubit 1, then half of the terms in the expansion (3.2) of $A(t)$ commute with B and half of them do not. Thus,

$$\begin{aligned}
&\langle [A(t), B]^\dagger [A(t), B]\rangle \\
&= 4 \sum_{k_2,k_3,\ldots,k_n} |a_{yk_2k_3\cdots k_n}|^2 + |a_{zk_2k_3\cdots k_n}|^2 \\
&\approx 4 \cdot 0.5 = 2.
\end{aligned} \tag{3.4}$$

The approximation step follows from Eq. (3.3) and the fact that we sum over half of the random variables. Substituting Eq. (3.4) into Eq. (3.1), we see that OTOC approaches 0 at late times.

Equation (3.2) with random coefficients is a very simple way to approximate $A(t)$ for large t in chaotic systems and it is oversimplified in some respects. For example, one major difference between this approximation and the exact evolution $A(t) = e^{iHt}Ae^{-iHt}$ is that the latter preserves the spectrum of A while the former does not. How does this discrepancy affect our understanding of the late-time behavior of OTOC? Is it necessary to use more refined and sophisticated approximations in order to fully capture the essence of chaotic dynamics at late times?

We focus on the scaling of late-time OTOC with system size. In finite-size systems, OTOC may converge to a small but finite value, which goes to 0 when the system size goes to infinity. One might expect this residual value to be exponentially small in the system size because we sum over an exponential number of random variables in Eq. (3.4). However, using a more refined approximation we show that the finite-size scaling of generic late-time OTOC should be inverse polynomial. In fact, the power-law scaling is closely related to energy conservation during the time evolution, which is not captured by simply setting the coefficients in the expansion (3.2) to be random.

3.1 Results

In this section, we introduce basic definitions and provide a summary of results.

Throughout this paper, asymptotic notations are used extensively. Let $f, g : \mathbb{R}^+ \to \mathbb{R}^+$ be two positive functions. One writes $f(x) = O(g(x))$ if and only if there exist positive numbers M, x_0 such that $f(x) \leq Mg(x)$ for all $x > x_0$; $f(x) = \Omega(g(x))$ if and only if there exist positive numbers M, x_0 such that $f(x) \geq Mg(x)$ for all $x > x_0$; $f(x) = \Theta(g(x))$ if and only if there exist positive numbers M_1, M_2, x_0 such that $M_1 g(x) \leq f(x) \leq M_2 g(x)$ for all $x > x_0$. To simplify the notation, we use a tilde to hide a polylogarithmic factor, e.g., $\tilde{O}(f(x)) := O(f(x) \operatorname{poly} \log f(x))$.

For concreteness, consider a chain of n qubits or spin-1/2's with total Hilbert space dimension $d = 2^n$ governed by a translationally invariant Hamiltonian $H = \sum_{i=1}^{n} H_i$, where H_i acts on spins $i, i+1$ (nearest-neighbor interaction). While our discussion is based on a one-dimensional spin system, our results do not rely on the dimensionality of the system or the degrees of freedom being spins. A minor modification of our method leads to similar results in other settings, e.g., fermionic systems in higher dimensions. Assume without loss of generality that $\operatorname{tr} H_i = 0$ (traceless) and $\|H_i\| \leq 1$ (bounded operator norm).

Let A, B, C, D be local (not necessarily unitary) operators with unit operator norm. The residual value of late-time OTOC is

$$OTOC_\infty(A, B, C, D) := \lim_{\tau \to \infty} \frac{1}{\tau} \int_0^\tau \mathrm{d}t \langle AB(t)CD(t) \rangle, \tag{3.5}$$

where $\langle X \rangle := \frac{1}{d} \operatorname{tr} X$ denotes the expectation value of an operator at infinite temperature.

Let $\{|1\rangle, |2\rangle, \ldots, |d\rangle\}$ be a complete set of eigenstates of H with corresponding energies $E_1 \leq E_2 \leq \cdots \leq E_d$ in nondescending order. Let $X_{jk} = \langle j|X|k\rangle$ be the matrix element of an operator in the energy basis. Define

$$\langle A, B, C, D \rangle_j = (AC)_{jj} B_{jj} D_{jj} + A_{jj} C_{jj} (BD)_{jj} - A_{jj} B_{jj} C_{jj} D_{jj}. \tag{3.6}$$

In strongly chaotic systems, we propose the following formula for late-time OTOC:

$$OTOC_\infty(A, B, C, D) \approx \frac{1}{d} \sum_j \langle A, B, C, D \rangle_j. \tag{3.7}$$

Based on this formula, we argue for

types of dynamics	late-time OTOC	references
Haar random unitary	$e^{-\Theta(n)}$	[49, 101]
chaotic Hamiltonian dynamics	$1/\text{poly}\, n$	this work
many-body localization	$\Theta(1)$	[55, 56, 58–60, 102]

Table 3.1: Finite-size scaling of generic late-time OTOC for various types of quantum dynamics.

- $OTOC_\infty(A, B, A^\dagger, B^\dagger)$ for traceless local operators A, B vanishes in the thermodynamic limit $n \to \infty$.
- In finite-size systems, OTOC $\langle AB(t)A^\dagger B^\dagger(t)\rangle$ saturates to $\Theta(1/n)$ if either A or B (or both) has a finite overlap with the Hamiltonian H. We not only derive the prefactor hidden in the big-Theta notation, but also provide a (not necessarily tight) upper bound on the remainder:

$$OTOC_\infty(A, B, A^\dagger, B^\dagger) = \frac{\langle AA^\dagger\rangle|\langle HB\rangle|^2 + \langle BB^\dagger\rangle|\langle HA\rangle|^2}{\langle HH_i\rangle n} + \tilde{O}(n^{-1.5}). \quad (3.8)$$

This is our main result. It is an example where certain properties of quantum chaotic systems can be calculated analytically. For comparison, Table 3.1 summarizes the finite-size scaling of late-time OTOC of generic traceless local operators for various types of quantum dynamics.

The remainder of this paper is organized as follows. In Section 3.2, assuming a "generic" energy spectrum, we present a simple derivation of Eq. (3.8) for the special case where the local operators in OTOC are terms in the Hamiltonian. In Section 3.3, we extend the approach to the general case using the eigenstate thermalization hypothesis (ETH) [4–6]. Thus, we give a rigorous proof of Eqs. (3.7), (3.8) based on two very mild assumptions for chaotic systems: a generic spectrum and ETH. In Section 3.4, we propose a heuristic physical picture for our results from the perspective of interpreting chaotic dynamics with random unitaries. We first introduce a previous approach, which takes into account the unitarity of the dynamics by approximating the time evolution operator e^{-iHt} with a random unitary. Unfortunately, this approximation remains too crude, for it still suggests that the residual value of late-time OTOC is exponentially small in the system size. We show that once energy conservation is also taken into account by requiring the random unitary to act within small energy windows, the finite-size scaling of late-time OTOC becomes inverse polynomial. In Section 3.5, we support our analytical

arguments with numerical simulations of a nonintegrable spin chain. The numerical results suggest that the remainder in Eq. (3.8) can be improved to $O(n^{-2})$.

3.2 Special case

In the case where the local operators in OTOC are terms in the Hamiltonian, we give a simple rigorous proof of Eq. (3.8) assuming only a generic spectrum.

In strongly chaotic systems, one might expect that the energy spectrum satisfies the "generic" condition:

Assumption 1 (generic spectrum; see, e.g., Ref. [103])**.**

$$E_p + E_r = E_q + E_s \implies ((p = q) \text{ and } (r = s)) \text{ or } ((p = s) \text{ and } (r = q)). \tag{3.9}$$

This assumption is necessary in the sense that it rules out certain integrable (e.g., free-fermion) systems.

Writing out the matrix elements,

$$\langle AB(t)CD(t)\rangle = \frac{1}{d}\sum_{p,q,r,s} A_{pq}B_{qr}C_{rs}D_{sp}e^{i(E_q-E_r+E_s-E_p)t}. \tag{3.10}$$

Substituting into Eq. (3.5), we obtain

$$OTOC_\infty(A,B,C,D) = \frac{1}{d}\sum_{p,q,r,s} A_{pq}B_{qr}C_{rs}D_{sp}\delta_{E_p+E_r,E_q+E_s}, \tag{3.11}$$

where δ is the Kronecker delta. Assumption 1 implies

$$\begin{aligned} &OTOC_\infty(A,B,C,D) \\ &= \frac{1}{d}\sum_{j,k} A_{jj}B_{jk}C_{kk}D_{kj} + \frac{1}{d}\sum_{j,k} A_{jk}B_{kk}C_{kj}D_{jj} - \frac{1}{d}\sum_{j} A_{jj}B_{jj}C_{jj}D_{jj}. \end{aligned} \tag{3.12}$$

Given a Hamiltonian H, there are multiple ways to write it as a sum of local terms: $H = \sum_i H_i$. Without loss of generality, we fix this ambiguity by expanding H in the Pauli basis and assigning all Pauli string operators starting at site i to H_i (see Eq. (3.51) for an example). This convention implies $\mathrm{tr}(H_jH_k) = 0$ for $j \neq k$. Hence, $\langle H_i^2\rangle = \langle HH_i\rangle = \langle H^2\rangle/n$ for any i due to translational invariance. Using this convention,

Theorem 1. *Assumption 1 implies*

$$OTOC_\infty(H_1,H_i,H_1,H_i) = 2\langle H_i^2\rangle^2/n + O(n^{-2}). \tag{3.13}$$

Proof. We will use the observation that $(H_i)_{jj} = E_j/n$ for any i due to translational invariance. For the present choice of local operators in OTOC, the first term on the right-hand side of Eq. (3.12) reads

$$\begin{aligned}
&\frac{1}{d}\sum_{j,k=1}^{d}(H_1)_{jj}(H_i)_{jk}(H_1)_{kk}(H_i)_{kj} \\
&= \frac{1}{dn^2}\sum_{j,k=1}^{d} E_j\langle j|H_i|k\rangle E_k\langle k|H_i|j\rangle \\
&= \frac{1}{dn^2}\,\mathrm{tr}\left(\sum_{j=1}^{d}|j\rangle E_j\langle j|H_i\sum_{k=1}^{d}|k\rangle E_k\langle k|H_i\right) \\
&= \frac{\mathrm{tr}(HH_iHH_i)}{dn^2} = \frac{1}{n^2}\sum_{j,k=1}^{n}\langle H_jH_iH_kH_i\rangle. \qquad (3.14)
\end{aligned}$$

In the last sum, there are n^2 terms, most of which are zero because $\mathrm{tr}\,H_j = \mathrm{tr}\,H_k = 0$. Furthermore, the convention stated above implies $\mathrm{tr}(H_jH_k) = 0$ for $j \neq k$. Hence, the number of nonvanishing terms in the last sum of Eq. (3.14) is $n + O(1)$ (n comes from the terms with $j = k$ and $O(1)$ accounts for the remainder). Equation (3.14) equals

$$\begin{aligned}
&\frac{1}{n^2}\sum_{j=1}^{n}\langle H_jH_iH_jH_i\rangle + O(n^{-2}) \\
&= \langle H_i^2\rangle^2/n + O(n^{-2}) + O(n^{-2}) = \langle H_i^2\rangle^2/n + O(n^{-2}). \qquad (3.15)
\end{aligned}$$

The second term on the right-hand side of Eq. (3.12) gives the same result. The last term on the right-hand side of Eq. (3.12) equals

$$\frac{1}{dn^4}\sum_j E_j^4 = \Theta(n^{-2}), \qquad (3.16)$$

where we used Eq. (3.17) with $m = 4$. This completes the proof. □

3.3 General case: Implications of eigenstate thermalization

In this section, we provide an argument for Eqs. (3.7), (3.8). The argument is rigorous assuming a generic spectrum and ETH.

Lemma 1 (moments)**.**

$$\frac{1}{d}\sum_j E_j^m = \langle H^m\rangle = \Theta(n^{m/2}), \quad \forall \textit{ even positive integer } m, \tag{3.17}$$

$$\left|\frac{1}{d}\sum_j E_j^3\right| = |\langle H^3\rangle| = O(n). \tag{3.18}$$

Proof. Expanding H in the Pauli basis, it suffices to count the number of terms that do not vanish upon taking the trace in the expansion of H^m or H^3. □

Lemma 2 (concentration of eigenvalues)**.** *Almost all eigenstates have zero energy density:*

$$|\{j : |E_j| \geq n^{0.51}\}|/d \leq O(n^{-0.01m}), \quad \forall m > 0. \tag{3.19}$$

Proof. It follows from Eq. (3.17) and Markov's inequality. □

This lemma allows us to upper bound the total contribution of all eigenstates away from the middle of the spectrum, e.g.,

$$\frac{1}{d}\sum_{j:|E_j|\geq n^{0.51}} E_j^2 \leq O(n^{2-0.01m}), \quad \forall m > 0. \tag{3.20}$$

Lemmas 2 and Eqs. (3.17), (3.20) are related to the fact that E_j's approach a normal distribution in the thermodynamic limit $n \to \infty$ [104, 105]. Indeed, $|E_j| = \Theta(\sqrt{n})$ for almost all j.

It suffices to assume ETH for eigenstates in the middle of the spectrum.

Assumption 2 (eigenstate thermalization hypothesis in the middle of the spectrum)**.** Let δ be an arbitrarily small positive constant. For any local operator X with $\|X\| \leq 1$, there is a function $f_X : [-\delta, \delta] \to [-1, 1]$ such that

$$|X_{jj} - f_X(E_j/n)| \leq 1/\mathrm{poly}\, n \tag{3.21}$$

for all j with $|E_j| \leq \delta n$, where $\mathrm{poly}\, n$ denotes a polynomial of sufficiently high degree in n. We assume that f_X is smooth in the sense of having a Taylor expansion to some low order.

It was proposed analytically [103] and supported by numerical simulations [106] that the right-hand side of Eq. (3.21) can be improved to $e^{-\Omega(n)}$. For our purposes, however, a (much weaker) inverse polynomial upper bound suffices.

Lemma 3. *For any local operator X and traceless local operator A, Assumption 2 implies*

$$f_X(0) = \frac{1}{d}\operatorname{tr} X, \tag{3.22}$$

$$f_A'(0) = \operatorname{tr}(HA)/\operatorname{tr}(HH_i), \tag{3.23}$$

$$\frac{1}{d}\sum_j |A_{jj}|^2 = \frac{|\operatorname{tr}(HA)|^2}{dn\operatorname{tr}(HH_i)} + O(n^{-2}), \tag{3.24}$$

$$\frac{1}{d}\sum_j |A_{jj}|^4 = O(n^{-2}). \tag{3.25}$$

For a generic traceless local operator A, the right-hand side of Eq. (3.23) (the normalized overlap between A and the Hamiltonian) is finite and the first term on the right-hand side of Eq. (3.24) is $\Theta(1/n)$.

Proof of Eq. (3.22).

$$\begin{aligned}\frac{1}{d}\operatorname{tr} X &= \frac{1}{d}\sum_j X_{jj} \approx \frac{1}{d}\sum_{j:|E_j|<n^{0.51}} X_{jj} \\ &\approx \frac{1}{d}\sum_{j:|E_j|<n^{0.51}} f_X(0) \approx \frac{1}{d}\sum_j f_X(0) = f_X(0),\end{aligned} \tag{3.26}$$

where we used Lemma 2 in the second and fourth steps. The third step follows from the continuity of $f_X(x)$ at $x = 0$. Taking the limit $n \to \infty$, all errors in Eq. (3.26) vanish and thus we obtain Eq. (3.22). In particular, $f_A(0) = 0$ for any traceless local operator A. □

Proof of Eq. (3.23).

$$\begin{aligned}\frac{1}{d}\operatorname{tr}(HA) &= \frac{1}{d}\sum_j E_j A_{jj} \\ &\approx \frac{1}{d}\sum_{j:|E_j|<n^{0.51}} E_j A_{jj} \approx \frac{1}{d}\sum_{j:|E_j|<n^{0.51}} \frac{E_j^2}{n} f_A'(0) \\ &\approx \frac{1}{d}\sum_j \frac{E_j^2}{n} f_A'(0) = \operatorname{tr}(HH_i) f_A'(0)/d,\end{aligned} \tag{3.27}$$

where we used Lemma 2 and Eq. (3.20) in the second and fourth steps, respectively. In the third step, we used Eq. (3.21) and the Taylor expansion

$$f_A(E_j/n) = f_A(0) + f_A'(0)E_j/n + 0.5 f_A''(0)E_j^2/n^2 + O(|E_j|^3/n^3) \tag{3.28}$$

so that the approximation error in this step is upper bounded by

$$\frac{O(1)}{d}\sum_{j:|E_j|<n^{0.51}}\frac{|E_j|^3}{n^2}\le O(n^{-0.47}). \tag{3.29}$$

Taking the limit $n\to\infty$, all errors in Eq. (3.27) vanish and thus we obtain Eq. (3.23). □

Proof of Eq. (3.24).

$$\begin{aligned}\frac{1}{d}\sum_j |A_{jj}|^2 &\approx \frac{1}{d}\sum_{j:|E_j|<n^{0.51}}|A_{jj}|^2\\ &\approx \frac{|f_A'(0)|^2}{d}\sum_{j:|E_j|<n^{0.51}}\frac{E_j^2}{n^2}\approx\frac{|f_A'(0)|^2}{d}\sum_j\frac{E_j^2}{n^2}\\ &= \frac{|\operatorname{tr}(HA)|^2}{dn\operatorname{tr}(HH_i)},\end{aligned} \tag{3.30}$$

where we used Lemma 2 and Eqs. (3.20), (3.23) in the first, third, and last steps, respectively. In the second step, we used Eqs. (3.21), (3.28) with the approximation error upper bounded by

$$\begin{aligned}&\frac{O(1)}{d}\left|\sum_{j:|E_j|<n^{0.51}}\frac{E_j^3}{n^3}\right|+\frac{O(1)}{d}\sum_{j:|E_j|<n^{0.51}}\frac{E_j^4}{n^4}+1/\operatorname{poly} n\\ &\approx\frac{O(1)}{d}\left|\sum_j\frac{E_j^3}{n^3}\right|+\frac{O(1)}{d}\sum_j\frac{E_j^4}{n^4}\\ &= O(n^{-2})+O(n^{-2})=O(n^{-2}),\end{aligned} \tag{3.31}$$

where we used Eqs. (3.17), (3.18). □

Proof of Eq. (3.25).

$$\begin{aligned}\frac{1}{d}\sum_j |A_{jj}|^4 &\approx \frac{1}{d}\sum_{j:|E_j|<n^{0.51}}|A_{jj}|^4\\ &\approx\frac{O(1)}{d}\sum_{j:|E_j|<n^{0.51}}\frac{E_j^4}{n^4}\approx\frac{O(1)}{d}\sum_j\frac{E_j^4}{n^4}=O(n^{-2}).\end{aligned} \tag{3.32}$$

□

Let $J \subseteq \mathbb{R}$ be an energy interval. Define

$$P_J = \sum_{j:E_j \in J} |j\rangle\langle j| \tag{3.33}$$

as the projector onto J.

Lemma 4 ([107])**.** *Let $\epsilon < \epsilon'$. For any local operator X,*

$$\|P_{(-\infty,\epsilon)} X P_{(\epsilon',\infty)}\| \le \|X\| e^{-\Omega(\epsilon'-\epsilon)}. \tag{3.34}$$

This lemma states that local operators cannot (up to an exponentially small error) connect projectors that are far away from each other in the spectrum.

Justification of Eq. (3.7). Let c be a sufficiently large constant. Consider the first term on the right-hand side of Eq. (3.12):

$$\begin{aligned}
&\frac{1}{d}\sum_{j,k} A_{jj}B_{jk}C_{kk}D_{kj} \approx \frac{1}{d}\sum_{j}\sum_{k:|E_j-E_k|<c\ln n} A_{jj}B_{jk}C_{kk}D_{kj} \\
&\approx \frac{1}{d}\sum_{j}\sum_{k:|E_j-E_k|<c\ln n} A_{jj}B_{jk}C_{jj}D_{kj} \approx \frac{1}{d}\sum_{j,k} A_{jj}C_{jj}B_{jk}D_{kj} \\
&= \frac{1}{d}\sum_{j} A_{jj}C_{jj}(BD)_{jj},
\end{aligned} \tag{3.35}$$

where we used Lemma 4 in the first and third steps: Due to the presence of off-diagonal matrix elements B_{jk}, D_{kj}, the total contribution of all terms with $|E_k - E_j| \ge c\ln n$ is upper bounded by $1/\mathrm{poly}\, n$. In the second step of Eq. (3.35), we replace C_{kk} by C_{jj} using ETH (Assumption 2), which states that eigenstates with similar energies have similar local expectation values. A detailed and rigorous error analysis for Eq. (3.35) is given in Propositions 1, 2 below.

Equation (3.35) shows that the first term on the right-hand side of Eq. (3.12) corresponds to the second term on the right-hand side of Eq. (3.6). Similarly, the second term on the right-hand side of Eq. (3.12) corresponds to the first term on the right-hand side of Eq. (3.6). Obviously, the last terms on the right-hand sides of Eqs. (3.6), (3.12) are the same. Thus, we obtain Eq. (3.7). □

Proposition 1. *The approximation errors in the first and third steps of Eq. (3.35) are $1/\mathrm{poly}\, n$, where $\mathrm{poly}\, n$ denotes a polynomial of sufficiently high degree in n.*

Proof. Let

$$Q_j = \sum_{k:|E_j-E_k|\geq c\ln n} |k\rangle\langle k|, \quad \tilde{C} = \sum_k C_{kk}|k\rangle\langle k|. \tag{3.36}$$

Since $\tilde{C}$ is the diagonal part of C (in the energy basis), it is easy to see $\|\tilde{C}\| \leq \|C\|$. The approximation error in the first step of Eq. (3.35) is

$$\begin{aligned}
&\frac{1}{d}\left|\sum_j \sum_{k:|E_j-E_k|\geq c\ln n} A_{jj}B_{jk}C_{kk}D_{kj}\right| \\
&\leq \frac{1}{d}\sum_j |A_{jj}|\left|\sum_{k:|E_j-E_k|\geq c\ln n} B_{jk}C_{kk}D_{kj}\right| \leq \frac{\|A\|}{d}\sum_j |\langle j|BQ_j\tilde{C}Q_jD|j\rangle| \\
&\leq \frac{\|A\|}{d}\sum_j \|Q_jB^\dagger|j\rangle\|\|\tilde{C}\|\|Q_jD|j\rangle\| \leq \|A\|\|B\|\|C\|\|D\|/\mathrm{poly}\, n,
\end{aligned} \tag{3.37}$$

where we used Lemma 4. The approximation error in the third step of Eq. (3.35) can be upper bounded similarly. □

Proposition 2. *The approximation error in the second step of Eq. (3.35) is* $\tilde{O}(n^{-1.5})$.

Proof. Let n be sufficiently large such that $n^{0.51} + c\ln n < \delta n$, and define

$$\tilde{C}^{(j)} := \sum_{k:|E_j-E_k|<c\ln n} (C_{jj} - C_{kk})|k\rangle\langle k|. \tag{3.38}$$

For j, k such that $|E_j| < n^{0.51}$ and $|E_j - E_k| < c\ln n$, Assumption 2 implies

$$|C_{jj}-C_{kk}| \leq |f_C(E_j/n)-f_C(E_k/n)|+1/\mathrm{poly}\, n = O(|E_j-E_k|)/n+1/\mathrm{poly}\, n. \tag{3.39}$$

Hence, $\|\tilde{C}^{(j)}\| = \tilde{O}(1/n)$ for any j such that $|E_j| < n^{0.51}$. The approximation error

in the second step of Eq. (3.35) is

$$\begin{aligned}
&\frac{1}{d}\left|\sum_j \sum_{k:|E_j-E_k|<c\ln n} A_{jj}B_{jk}(C_{jj}-C_{kk})D_{kj}\right| \\
&\le \frac{1}{d}\sum_j |A_{jj}|\left|\sum_{k:|E_j-E_k|<c\ln n} B_{jk}\tilde{C}^{(j)}_{kk}D_{kj}\right| = \frac{1}{d}\sum_j |A_{jj}||\langle j|B\tilde{C}^{(j)}D|j\rangle| \\
&\le \frac{1}{d}\sum_j |A_{jj}|\left\|\tilde{C}^{(j)}\right\| = \frac{1}{d}\sum_{j:|E_j|<n^{0.51}} |A_{jj}|\left\|\tilde{C}^{(j)}\right\| + \frac{1}{d}\sum_{j:|E_j|\ge n^{0.51}} |A_{jj}|\left\|\tilde{C}^{(j)}\right\| \\
&\le \frac{1}{d}\sum_{j:|E_j|<n^{0.51}} |A_{jj}|\tilde{O}(1/n) + \frac{1}{d}\sum_{j:|E_j|\ge n^{0.51}} |A_{jj}|O(1) \\
&\le \frac{\tilde{O}(1/n)}{d}\sum_j |A_{jj}| + \frac{1}{d}\sum_{j:|E_j|\ge n^{0.51}} O(1) \\
&\le \tilde{O}(1/n)\sqrt{\frac{1}{d}\sum_j |A_{jj}|^2} + 1/\mathrm{poly}\, n = \tilde{O}(n^{-1.5}),
\end{aligned} \tag{3.40}$$

where we used Eq. (3.24) in the last step. □

Justification of Eq. (3.8). Specializing to $\langle AB(t)A^\dagger B^\dagger(t)\rangle$, the derivation above yields

$$\begin{aligned}
&OTOC_\infty(A,B,A^\dagger,B^\dagger) \\
&= \frac{1}{d}\sum_j (AA^\dagger)_{jj}|B_{jj}|^2 + |A_{jj}|^2(BB^\dagger)_{jj} - |A_{jj}B_{jj}|^2 + \tilde{O}(n^{-1.5}).
\end{aligned} \tag{3.41}$$

Consider the first term on the right-hand side:

$$\begin{aligned}
\frac{1}{d}\sum_j (AA^\dagger)_{jj}|B_{jj}|^2 &\approx \frac{1}{d}\sum_{j:|E_j|<n^{0.51}} (AA^\dagger)_{jj}|B_{jj}|^2 \\
&\approx \frac{1}{d}\sum_{j:|E_j|<n^{0.51}} f_{AA^\dagger}(0)|B_{jj}|^2 \approx \frac{f_{AA^\dagger}(0)}{d}\sum_j |B_{jj}|^2 \\
&\approx \frac{\mathrm{tr}(AA^\dagger)|\,\mathrm{tr}(HB)|^2}{d^2 n\,\mathrm{tr}(HH_i)},
\end{aligned} \tag{3.42}$$

where we used Lemma 2 in the first and third steps; the continuity of $f_{AA^\dagger}(x)$ at $x = 0$ in the second step; and Eqs. (3.22), (3.24) in the last step. A rigorous error analysis for Eq. (3.42) is given in Proposition 3 below.

The second term on the right-hand side of Eq. (3.41) can be estimated similarly. The third term on the right-hand side of Eq. (3.41) is

$$\frac{1}{d}\sum_j |A_{jj}B_{jj}|^2 \le \frac{1}{2d}\sum_j |A_{jj}|^4 + |B_{jj}|^4 = O(n^{-2}), \tag{3.43}$$

where we used Eq. (3.25). Thus, Eq. (3.8) is proved based on Assumptions 1, 2. □

Proposition 3. *The error in Eq. (3.42) is* $O(n^{-2})$.

Proof. The approximation error in the last step of Eq. (3.42) is $O(n^{-2})$ as given by Eq. (3.24). Using the Taylor expansion of $f_{AA^\dagger}(x)$ at $x = 0$, we estimate the approximation error in the second step of Eq. (3.42):

$$\frac{O(1)}{d}\left|\sum_{j:|E_j|<n^{0.51}}\frac{|B_{jj}|^2E_j}{n}\right| + \frac{O(1)}{d}\sum_{j:|E_j|<n^{0.51}}\frac{|B_{jj}|^2E_j^2}{n^2} + 1/\mathrm{poly}\, n \lesssim \frac{O(1)}{d}\left|\sum_{j:|E_j|<n^{0.51}}\frac{E_j^3}{n^3}\right|$$
$$+ \frac{O(1)}{d}\sum_{j:|E_j|<n^{0.51}}\left(\frac{E_j^4}{n^4} + |B_{jj}|^4\right) \approx \frac{O(1)}{d}\left|\sum_j \frac{E_j^3}{n^3}\right| + \frac{O(1)}{d}\sum_j\left(\frac{E_j^4}{n^4} + |B_{jj}|^4\right)$$
$$\approx O(n^{-2}) + O(n^{-2}) + O(n^{-2}) = O(n^{-2}), \tag{3.44}$$

where we used the Taylor expansion of $f_B(x)$ at $x = 0$ and the inequality of arithmetic and geometric means in the first step; Lemma 2 in the second step; and Eqs. (3.17), (3.18), (3.25) in the third step. □

3.4 Chaotic dynamics as random unitary

In this section, we rederive Eq. (3.7) using techniques from the theory of random unitaries. The derivation is not rigorous, but provides a heuristic picture showing the extent to which chaotic dynamics can be approximated by a random unitary.

To improve the approximation described by Eq. (3.2), we first take into account the unitarity of the dynamics. In strongly chaotic systems, it is tempting to expect

Assumption 3. The time evolution operator e^{-iHt} for large t behaves like a random unitary.

Based on this assumption, late-time OTOC can be estimated from

$$OTOC_\infty(A,B,C,D) = \int \mathrm{d}U\langle A(U^\dagger BU)C(U^\dagger DU)\rangle, \tag{3.45}$$

where U is taken from the unitary group $\mathcal{U}(d)$ with respect to the Haar measure.

Lemma 5 ([49, 101])**.**

$$\int \mathrm{d}U\langle AU^\dagger BUCU^\dagger DU\rangle = \langle A,B,C,D\rangle - \frac{\langle AC\rangle_c\langle BD\rangle_c}{d^2-1}, \tag{3.46}$$

where $\langle XY\rangle_c := \langle XY\rangle - \langle X\rangle\langle Y\rangle$ *is the connected correlator and*

$$\langle A,B,C,D\rangle := \langle AC\rangle\langle B\rangle\langle D\rangle + \langle A\rangle\langle C\rangle\langle BD\rangle - \langle A\rangle\langle B\rangle\langle C\rangle\langle D\rangle. \tag{3.47}$$

Note that the right-hand side of Eq. (3.6) resembles that of Eq. (3.47) in the sense of replacing every $\langle\cdots\rangle$ (expectation value at infinite temperature) by $\langle j|\cdots|j\rangle$ (expectation value in an eigenstate).

Corollary 1 ([49, 101])**.** *Assumption 3 and Lemma 5 imply*

$$OTOC_\infty(A,B,C,D) = \langle A,B,C,D\rangle - \frac{\langle AC\rangle_c\langle BD\rangle_c}{d^2-1}. \tag{3.48}$$

Therefore,

- $OTOC_\infty(A,B,A^\dagger,B^\dagger)$ *for traceless operators* A,B *vanishes in the thermodynamic limit* $n\to\infty$.
- *In finite-size systems, the saturation value of OTOC* $\langle AB(t)A^\dagger B^\dagger(t)\rangle$ *is exponentially small in the system size (because* $d=2^n$*).*

The approximation stated in Assumption 3 is still too crude. We propose a refined version of Assumption 3 by incorporating energy conservation and argue (nonrigorously) that Eq. (3.7) follows from this refinement.

We observe that the time evolution conserves energy and that local operators can only additively change the energy of a state by $O(1)$ (Lemma 4). Thus, the action of OTOC $AB(t)CD(t)$ is approximately restricted to each microcanonical ensemble. This observation motivates a refinement of Assumption 3 in strongly chaotic systems:

Assumption 4. The time evolution operator e^{-iHt} for large t behaves like a random unitary in each microcanonical ensemble.

Conceptually, this assumption is related to the notion of random diagonal unitaries [108, 109].

Based on Assumption 4, we argue for Eq. (3.7). Since the bandwidth of H is $\Theta(n)$, we decompose the energy spectrum into a disjoint union of $\Theta(n/\Delta)$ microcanonical ensembles with bandwidth Δ. Let $J_k := [k\Delta,(k+1)\Delta)$ and define $[A,B,C,D]_k$ as

the right-hand side of Eq. (3.47) with every $\langle \cdots \rangle$ replaced by the expectation value $\mathrm{tr}(P_{J_k} \cdots)/\mathrm{tr}\, P_{J_k}$ in the microcanonical ensemble. We expect

$$\lim_{\tau\to\infty} \frac{1}{\tau} \int_0^\tau \mathrm{d}t \frac{\mathrm{tr}(P_{J_k} AB(t)CD(t))}{\mathrm{tr}\, P_{J_k}} \approx [A,B,C,D]_k \approx \frac{1}{\mathrm{tr}\, P_{J_k}} \sum_{j:E_j\in J_k} \langle A,B,C,D\rangle_j. \tag{3.49}$$

The first step is a consequence of Lemma 5 and Assumption 4. Indeed, it is just Eq. (3.48) restricted to the microcanonical ensemble P_{J_k}. The last step of Eq. (3.49) used ETH. Equation (3.7) follows immediately from Eq. (3.49).

An important subtlety here, which does not appear in the derivation of Eq. (3.48), requires further explanation. For an eigenstate $|j\rangle$ in a microcanonical ensemble P_{J_k}, the state $AB(t)CD(t)|j\rangle$ may not be completely in the microcanonical ensemble. As long as A, B, C, D are local operators, Lemma 4 implies

$$\|(1 - P_{J_k})AB(t)CD(t)|j\rangle\| \le \|A\|\|B\|\|C\|\|D\| e^{-\Omega(\min\{E_j - k\Delta, (k+1)\Delta - E_j\})}, \tag{3.50}$$

i.e., the "leakage" out of the microcanonical ensemble P_{J_k} is exponentially small. This is why Eq. (3.7) requires the locality of A, B, C, D, although Corollary 1 does not.

3.5 Numerics

In this section, we support Eq. (3.8) with numerical simulations. Consider the spin-1/2 chain

$$H = \sum_{i=1}^n H_i, \quad H_i = \sigma_i^z \sigma_{i+1}^z - 1.05\sigma_i^x + 0.5\sigma_i^z + g\sigma_i^y \sigma_{i+1}^z \tag{3.51}$$

with periodic boundary conditions ($\sigma_{n+1}^z := \sigma_1^z$), where $\sigma_i^x, \sigma_i^y, \sigma_i^z$ are the Pauli matrices at site i. For $g = 0$, this model is nonintegrable in the sense of Wigner-Dyson level statistics [10, 110]. Reference [41] calculated OTOC, focusing on the butterfly effect rather than the late-time behavior. Note that for $g = 0$, most energy levels are two-fold degenerate so that Assumption 1 does not hold.

We fix $g = 0.1$. Intuitively, the model is nonintegrable for any value of g. We have numerically confirmed the validity of Assumption 1 for $n = 5, 6, \ldots, 12$. Presumably, Assumption 1 holds for any integer $n \ge 5$. Let

$$F_n^x := OTOC_\infty(\sigma_1^x, \sigma_i^x, \sigma_1^x, \sigma_i^x), \quad F_n^z := OTOC_\infty(\sigma_1^z, \sigma_i^z, \sigma_1^z, \sigma_i^z). \tag{3.52}$$

Note that the values of F_n^x, F_n^z are independent of i. We compute F_n^x, F_n^z using exact diagonalization. The results are shown in the left panel of Fig. 3.1.

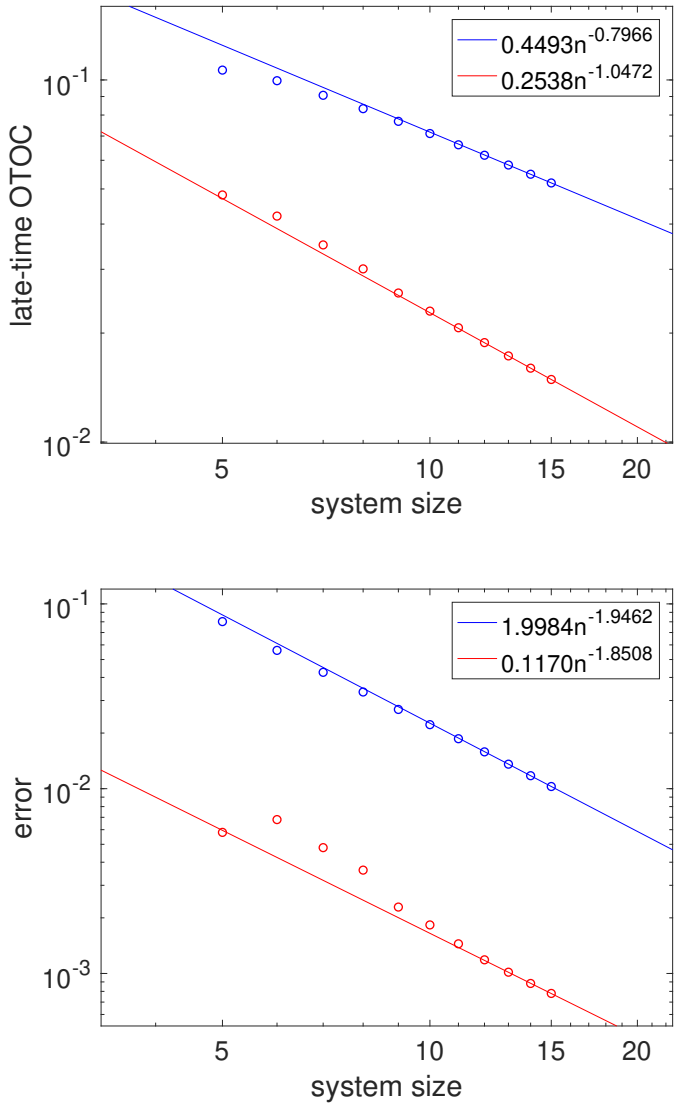

Figure 3.1: Upper panel: Finite-size scaling of late-time OTOC F_n^x (blue), F_n^z (red) for $n = 5, 6, \ldots, 15$. The lines are power-law fits $0.4493n^{-0.7966}$ (blue), $0.2538n^{-1.0472}$ (red) to the last few data points. Lower panel: Finite-size scaling of the errors $|F_n^x - G_n^x|$ (blue), $|F_n^z - G_n^z|$ (red) for $n = 5, 6, \ldots, 15$. The lines are power-law fits $1.9984n^{-1.9462}$ (blue), $0.1170n^{-1.8508}$ (red) to the last few data points.

The leading terms in the finite-size scaling of F_n^x, F_n^z are calculated analytically from Eq. (3.8):

$$G_n^x := \frac{14}{15n} \approx \frac{0.9333}{n}, \quad G_n^z := \frac{40}{189n} \approx \frac{0.2116}{n}. \tag{3.53}$$

We expect that the noticeable differences between G_n^x, G_n^z and the power-law fits to F_n^x, F_n^z are due to finite-size effects. To justify this claim, we perform a scaling analysis of the errors $|F_n^x - G_n^x|$, $|F_n^z - G_n^z|$ in the right panel of Fig. 3.1. The numerics suggest that the errors should vanish as $\Theta(n^{-2})$ in the thermodynamic limit $n \to \infty$.

3.6 Conclusions and Discussions

We propose that in order to better approximate the late-time behavior of chaotic dynamics generated by a time-independent Hamiltonian, one needs to take into account energy conservation. In particular, we show that approximation schemes with and without energy conservation make different predictions about OTOC at late times: without energy conservation, late-time OTOC scales inverse exponentially with system size; with energy conservation, the scaling is inverse polynomial. The latter prediction has been rigorously confirmed based on two very mild assumptions and is consistent with numerical simulations of a nonintegrable spin chain.

An immediate open question is how good the energy-preserving approximation scheme proposed in this paper is in predicting the late-time behavior of higher-order time-ordered or out-of-time-ordered correlators. A more general problem for future study is how to approximate the time evolution process and capture other universal features of chaotic dynamics. See Refs. [75, 76, 111, 112] for recent progress in this direction.

Chapter 4

INFORMATION SCRAMBLING IN CHAOTIC SYSTEMS WITH DISSIPATION

Chaos happens not just in classical systems, but in quantum systems as well [79, 113–119]. One characteristic signature of quantum chaos is the scrambling of quantum information which can be quantitatively described by the out-of-time-ordered correlator (OTOC) [34–63]. More specifically, suppose that information is encoded initially in a local operator A. Under the dynamics generated by a local Hamiltonian $H = \sum_i h_i$, $A(t) = e^{iHt}Ae^{-iHt}$ grows in size and becomes non-local as t increases. As A grows in size, it starts to overlap with local operators B at other spatial locations and ceases to commute with them. The effect of information scrambling is then manifested as the growth in the norm of the commutator $[A(t), B]$. Correspondingly, it is also manifested as the decay of (the real part of) the OTOC $\langle A^\dagger(t)B^\dagger A(t)B\rangle_\beta$ which is related to the commutator as

$$\Re\,\langle A^\dagger(t)B^\dagger A(t)B\rangle_\beta = 1 - \frac{1}{2}\langle [A(t),B]^\dagger [A(t),B]\rangle_\beta, \tag{4.1}$$

where local operators A, B are both unitary, $\langle\cdot\rangle_\beta$ represents the thermal average at the inverse temperature $\beta = 1/T$, and $\Re$ denotes the real part.

In a chaotic system, the decay of OTOC is usually expected to exhibit the following features: First, after time evolution for a very long time, information initially encoded in A becomes highly nonlocal and cannot be accessed with any individual local operator B. Therefore, all OTOCs at infinite temperature $\beta = 0$ decay to zero at late time [40, 43, 49, 51]

$$\lim_{t\to\infty} \Re\,\langle A^\dagger(t)B^\dagger A(t)B\rangle_{\beta=0} = 0, \tag{4.2}$$

where the local operators A and B are traceless.

Secondly, in chaotic zero-dimensional systems, the OTOC starts to decay at early time in an exponential way [43]

$$\Re\,\langle A^\dagger(t)B^\dagger A(t)B\rangle_\beta = f_1 - \frac{f_2}{n}e^{\lambda_L t} + O\left(\frac{1}{n^2}\right), \tag{4.3}$$

where the constants f_1, f_2 depend on the choice of operators A, B, and n is the total number of degrees of freedom. The exponent of the exponential – the Lyapunov

exponent – characterizes how chaotic the quantum dynamics is. It is bounded by $\lambda_L \leq \frac{2\pi}{\beta}$ [42–45] and is expected to be saturated by quantum systems corresponding to black holes.

Thirdly, in a system with spatial locality, information spreads at a certain speed, giving rise to a delay time before OTOC starts to decay. In some simple cases [42, 43, 47, 120, 121], the early-time behavior of OTOC is approximately described by

$$f_1' - f_2' e^{\lambda_L (t - d_{BA}/v_B)} + \text{higher-order terms} \tag{4.4}$$

with f_1', f_2' that depend on A, B and the local degrees of freedom. d_{BA} is the distance between the local operators A and B. The higher-order terms can be described by $O(\frac{1}{n^2})$ in large-n systems [42] or $O(e^{-2\lambda_L d_{BA}/v_B})$ in spin systems [43]. That is, information spreads with a finite velocity v_B – the butterfly velocity – and forms a 'light cone' [41–43]. In general quantum chaotic spin systems with small local Hilbert space dimensions and short-range interactions, like random circuit models [70–76], the wave front of the light cone becomes wider while propagating out and Refs. [77, 78] give an in-depth study of the general form of the early time decay of OTOC. The deep connection between OTOC and quantum chaos generated a lot of interest in the topic, both theoretically and experimentally. Several protocols have been proposed to measure these unconventional correlators in real experimental systems [85–87, 122–129].

The measurement of OTOC in real experimental systems is complicated by the fact that the system is not exactly closed and suffers from dissipation through coupling to the environment. How does dissipation affect the measured signal of OTOC? More generally, we can ask how does dissipation affect information scrambling in a chaotic system? Dissipation leads to leakage of information, and therefore it is natural to expect that any signal of information scrambling would decay. Is it then possible to recover the signatures of information scrambling in a dissipative system and observe the existence of a light cone?

To address these questions, we numerically study a prototypical model of chaotic spin chain [37, 41, 43, 110] – the Ising model with both transverse and longitudinal fields – in the presence of some common types of dissipation: amplitude damping, phase damping and phase depolarizing. Due to the lack of a "small parameter" as explained in Ref. [78], there is no well-defined Lyapunov exponent in this system. Thus, we focus on the structural changes of the light cone, which manifests information scrambling.

The Hamiltonian of the system with open boundary condition is

$$H_s = -J\Big[\sum_{i=1}^{N-1}\sigma_i^z\sigma_{i+1}^z + \sum_{i=1}^{N}(h_x\sigma_i^x + h_z\sigma_i^z)\Big], \tag{4.5}$$

where N is the number of spins, and we choose the parameters to be $J = 1$, $h_x = -1.05$, and $h_z = 0.5$. This model, far from any integrability limits [110], is believed to have chaotic dynamics. We find that if OTOC is measured using the protocol given in Ref. [85], dissipation leads to the decay of the signal not only due to information leaking into the environment, but also information re-structuring. We define a corrected OTOC to remove the effect of leaking, so that the light cone can be recovered to some extent. However, due to the re-structuring, the recovered light cone only persists to a finite distance.

The paper is organized as follows. In Sec. 4.1, we review the dynamics of dissipative systems and define a dissipative version of OTOC based on the measurement protocol given in Ref. [85]. In Sec. 4.2, after observing the fast overall decay of the dissipative OTOC, we define a corrected OTOC to remove the effect of overall information leaking in the hope of recovering the information light cone. However, we see that the corrected light cone still only persists for a finite distance. In Sec. 4.3, we point out that the corrected light cone is finite due to information re-structuring and investigate the relationship between the width of the partially recovered light cone and the strength of dissipation. In Sec. 4.4, we conjecture a modified Lieb-Robinson bound for dissipative systems based on our observation regarding OTOC in the previous sections.

4.1 Measurement of OTOC in dissipative systems

In this section, we provide a brief review of the dynamics of dissipative systems, and then generalize the definition of OTOC to dissipative systems based on the measurement protocol in Ref. [85].

A dissipative system is an open quantum system S coupled to its environment E. In this coupled system, the total Hamiltonian is $H = H_s + H_e + H_{int}$, where $H_s(H_e)$ is the Hamiltonian of the system (environment) and H_{int} is the interaction term. The reduced density matrix of the system S changes as a consequence of its internal dynamics and the interaction with the environment E. In most cases, the initial state is assumed to be a product state $\rho_s(0) \otimes \rho_e(0)$. Under the Born, Markov and secular approximations, the dynamical evolution of a dissipative system $\rho_s(t) = \mathrm{tr}_e[e^{-iHt}\rho_s(0) \otimes \rho_e(0)e^{iHt}] = \mathcal{V}(t) \cdot \rho_s(0)$ can be described by the Lindblad

master equation [130]

$$\frac{d\rho_s(t)}{dt} = \mathcal{L}\cdot\rho_s(t) = -i[H_s,\rho_s(t)]+ \\ \sum_k \frac{\Gamma}{2}\Big(2L_k\rho_s(t)L_k^\dagger - \rho_s(t)L_k^\dagger L_k - L_k^\dagger L_k\rho_s(t)\Big), \tag{4.6}$$

where $\mathcal{V}(t)$ is the dynamical map that connects $\rho_s(0)$ to $\rho_s(t)$, $\mathcal{L}$ is the Liouvillian super-operator, the first commutator with H_s represents the unitary dynamics, the dissipation rate Γ is a positive number, and the Lindblad operators L_k describe the dissipation. Some common types of dissipation [130, 131] act locally on each spin via the Lindblad operators in three different scenarios:

$$\text{amplitude damping:}\ \ L_k = \sqrt{\frac{1}{2}}(\sigma_k^x - i\sigma_k^y), \tag{4.7}$$

$$\text{phase damping:}\ \ L_k = \sqrt{\frac{1}{2}}\sigma_k^z, \tag{4.8}$$

$$\text{phase depolarizing:}\ \ L_k = \frac{1}{2}\sigma_k^x, \frac{1}{2}\sigma_k^y, \frac{1}{2}\sigma_k^z, \tag{4.9}$$

where k denotes the k-th spin. Different pre-factors are selected to ensure that the Liouvillian super-operator at site k has the same largest nonzero eigenvalue $-\Gamma$ in different dissipative channels.

In the Heisenberg picture, the adjoint dynamical map $\mathcal{V}^\dagger(t)$ acting on the Hermitian operators is defined by $\mathrm{tr}[O(\mathcal{V}(t)\cdot\rho_s)] = \mathrm{tr}[(\mathcal{V}^\dagger(t)\cdot O)\rho_s]$ for all states ρ_s. If the Lindblad operators do not depend on time, then the adjoint master equation describing the evolution of the operator $O_H(t) = \mathcal{V}^\dagger(t)\cdot O$ is [130]

$$\frac{dO_H(t)}{dt} = \mathcal{L}^\dagger\cdot O_H(t) = i[H_s,O_H(t)]+ \\ \sum_k \frac{\Gamma}{2}\Big(2L_k^\dagger O_H(t)L_k - O_H(t)L_k^\dagger L_k - L_k^\dagger L_k O_H(t)\Big), \tag{4.10}$$

where $\mathcal{L}^\dagger$ is the adjoint Liouvillian super-operator.

Given both the dynamical and the adjoint dynamical map, how should we define the OTOC in a dissipative system? Should we just replace $A(t)$ with $\mathcal{V}^\dagger(t)\cdot A$ or do something more complicated? In order to give a meaningful answer to this question, we need to specialize to a particular measurement scheme of OTOC and see how the measured quantity changes due to dissipation. We choose to focus on the measurement scheme given in Ref. [85].

Let us analyze in more detail how the measurement scheme would be affected if dissipation is present. Without dissipation, the protocol involves the system whose unitary dynamics generated by H_s is to be probed and a control qubit c. The system is initialized in a thermal state ρ_s or eigenstate $|\psi\rangle_s$ and the control qubit is initialized in state $|+\rangle_c = \frac{1}{\sqrt{2}}(|0\rangle_c + |1\rangle_c)$. Ignoring dissipation, the measurement scheme involves the following steps of unitary operations:

$$
\begin{aligned}
(1): \quad & U_1 = I_s \otimes |0\rangle\langle 0|_c + B_s \otimes |1\rangle\langle 1|_c, \\
(2): \quad & U_2 = e^{-itH_s} \otimes I_c \\
(3): \quad & U_3 = A_s \otimes I_c, \\
(4): \quad & U_4 = e^{itH_s} \otimes I_c, \\
(5): \quad & U_5 = B_s \otimes |0\rangle\langle 0|_c + I_s \otimes |1\rangle\langle 1|_c,
\end{aligned}
$$

where A_s and B_s are both local unitary operators in the system. Finally, measurement of σ_c^x is performed to get the real part of OTOC. A nice property of this protocol is that it works for both pure states and mixed states, which allows straightforward generalization to open systems.

Note that the above protocol involves both forward and backward time evolution. With dissipation, we assume that only the Hamiltonian of the system is reversed during the backward time evolution while the effect of the environment is unchanged. The reason is that H_e and H_{int} are usually out of control in experiments. Under this setup, if forward time evolution is governed by $H_f = H_s + H_e + H_{int}$, then backward time evolution is governed by $H_b = -H_s + H_e + H_{int}$. Correspondingly, the backward dynamical map $\mathcal{V}_b$ and adjoint dynamical map $\mathcal{V}_b^\dagger$ differ from the forward ones $\mathcal{V}_f = \mathcal{V}$, $\mathcal{V}_f^\dagger = \mathcal{V}^\dagger$ by a minus sign in front of H_s.

This setup is different from the naive time reversal described by $H_b' = -H_f = -(H_s + H_e + H_{int})$. Under the setup of naive time reverse, if the dynamics of the total system is believed to be chaotic, then the expectation is that OTOCs $F(t, A_s, B_s)$ of local operators in subsystem s have the capability to detect the ballistic butterfly light cone. Reference [76] confirms this expectation via investigating the OTOCs of local operators in subsystem s in the random circuit model of composite spins.

In the presence of dissipation, and assuming that the dissipative part of the dynamics cannot be naively reversed, the full protocol now proceeds as follows. Initially the system is prepared with density matrix $\rho_s(0)$. In addition, a control qubit c is initialized in the state $|+\rangle_c = \frac{1}{\sqrt{2}}(|0\rangle_c + |1\rangle_c)$. The total initial state is $\rho_{\text{init}} =$

$\rho_s(0) \otimes |+\rangle\langle+|_c$. The final state is ρ_f after sequentially applying the following super-operators

$$\begin{aligned}
(1): \quad & \mathcal{S}_1 = C(I_s \otimes |0\rangle\langle 0|_c + B_s \otimes |1\rangle\langle 1|_c), \\
(2): \quad & \mathcal{S}_2 = \mathcal{V}_f(t) \otimes \mathcal{I}_c, \\
(3): \quad & \mathcal{S}_3 = C(A_s \otimes I_c), \\
(4): \quad & \mathcal{S}_4 = \mathcal{V}_b(t) \otimes \mathcal{I}_c, \\
(5): \quad & \mathcal{S}_5 = C(B_s \otimes |0\rangle\langle 0|_c + I_s \otimes |1\rangle\langle 1|_c), \\
& \rho_f = \mathcal{S}_5 \cdot \mathcal{S}_4 \cdot \mathcal{S}_3 \cdot \mathcal{S}_2 \cdot \mathcal{S}_1 \cdot \rho_{init},
\end{aligned} \tag{4.11}$$

where $\mathcal{I}$ is the identity super-operator, and the conjugation super-operator is defined by $C(U) \cdot \rho = U\rho U^\dagger$. Finally, we perform the measurement σ_c^x to get the real part of OTOC

$$\begin{aligned}
& F(t, A, B) := \mathrm{tr}(\sigma_c^x \rho_f) \\
& = \Re \ \mathrm{tr}\left(\left(\mathcal{V}_b^\dagger(t) \cdot B_s^\dagger\right) A_s \left(\mathcal{V}_f(t) \cdot \left(B_s \rho_s(0)\right)\right) A_s^\dagger\right).
\end{aligned} \tag{4.12}$$

In this paper, we focus on the case where the initial state of the system is prepared in the equilibrium state at infinite temperature, i.e. $\rho_s(0) = I_s/2^N$ and the unitary operators A_s and B_s are selected as local Pauli operators, for example, $B_s = \sigma_1^z, A_s = \sigma_i^z$.

4.2 Dissipative OTOC corrected for overall decay

In this section, we observe that the information light cone disappears due to the fast overall decay of OTOC in dissipative systems. In order to recover the light cone as much as possible, we propose a corrected OTOC to remove the effect of overall decay due to the information leaking in dissipative systems.

In a quantum system without dissipation, the OTOC $F(t, A, B) = \Re\langle A^\dagger B_b^\dagger(t) A B_b(t)\rangle_{\beta=0}$ has the same capability to reveal the light cones with different time scaling as the operator norm of the commutator $[B_b^\dagger(t), A^\dagger]$ in the Lieb-Robinson bound [41, 42, 55], where $B_b^\dagger(t)$ is the operator $e^{itH_b} B^\dagger e^{-itH_b} = e^{-itH_s} B^\dagger e^{itH_s}$ in the Heisenberg picture. When $t < d_{BA}/v_B$, the support of $B_b^\dagger(t)$ and $A^\dagger$ are approximately disjoint, so $F(t, A, B)$ is almost equal to 1, where d_{BA} is the distance between the local operators A and B and v_B is the butterfly velocity. The OTOC begins to decay [40–44] when the support of $B_b^\dagger(t)$ grows to $A^\dagger$. Furthermore, in chaotic systems, OTOC decays to zero at late time in the thermodynamic limit [40, 43, 49, 51]. As shown in the upper

left panel of FIG. (4.1), the OTOC $F(t, A, B)$ is able to reveal the ballistic light cone of information scrambling.

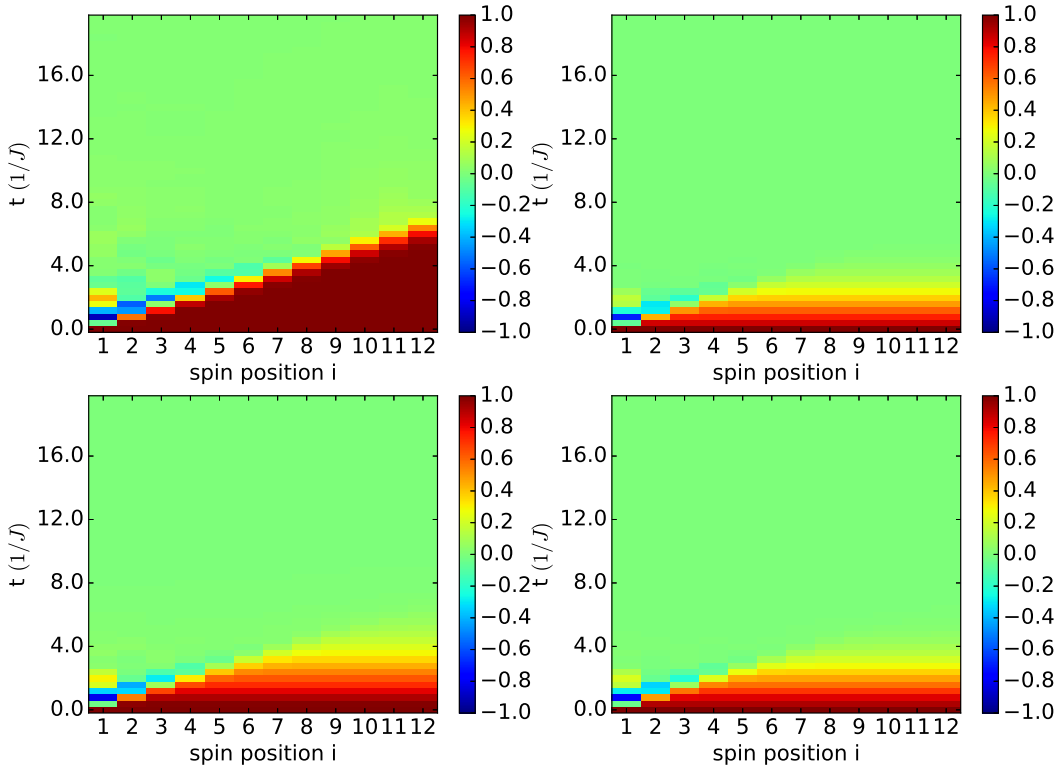

Figure 4.1: OTOC $F(t, \sigma_i^z, \sigma_1^z)$ in the chaotic Ising chain (4.5) with no dissipation (upper left), amplitude damping (upper right), phase damping (lower left), and phase depolarizing (lower right). The dissipation rate is $\Gamma = 0.1$ in these three dissipative channels.

In the presence of dissipation, information is leaking into the environment while being scrambled. Thus $\mathcal{V}_b^\dagger(t) \cdot B^\dagger$ and the OTOC begin to decay when $t > 0$. Intuitively, dissipation destroys the light cone revealed by the OTOC $F(t, A, B)$ because the OTOC decays to zero in a short time which is independent of the spatial distance between local operators A and B. In FIG. (4.1), our numerical calculations confirm that the light cone is destroyed. The OTOC $F(t, \sigma_i^z, \sigma_1^z)$ decays to zero for all i approximately when $t > 4/J$.

In dissipative systems, there are two factors leading to the decay of $F(t, A, B)$: (i) the decay of $\mathcal{V}_b^\dagger(t) \cdot B^\dagger$ related to the information leaking caused by dissipation, and (ii) the non-commutativity between $\mathcal{V}_b^\dagger(t) \cdot B^\dagger$ and $A^\dagger$. Information scrambling is manifested only in (ii), but it might be overshadowed by (i). Is it possible to remove the effect of information leaking and recover the destroyed light cone? One natural

idea is to divide the OTOC $F(t, A, B)$ by a factor representing the decay related to information leaking. The identity operator I commutes with arbitrary operator, and therefore $F(t, I, B)$ is a factor representing the overall decay of quantum information due to leaking only. Therefore, we propose a corrected OTOC to detect the light cone

$$\frac{F(t, A, B)}{F(t, I, B)}. \tag{4.13}$$

The numerical results in FIG. (4.2) show that the corrected OTOC is able to recover the information light cone to some extent in small systems ($N = 12$), with either the dissipation of amplitude damping, phase damping, or phase depolarizing.

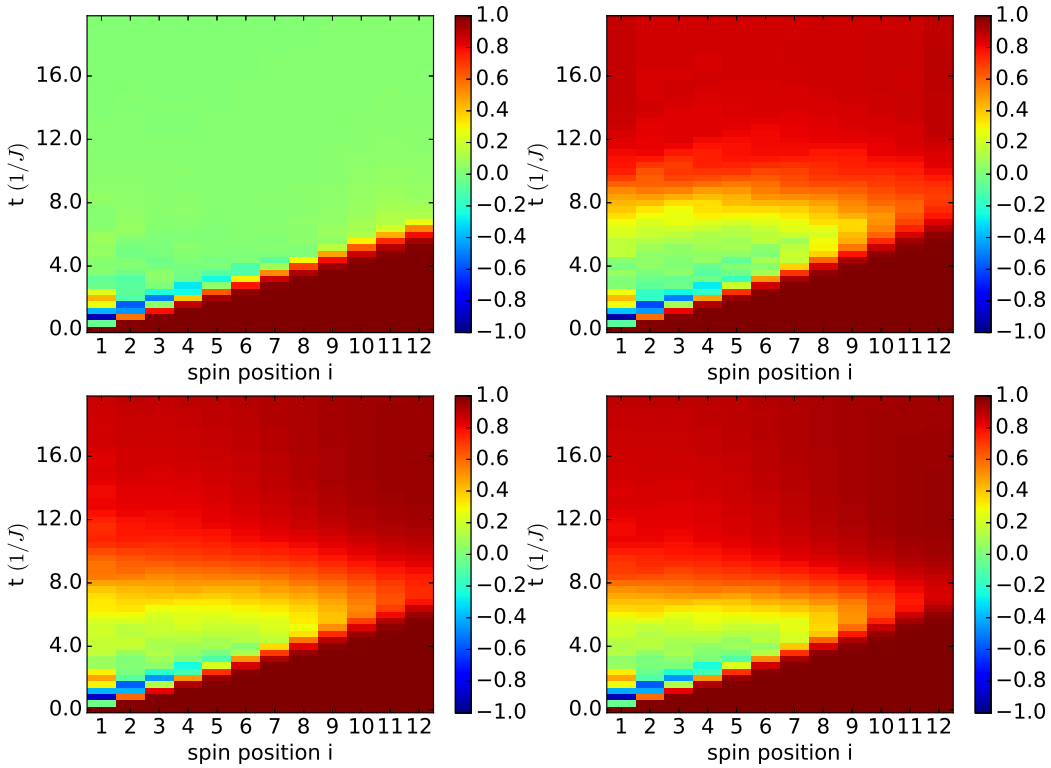

Figure 4.2: Corrected OTOC $F(t, \sigma_i^z, \sigma_1^z)/F(t, I, \sigma_1^z)$ in the chaotic Ising chain (4.5) with no dissipation (upper left), amplitude damping (upper right), phase damping (lower left), and phase depolarizing (lower right). The dissipation rate is $\Gamma = 0.1$ in these three dissipative channels.

For small dissipation rate, does the corrected OTOC have the capability to recover the destroyed light cone in the thermodynamic limit? The answer is no. Due to the limited computational resources, we simulate a relatively large system with 24 spins. FIG. (4.3) shows that the boundary of the light cone revealed by the corrected OTOC

gradually disappears in space. Based on this result, we expect that the corrected OTOC only has a finite extent in the thermodynamic limit.

Here, let us briefly talk about the numerical methods we used. When $N = 12$, quantum toolbox in Python [132, 133] is used to numerically solve the master and adjoint master differential equations [Eqs. (4.6) and (4.10)]. When $N = 24$, our numerical simulations are based on the time-evolving block decimation (TEBD) algorithm after mapping matrix product operators to matrix product states [134–136], which is able to efficiently simulate the evolution of operators or mixed states. In the singular value decomposition, we ignore the singular values s_k if $s_k/s_1 < 10^{-8}$, where s_1 is the maximal one. The bond dimension is enforced as $\chi \leq 500$. Due to the presence of dissipation, the entanglement growth in the matrix product operator is bounded. Therefore, the OTOC can be efficiently calculated using the TEBD algorithm.

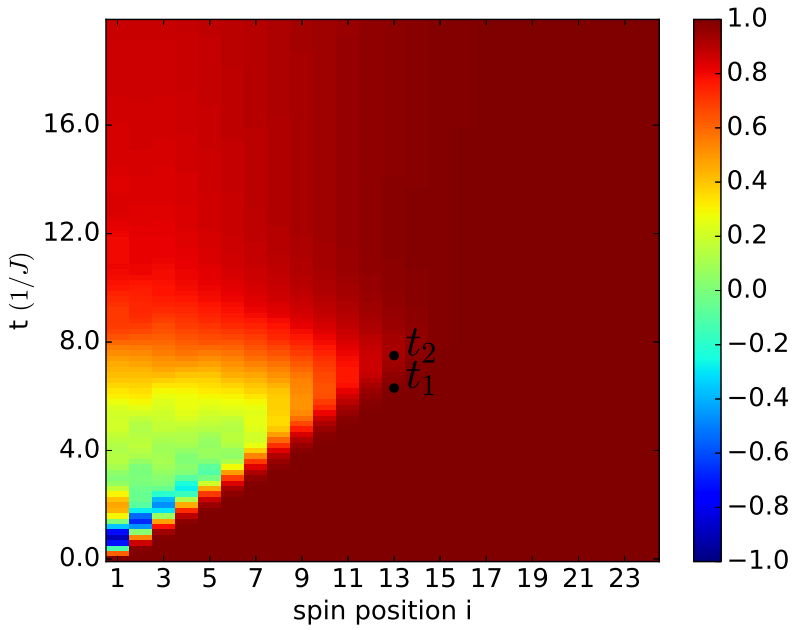

Figure 4.3: Corrected OTOC $F(t, \sigma_i^z, \sigma_1^z)/F(t, I, \sigma_1^z)$ recovers some part of the light cone in the channel of phase depolarizing with dissipation rate $\Gamma = 0.1$ and system size $N = 24$.

4.3 The width of the partially recovered light cone

The finite extent of the light cone revealed by the corrected OTOC indicates that, besides the overall decay of quantum information, dissipation also leads to structural changes in the scrambled information. In this section, we are going to give a qualitative argument as to why and how the structural change happens.

In particular, we find that the re-structuring happens at late time in two aspects: (i) few-body terms dominate when compared with many-body terms, and (ii) at fixed time, the weight of few-body terms decays in space.

Let us define the few-body and many-body terms, and their weights. Consider the operator $B_b^\dagger(t) = \mathcal{V}_b^\dagger(t) \cdot B^\dagger$ which can be written in the basis of products of Pauli matrices as

$$B_b^\dagger(t) = \sum_S b_S(t) S = \sum_{i_1 i_2 \cdots i_N} b_{i_1 i_2 \ldots}(t) \sigma_1^{i_1} \sigma_2^{i_2} \cdots \sigma_N^{i_N}, \tag{4.14}$$

where the Pauli string S is a product of Pauli matrices $\sigma_1^{i_1}\sigma_2^{i_2}\cdots\sigma_N^{i_N}$ with $i_k = 0, x, y,$ or z. In the above decomposition, a few-body (many-body) term is a Pauli string with few (many) non-trivial Pauli matrices. $|b_S(t)|^2 / \sum_{S'} |b_{S'}(t)|^2$ represents the weight of the Pauli string S.

Our qualitative arguments are mainly based on the Suzuki-Trotter expansion of the adjoint propagator in the infinitesimal time steps

$$B_b^\dagger(t+\tau) = \mathcal{V}_b^\dagger(\tau) \cdot B_b^\dagger(t) \approx e^{\mathcal{L}_D^\dagger \tau} \cdot (B_b^\dagger(t) - i\tau[H_s, B_b^\dagger(t)]), \tag{4.15}$$

where $\mathcal{L}_D^\dagger$ is the adjoint super-operator of the dissipation and τ is the infinitesimal time interval. Based on this expression, we are able to qualitatively discuss the operator spreading in the space of operators during the time evolution.

The nearest-neighbor interactions in H_s lead to operator growth in space. If there is no dissipation, every term inside the light cone is expected to have approximately equal weight at late time [51], so $F(t, A, B)$ is approximately equal to zero inside the light cone.

Intuitively, dissipation leads to operator decay. Many-body terms decay at a higher rate than few-body terms, so few-body terms dominate at late time in dissipative systems. In the channel of phase depolarization, $e^{\mathcal{L}_D^\dagger \tau} \cdot \sigma^{k_i} = e^{-\Gamma\tau}\sigma^{k_i} (k_i = x, y, z)$. In one step of evolution, the decaying factors of one-body, two-body and m-body terms are respectively $e^{-\Gamma\tau}$, $e^{-2\Gamma\tau}$, and $e^{-m\Gamma\tau}$. Many-body terms decay faster than few-body terms. Amplitude and phase damping channels have similar behaviors. In the dominating few-body terms, firstly we need to consider one-body terms. Secondly, the nearest-neighbor two-body terms cannot be ignored because the nearest-neighbor interactions in H_s [Eq. (4.15)] transform one-body operators into nearest-neighbor two-body operators. Our simulations support these qualitative arguments. FIG.

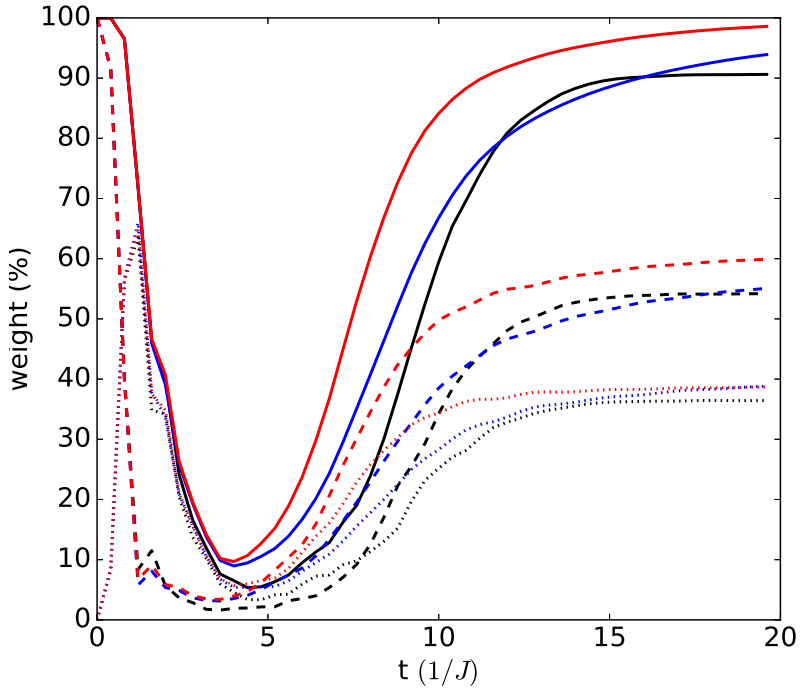

Figure 4.4: Color plot of the weights of few-body terms in the chaotic Ising chain (4.5) with $N = 12$ spins and dissipation rate $\Gamma = 0.1$. Dashed (dotted) line denotes the total weight of one-body (nearest-neighbor two-body) terms in the operator $\mathcal{V}_b^\dagger(t) \cdot \sigma_1^z$, while the solid line is the sum of dotted and dashed lines. Black, blue, and red lines are the results for dissipative channels of amplitude damping, phase damping, and phase depolarizing, respectively.

(4.4) shows that the sum of the weights of one-body and nearest-neighbor two-body terms approximately exceeds 90% at late time in the dissipative channels.

Moreover, because of dissipation, the weight of few-body terms decays in space at the same time. In the time-evolved operator $\mathcal{V}_b^\dagger(t) \cdot \sigma_1^z$, few-body terms on the right are sequentially generated from the ones on the left. For example, one-body term $\sigma_{i+1}^{k_{i+1}}$ is generated via the path $\sigma_i^{k_i} \to \sigma_i^{k_i'} \sigma_{i+1}^{k_{i+1}'} \to \sigma_{i+1}^{k_{i+1}}$, where $k_i, k_i', k_{i+1}', k_{i+1}$ are non-trivial indicies x, y or z. Considering the generating paths and the different decaying rate of few-body terms, we find that extra spatial decaying factor exists when comparing the coefficients of $\sigma_{i+1}^{k_{i+1}}$ and $\sigma_i^{k_i}$. Spacial decaying factors accumulate during the scrambling of information, so the weight of few-body terms decays in space at the same time. In FIG. (4.3), the corrected OTOC $F(t, \sigma_i^z, \sigma_1^z)/F(t, I, \sigma_1^z)$ approaches 1 from left to right at late time t. In the channel of phase depolarizing, $(1 - F(t, \sigma_i^z, \sigma_1^z)/F(t, I, \sigma_1^z))$ is proportional to the weight of few-body terms S_i near site i at late time, i.e. $|b_{S_i}(t)|^2 / \sum_{S'} |b_{S'}(t)|^2$. Thus the numerical result confirms that

the weight of few-body terms decays in space at the same time.

Besides the qualitative discussions, we are going to quantitatively study the relationship between the width $d(\Gamma)$ of the partially recovered light cone and the dissipation rate Γ. Appendix B provides a lower bound $\sqrt{\epsilon a v_{LR}/\Gamma}$, where a is the distance between two nearest neighbor sites, v_{LR} is the Lieb-Robinson velocity and ϵ is a small number. This inequality is shown to be satisfied for the width of the light cone revealed by the corrected OTOC in the channel of phase damping or phase depolarizing. In general, we expect that $d(\Gamma)$ obeys a power law c/Γ^{α} when the dissipation rate Γ is sufficiently small.

Now, we discuss how to find the width $d(\Gamma)$ of the partially recovered light cone in the numerical calculations. Our criterion is that if the difference of corrected OTOCs at $(t_1 = (d_{BA} - w/2)/v_B, d_{BA})$ and $(t_2 = (d_{BA} + w/2)/v_B, d_{BA})$ (see FIG. 4.3) is less than a threshhold value δ, for example 0.1, then it is impossible to recognize the boundary of the light cone and we identify the smallest such d_{BA} as the width of the recovered light cone. Here w is the width of the boundary of the light cone in the system without dissipation and v_B is the corresponding butterfly velocity.

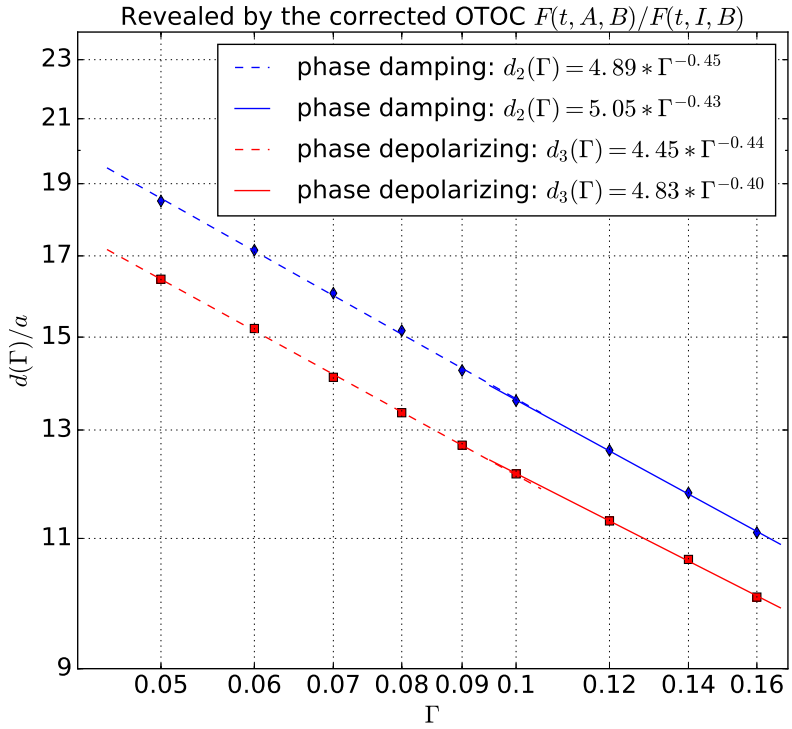

Figure 4.5: The log-log plot of $d(\Gamma)$ and Γ.

Our numerical simulation supports that $d(\Gamma)$ obeys a power law c/Γ^{α}. In FIG.

(4.5), our fitting results are: $\alpha_2 \approx 0.45, \alpha_3 \approx 0.44$ when $0.05 \leq \Gamma \leq 0.1$, and $\alpha_2 \approx 0.43, \alpha_3 \approx 0.40$ when $0.1 \leq \Gamma \leq 0.16$, where the subscripts $2, 3$ represent the channels of phase damping and phase depolarizing respectively. If Γ is sufficiently small, the power-law value c/Γ^{α} is expected to be greater than or equal to the lower bound $\sqrt{\epsilon a v_{LR}/\Gamma}$. This implies that α should be greater than or equal to 0.5. Here in our simulation, α_2 and α_3 are smaller than 0.5. The reason is that the dissipation rates in the range of $[0.05, 0.1]$ are not small enough. Theoretically, the derivations in Appendix B give the condition of sufficiently small Γ via comparing $\sqrt{\epsilon a v_{LR}/\Gamma}$ with ξ. Γ is sufficiently small if it is much less than $\epsilon a v_{LR}/\xi^2$. In this chaotic Ising model, after selecting $\epsilon \sim 0.1$, and estimating the parameters $v_{LR} \sim 2Ja, \xi \sim a$, then we obtain that $\Gamma \ll 0.1$ is sufficiently small. Therefore, our numerical result does not contradict the lower bound proved in Appendix B. Numerically, we see that α decreases when the range of Γ increases.

Even though amplitude damping has different properties when compared with phase damping and phase depolarizing, we numerically verify that $d(\Gamma)$ still scales as a power law of the dissipation rate Γ. In the channel of amplitude damping, the corrected OTOC depends on $\mathcal{V}_b^{\dagger}(t)$ and $\mathcal{V}_f(t)$ which have different properties. The identity is a fixed point of $\mathcal{V}_b^{\dagger}(t)$ while $\mathcal{V}_f(t)$ is trace-preserving. The proof in Appendix B does not apply to amplitude damping, thus the lower bound $\sqrt{\frac{\epsilon a v_{LR}}{\Gamma}}$ does not work for the corrected OTOC in this channel. In the numerical simulation, we confirm that the general expectation of power-law decay is still correct. FIG. (4.6) shows that $d(\Gamma)$ scales as a power law of Γ with the power $\alpha_1 \approx 0.31$ when $0.05 \leq \Gamma \leq 0.1$, where the subscript 1 represents the channel of amplitude damping.

4.4 Lieb-Robinson bound in dissipative systems

Now we would like to discuss the Lieb-Robinson bound and its connections with OTOC in open quantum systems. Based on the observation of corrected OTOC, we conjecture a tighter Lieb-Robinson bound for dissipative systems.

The Lieb-Robinson inequality provides an upper bound for the speed of information propagation in quantum systems with local interactions. Let us briefly review the Lieb-Robinson bound.

Two observers, Alice and Bob, have access to the quantum system. The system is initially in the state $\rho(0)$ and its dynamics is governed by the dynamical map $\mathcal{V}_b(t)$ related to the Hamiltonian $H_b = -H_s + H_e + H_{int}$. The sender Alice has the option to perform some local actions in her region. After some time t, the

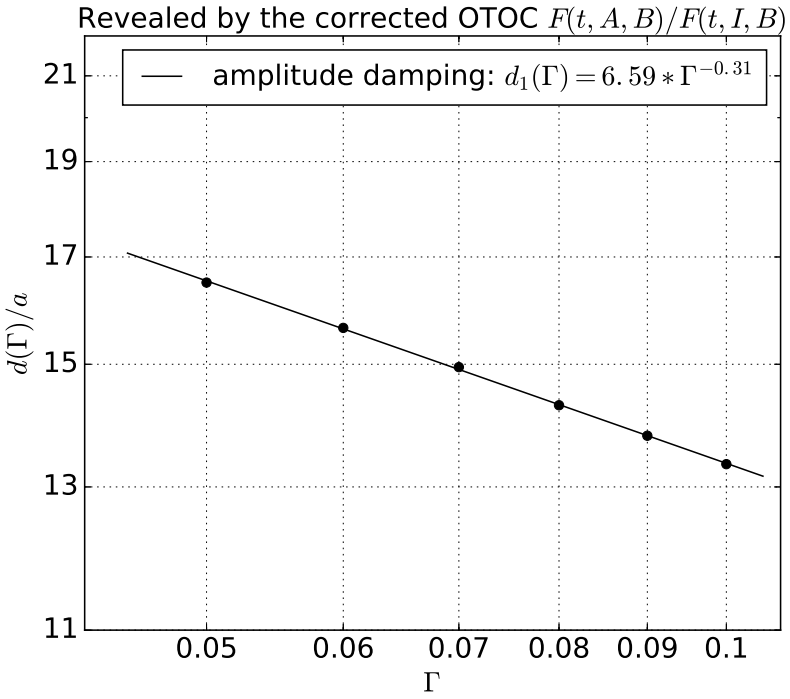

Figure 4.6: The log-log plot of $d(\Gamma)$ and Γ.

receiver Bob performs some measurements to detect the signal. No signal is sent to Bob if Alice does nothing. In order to send a signal, Alice performs a small local unitary perturbation $U_A = e^{-i\epsilon O_A}$ in her region, which maps the state $\rho_s(0)$ to $\rho_s'(0) = U_A \rho_s(0) U_A^\dagger \approx \rho_s(0) - i\epsilon[O_A, \rho_s(0)]$, where O_A is a local Hermitian operator. At time t, Bob makes a measurement described by the local Hermitian operator O_B. The difference of outcomes describing the capability to detect the signal is

$$\begin{aligned} &\left|\mathrm{tr}\left(O_B \mathcal{V}_b(t) \cdot \left(\rho_s'(0) - \rho_s(0)\right)\right)\right| \\ &= \epsilon |\,\mathrm{tr}(\rho_s(0)[\mathcal{V}_b^\dagger(t) \cdot O_B, O_A])| \\ &\leq \epsilon \| \,[\mathcal{V}_b^\dagger(t) \cdot O_B, O_A]\,\|, \end{aligned} \tag{4.16}$$

where the operator norm is defined by $\|O\| = \sup_{|\psi\rangle} \|O|\psi\rangle\|/\||\psi\rangle\|$. Following the Lieb-Robinson bound in closed systems [67–69], an inequality has been proved in open quantum systems [137–142]

$$\| \,[\mathcal{V}_b^\dagger(t) \cdot O_B, O_A]\,\| \leq c\, \|O_A\| \cdot \|O_B\|\, e^{-\frac{d_{BA} - v_{LR} t}{\xi}}, \tag{4.17}$$

where c, ξ are some constants, v_{LR} is the Lieb-Robinson velocity, and d_{BA} is the distance between the local operators O_A and O_B. The Lieb-Robinson velocity v_{LR} is an upper bound for the speed of information propagation, so it is greater than or

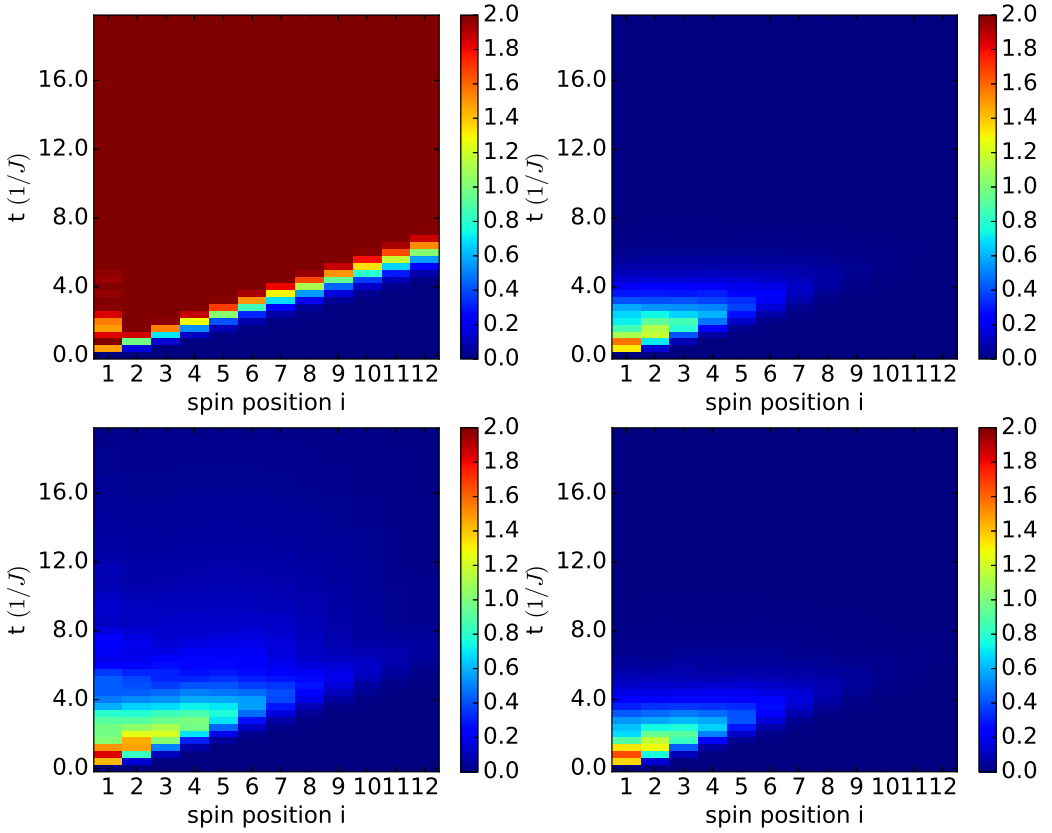

Figure 4.7: The operator norm of the commutator $\| [\mathcal{V}_b^\dagger(t) \cdot \sigma_1^z, \sigma_i^z] \|$ in the chaotic Ising chain (4.5) with no dissipation (upper left), amplitude damping (upper right), phase damping (lower left), and phase depolarizing (lower right). The dissipation rate is $\Gamma = 0.2$ in these three dissipative channels.

equal to the butterfly velocity v_B at $\beta = 0$ in Eq. (4.4) [41]. Refs. [42, 43, 52, 53] provide more discussions about the relationship between v_B and v_{LR}.

In dissipative systems, the left-hand side of Eq. (4.17) decays to zero at late time, so Eq. (4.17) is not tight enough. One reason is that the operator $\mathcal{V}_b^\dagger(t) \cdot O_B$ in the Heisenberg picture is overall decaying because of the dissipation. Ref. [139] has proved that the operator norm of $\mathcal{V}_b^\dagger(t) \cdot O_B$ is non-increasing because of the dissipation, i.e. $\|\mathcal{V}_b^\dagger(t + \mathrm{d}t) \cdot O_B\| \leq \|\mathcal{V}_b^\dagger(t) \cdot O_B\|$, where $\mathrm{d}t$ is an infinitesimal time step. This means that the non-trivial elements in the time-evolved operator are decaying during the time evolution. Our numerical simulations (FIG. 4.7) show that the left-hand side of Eq. (4.17) decays to zero at late time, and the boundary of the light cone gradually disappears when the distance d_{BA} increases.

Inspired by the corrected OTOC, we conjecture a tighter Lieb-Robinson bound in

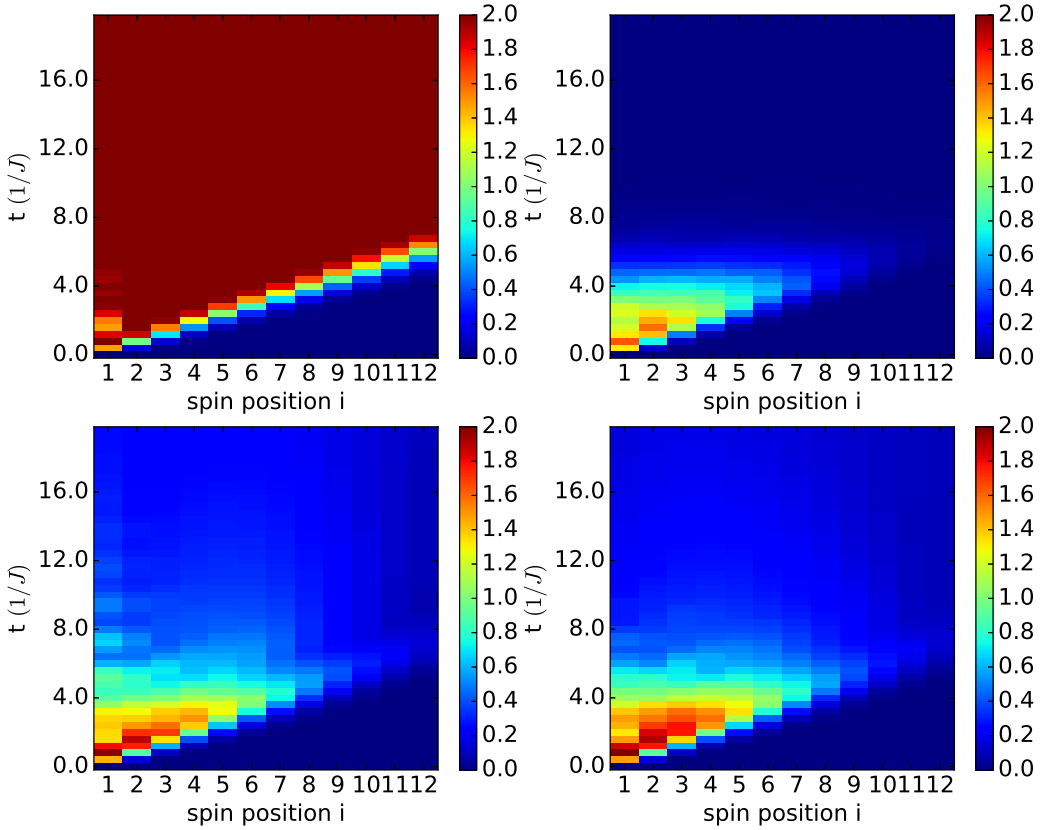

Figure 4.8: The corrected operator norm of the commutator $\| [\mathcal{V}_b^\dagger(t) \cdot \sigma_1^z, \sigma_i^z] \| / \| \mathcal{V}_b^\dagger(t) \cdot \sigma_1^z \|$ in the chaotic Ising chain (4.5) with no dissipation (upper left), amplitude damping (upper right), phase damping (lower left), and phase depolarizing (lower right). The dissipation rate is $\Gamma = 0.2$ in these three dissipative channels.

dissipative systems

$$\frac{\| [\mathcal{V}_b^\dagger(t) \cdot O_B, O_A] \|}{\|O_A\| \cdot \|\mathcal{V}_b^\dagger(t) \cdot O_B\|} \leq c\, e^{-\frac{d_{AB} - v_{LR} t}{\xi}}, \tag{4.18}$$

The above tighter bound has deep connections with the corrected OTOC. In the channel of phase damping or phase depolarizing, the adjoint dynamical map $\mathcal{V}_b^\dagger(t)$ is exactly equal to $\mathcal{V}_f(t)$. Then $2\left(1 - \frac{F(t,O_A,O_B)}{F(t,I,O_B)}\right) = \frac{\| [\mathcal{V}_b^\dagger(t) \cdot O_B, O_A] \|_F^2}{\|\mathcal{V}_b^\dagger(t) \cdot O_B\|_F^2}$ holds when the observables are also unitary, where $\|O\|_F = \sqrt{\mathrm{tr}(OO^\dagger)/2^N}$ is the normalized Frobenius norm of the operator O. We expect that the normalized Frobenius and operator norms exhibit similar behaviors during the time evolution. Based on this expectation, Eq. (4.18) is conjectured in dissipative systems via changing the normalized Frobenius norm to the operator norm. Similar to the corrected OTOC,

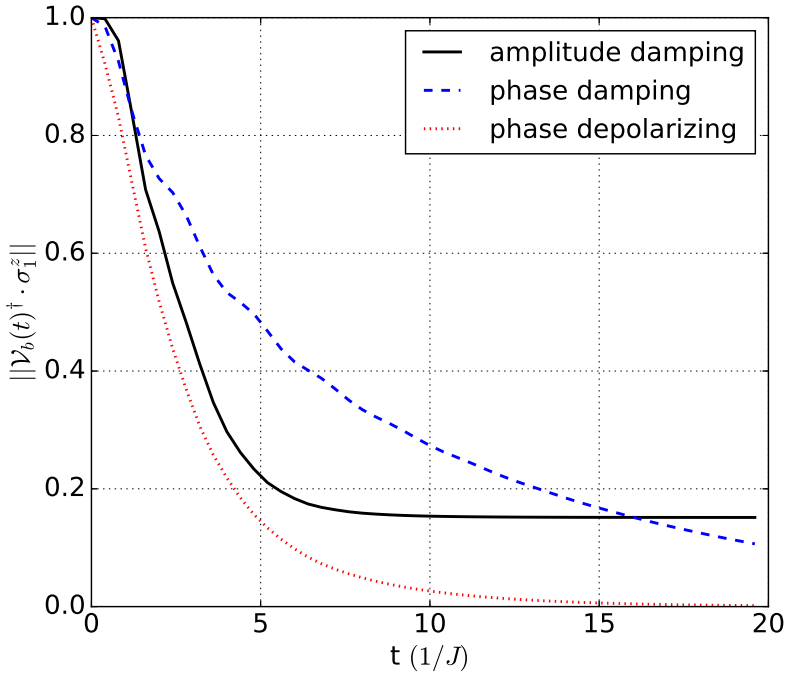

Figure 4.9: The decay of the operator norm $\|\mathcal{V}_b^\dagger(t) \cdot \sigma_1^z\|$ in different dissipative channels ($N = 12, \Gamma = 0.2$).

the left-hand side of the above modified version of the Lieb-Robinson bound is able to partially recover the destroyed light cone in the chaotic Ising chain with dissipation (see FIG. 4.8).

In the above tighter Lieb-Robinson bound, the correcting factor $1/\|\mathcal{V}_b^\dagger(t) \cdot O_B\|$ has different behaviors in different dissipative channels. $\|\mathcal{V}_b^\dagger(t) \cdot O_B\|$ decays to zero in the channel of phase damping or phase depolarizing, but converges to a positive constant in the channel of amplitude damping (see FIG. 4.9). In the channel of amplitude damping, the adjoint dynamical map $\mathcal{V}_b^\dagger(t)$ does not preserve the trace of an operator, the identity operator I appears in the decomposition of $\mathcal{V}_b^\dagger(t) \cdot O_B$ in terms of Pauli operators when O_B is traceless. Therefore, the operator norm of $\mathcal{V}_b^\dagger(t) \cdot O_B$ converges to a constant. This can also be observed in the upper right panel of FIG. (4.8) which is distinct from the lower ones. The operator norm of the commutator is decaying to zero while the denominator converges to a positive constant when $t > 7/J$. In the channel of amplitude damping, the correcting factor $1/\|\mathcal{V}_b^\dagger(t) \cdot O_B\|$ does not play an essential role to remove the effect of overall decay due to the information leaking.

4.5 Conclusion and discussion

In this paper, we study the effect of dissipation on information scrambling in open chaotic systems. By numerically calculating the measured OTOC signal in a chaotic spin chain in the presence of common types of dissipation, we find that dissipation leads to the decay of the signal not only due to information leaking, but also information re-structuring. We define a corrected OTOC to remove the effect of leaking and partially recover the information light cone. However, due to the re-structuring, the recovered light cone only persists to a finite distance. Based on this understanding of how dissipation affects information scrambling, we conjecture a tighter version of the Lieb-Robinson bound in open systems, which we support with numerical simulation.

As our study focuses on the overall shape of the light cone in OTOC and how it changes with dissipation, we do not expect the result to depend on model parameters either. The existence of a linear light cone shows up in both integrable and non-integrable systems [143]. For example, Ref. [63] studied the OTOC in an integrable Ising chain and found a linear shaped light cone just like in the random circuit model case [73, 74]. Some details of the light cone might differ, for example, the broadening of the wave front or the late time value of the OTOC. But if we focus on the shape of the light cone, there is no intrinsic difference between the integrable and the non-integrable case.

Given the observation we made in this paper, several open questions would be interesting to explore in future work. First, we qualitatively discussed the information re-structuring during scrambling. A more accurate estimation of the size of the light cone may be obtained by carefully modeling the dynamics as dissipative quantum walks. Secondly, although we were able to partially recover the light cone numerically, this is not practical experimentally, as the normalization factor we divide out in Eq. (4.13) decays exponentially in time and quickly becomes too small to be accessible experimentally. Is there a better way to see information scrambling in the presence of dissipation? Are there quantities which are also sensitive to information scrambling as OTOC, but more robust to the effect of dissipation? This is an important question to be addressed in future work. Finally, we conjectured the modified version of open system Lieb-Robinson bound based on numerical observation. It would be nice to see if this bound can be analytically proved.

Recently, we learned of the work by Swingle and Yunger Halpern [144] which also studies the problem of extracting OTOCs' early-time dynamics in the presence of

error and decoherence.

Chapter 5

ASYMMETRIC INFORMATION SCRAMBLING IN 2-LOCAL HAMILTONIANS

Understanding the quantum dynamics of thermalization in isolated many-body systems is a topic of central interest. While memory of a system's initial conditions is always preserved under unitary dynamics, this information can get "scrambled" and become inaccessible to local measurements, thereby enabling *local* subsystems to reach thermal equilibrium [4–6, 18]. This scrambling can be quantified by studying the spatial spreading of initially local operators under Heisenberg time evolution. Under dynamics governed by a local time-independent Hamiltonian H, an initially local operator near the origin, A_0, evolves into $A_0(t) = e^{iHt}A_0e^{-iHt}$. As $A_0(t)$ spreads in space, it starts to overlap with local operators B_x at spatially separated locations x. The effect of scrambling is thus manifested in the non-commutation between $A_0(t)$ and B_x, which can be quantified via an out-of-time-ordered correlator (OTOC): [34–61, 80, 85–87, 100, 122–129, 144–151]

$$\begin{aligned} C(x,t) &= \mathfrak{R}\langle A_0^\dagger(t)B_x^\dagger A_0(t)B_x\rangle \\ &= 1 - \frac{1}{2}\langle [A_0(t),B_x]^\dagger[A_0(t),B_x]\rangle, \end{aligned} \tag{5.1}$$

where A_0, B_x are local unitary operators, $\mathfrak{R}$ represents the real part, and the expectation value $\langle\rangle$ is with respect to the infinite temperature thermal ensemble.

The OTOC is expected to exhibit the following features in systems with scrambling dynamics [10, 35, 36, 40, 47, 64, 70–78, 81, 110, 145, 147, 152, 153]: At early times, $A_0(t)$ approximately commutes with B_x and the OTOC is nearly equal to one. At late times, $A_0(t)$ becomes highly non-local and spreads across the entire system, and the OTOC decays to zero [40, 43, 49, 51]. At intermediate times, the operator has most of its support within a region around the origin defined by left and right operator "fronts" that propagate outwards, and generically also broaden in time [73, 74]. As the operator front approaches and passes x, the OTOC $C(x,t)$ decays from nearly one to zero. We will restrict ourselves to translationally invariant systems where operators spread ballistically with a butterfly speed v_B, which is similar in spirit to the Lieb-Robinson speed [67] characterizing the speed of information propagation. In these cases, the operator fronts define a "light-cone" within which the OTOC is nearly zero.

A set of recent papers illustrated that the butterfly velocity can depend on the direction of information spreading [154, 155]. In one dimension, the asymmetry between the different directions can be quantified by the butterfly speeds v_B^r and v_B^l, where the superscript r (l) represent propagation directions to the right (left). While Ref. [154] showed how this asymmetry could be induced by anyonic particle statistics, Ref. [155] constructed models of asymmetric unitary circuits, and Hamiltonians inspired from such circuits.

In this work [156], we present a complementary and physically transparent way for constructing a family of Hamiltonians with asymmetric information propagation. Our construction does not rely on particle statistics, nor is it inspired by unitary circuits. Instead, we start with non-interacting integrable spin 1/2 models where the butterfly speed is related to quasiparticle propagation velocities and can be analytically calculated [63, 77, 78, 143]. We show how the butterfly speed can be made asymmetric in such models, before generalizing to non-integrable Hamiltonians by adding interactions.

5.1 Integrable Hamiltonians

In this section, we construct time-independent integrable Hamiltonians for spin 1/2 degrees of freedom living on an infinite one dimensional lattice. The Hamiltonians only have local terms acting on 2 spins at a time. These models are exactly solvable, so the butterfly velocities can be analytically calculated, and demonstrated to be asymmetric. This family of Hamiltonians parameterized by λ takes the form:

$$H_\lambda = -\frac{J(1-\lambda)}{2}\sum_j \left[h_{yz}\sigma_j^y\sigma_{j+1}^z + h_{zy}\sigma_j^z\sigma_{j+1}^y\right] \\ \frac{-J\lambda}{2}\sum_j \left[h_{zz}\sigma_j^z\sigma_{j+1}^z + h_x\sigma_j^x\right], \tag{5.2}$$

where $\sigma_j^x, \sigma_j^y, \sigma_j^z$ are the Pauli spin 1/2 operators located at site j, $J > 0, h_{zz}, h_x, h_{yz}, h_{zy}$ are constants, and the parameter λ lies in the range $[0, 1]$. This model can be mapped to a system of free fermions via a Jordan-Wigner representation. When $\lambda = 1$, the Hamiltonian is the well-known transverse Ising model with inversion symmetry about the center of the chain. On the other hand, for $\lambda < 1$, the Hamiltonian does not have inversion symmetry when $h_{yz} \neq h_{zy}$.

In order to detect the ballistic light cone and asymmetric butterfly velocities, we consider the OTOCs

$$C_{\mu\nu}(j,t) = \Re\langle\sigma_0^\mu(t)\sigma_j^\nu\sigma_0^\mu(t)\sigma_j^\nu\rangle_{\beta=0}, \tag{5.3}$$

where $\mu, \nu \in \{x, y, z\}$ and $\beta = 0$ represents the infinite temperature thermal state. We note that the mapping to free fermions allows Pauli operators to be written in terms of Majorana fermion operators which, in turn, allows an exact calculation of the OTOC (Appendix C). These OTOCs are shown in FIG. (5.1). For the case of $\lambda = 0$, the right and left butterfly velocities are equal to each other despite the lack of inversion symmetry (upper panel). For $\lambda = 1$, the Hamiltonian H_1 is the well-known Ising model and butterfly velocities are symmetric, as shown in the middle panel of FIG. 5.1. By contrast, for the general case $\lambda \in (0, 1)$, the Hamiltonian does not have inversion symmetry and the OTOCs show asymmetric butterfly velocities (lower panel).

The asymmetry in butterfly speeds for $0 < \lambda < 1$ can be directly understood using the quasiparticle description of the free model. It is known that the butterfly speed in an integrable model is the maximum quasiparticle group velocity [77, 78, 143], and the operator fronts generically broaden either diffusively or sub-diffusively depending on whether the integrable system is interacting or not [143].

The quasi-particle dispersion for the Hamiltonian in Eq. (5.2) is $\epsilon_{\lambda,1(2)}(q) = J\Big[(1-\lambda)(h_{yz}-h_{zy})\sin q + (-)\big((1-\lambda)^2(h_{yz}+h_{zy})^2\sin^2 q + \lambda^2(h_{zz}^2+h_x^2-2h_{zz}h_x\cos q)\big)^{1/2}\Big]$. The butterfly speed to the right (left) is the magnitude of the maximal (minimal) quasi-particle group velocity [77, 78, 143]

$$v^r_{B,\lambda} = \max_q \frac{d\epsilon_{\lambda,1(2)}(q)}{dq},\ v^l_{B,\lambda} = -\min_q \frac{d\epsilon_{\lambda,1(2)}(q)}{dq}. \tag{5.4}$$

These are plotted in FIG. (5.2), where asymmetric butterfly velocities are clearly observed when λ is $\in (0, 1)$. For the special cases of $\lambda = 0$ and $\lambda = 1$, the right and left butterfly speeds are the same

$$v^r_{B,0} = v^l_{B,0} = 2J\max(|h_{yz}|, |h_{zy}|), \tag{5.5}$$

$$v^r_{B,1} = v^l_{B,1} = J\min(|h_{zz}|, |h_x|). \tag{5.6}$$

The above results are consistent with the butterfly velocities demonstrated via the out-of-time-ordered correlations shown in FIG. (5.1).

5.2 Non-integrable Hamiltonians

In this section, we construct a non-integrable Hamiltonian by adding longitudinal fields to the free Hamiltonian H_λ [10, 110]. The asymmetric butterfly velocities are estimated from a variety of measures including out-of-time-ordered correlations, right/left weight of time-evolved operators, and operator entanglement.

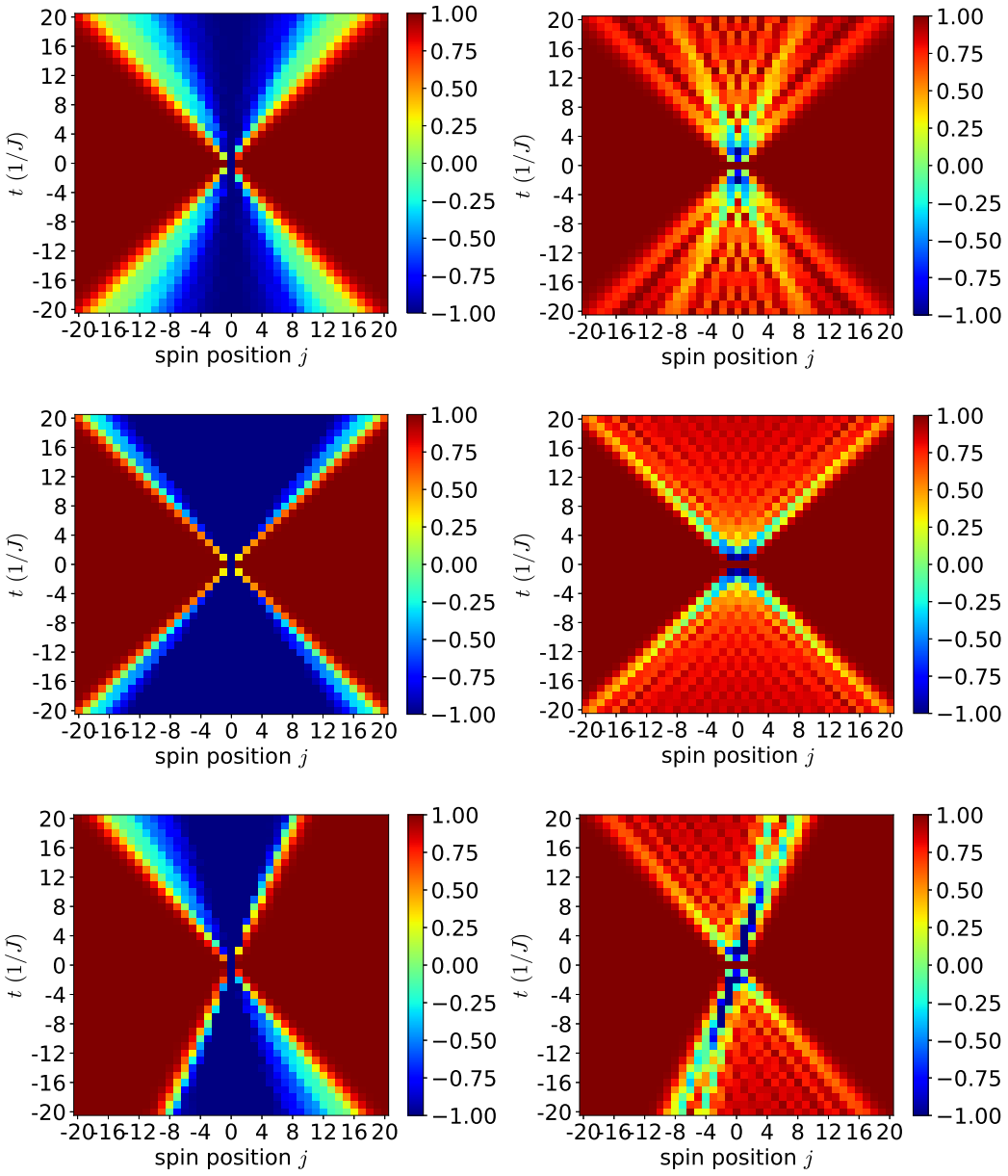

Figure 5.1: OTOCs $C_{xz}(j,t)$ (upper panel) and $C_{xx}(j,t)$ (lower panel) in the Hamiltonian H_λ [Eq. (5.2)] with parameters $h_{yz} = 0.5, h_{zy} = -0.25, h_{zz} = 1.0, h_x = -1.05$, and $\lambda = 0$ in the upper panel, $\lambda = 1$ in the middle panel, and $\lambda = 0.5$ in the lower panel. The asymmetric light-cone is clear in the lower panel.

The interacting Hamiltonian on a one-dimensional lattice with open boundary con-

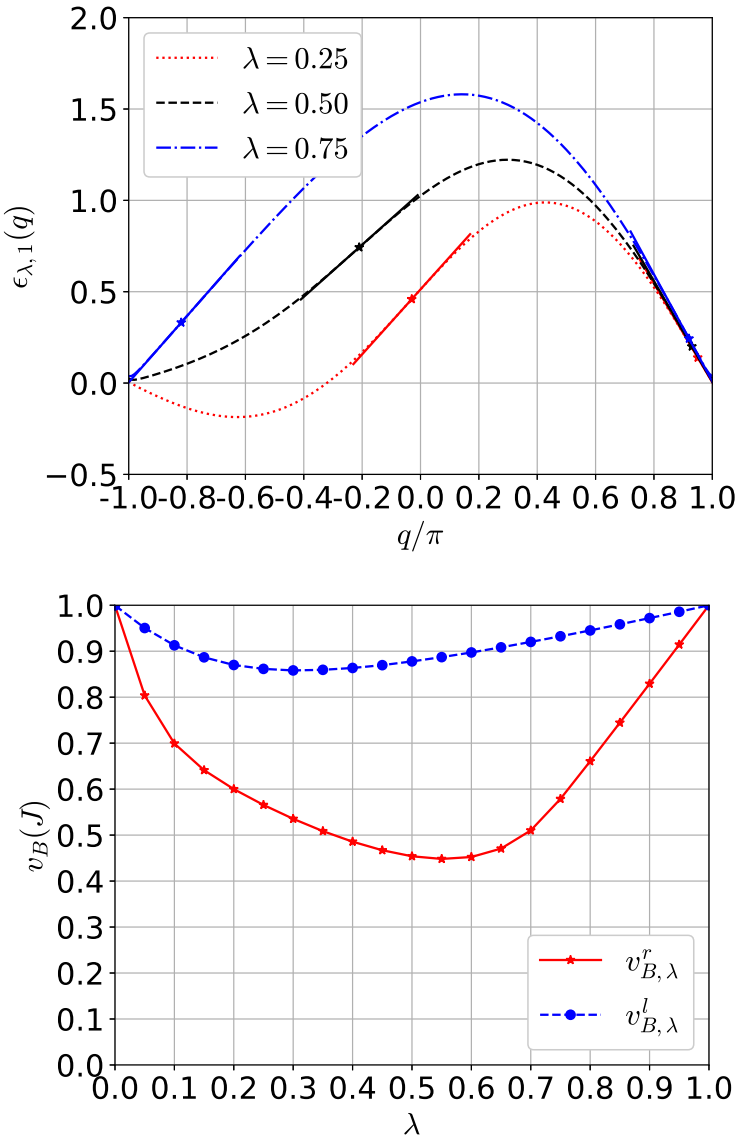

Figure 5.2: Quasi-particle dispersion relations $\epsilon_{\lambda,1}(q)$ (upper panel) and asymmetric butterfly speeds (right panel) for the Hamiltonian H_λ [Eq. (5.2)]. The parameters used are $h_{yz} = 0.5, h_{zy} = -0.25, h_{zz} = 1.0, h_x = -1.05$. In the lower panel, the star $\star$ denotes the place where the dispersion relation has maximal or minimal slope, and the solid lines represent the slope. In the right panel, asymmetric butterfly speeds are directly determined from the quasi-particle dispersion relations [Eq. (5.4)].

ditions is

$$H = \frac{-J(1-\lambda)}{2}\sum_{j=1}^{L-1}\left[h_{yz}\sigma_j^y\sigma_{j+1}^z + h_{zy}\sigma_j^z\sigma_{j+1}^y\right]$$
$$+ \frac{-J\lambda}{2}\left[h_{zz}\sum_{j=1}^{L-1}\sigma_j^z\sigma_{j+1}^z + \sum_{j=1}^{L}h_x\sigma_j^x\right] - \frac{J}{2}\left[\sum_{j=1}^{L}h_z\sigma_j^z\right], \tag{5.7}$$

where L is the system size, and h_z is a longitudinal field strength. We select the particular parameters $\lambda = 0.5, h_{yz} = 0.5, h_{zy} = -0.25, h_{zz} = 1.0, h_x = -1.05, h_z = 0.5$, although none of our results are fine tuned to this choice.

The longitudinal field breaks integrability and is expected to thermalize the system. For non-integrable Hamiltonians with thermalizing dynamics, the level statistics is consistent with the distribution of level spacings in random matrix ensembles [79]. Let $E_0 < \cdots < E_n < E_{n+1} < \cdots$ be the sequence of ordered energy eigenvalues and $s_n = (E_{n+1} - E_n)$ be the level spacings. One defines the ratio of consecutive level spacings $r_n = s_n/s_{n-1}$, and the distribution of r_n can be described by the Wigner-like surmises for non-integrable systems [13, 157]

$$p_W(r) = \frac{1}{Z_W} \frac{(r + r^2)^W}{(1 + r + r^2)^{1+3W/2}}, \tag{5.8}$$

where $W = 1, Z_1 = 8/27$ for Gaussian Orthogonal Ensemble (GOE), and $W = 2, Z_2 = 4\pi/(81\sqrt{3})$ for Gaussian Unitary Ensemble (GUE), while they are Poissonian for integrable systems. As shown in FIG. (5.3), the ratio distribution provides evidence supporting the non-integrability of the Hamiltonian. When $\lambda = 0.5$, the Hamiltonian is complex Hermitian, and its ratio distribution agrees with the Gaussian Unitary Ensemble (GUE). When $\lambda = 1$, the Hamiltonian is real, symmetric and has the inversion symmetry with respect to its center, and its level statistics in the sector with even parity agrees with the Gaussian Orthogonal Ensemble (GOE) [10, 110].

We now characterize the asymmetric spreading of quantum information in this model using a variety of different diagnostics that were discussed in [155].

Asymmetric butterfly velocities from OTOCs

In this subsection, we estimate the asymmetric butterfly velocities from OTOCs.

As discussed earlier, as the time-evolved operator spreads ballistically, OTOCs can detect the light cone and butterfly velocities. The saturated value of OTOCs equals approximately one outside the ballistic light cone and zero inside it. Near the boundary of the light cone, the OTOCs decay in a universal form $C(j,t) = 1 - f\, e^{-c(j-v_B t)^\alpha / t^{\alpha-1}}$ [77, 78], where c, f are constants, v_B describes the speed of operator spreading, and α controls the broadening of the operator fronts. In a generic "strongly quantum" system (*i.e.* away from large N/ semiclassical/weak coupling limits) the operator front shows broadening which corresponds to $\alpha > 1$ so that the OTOC is not a simple exponential in t [78].

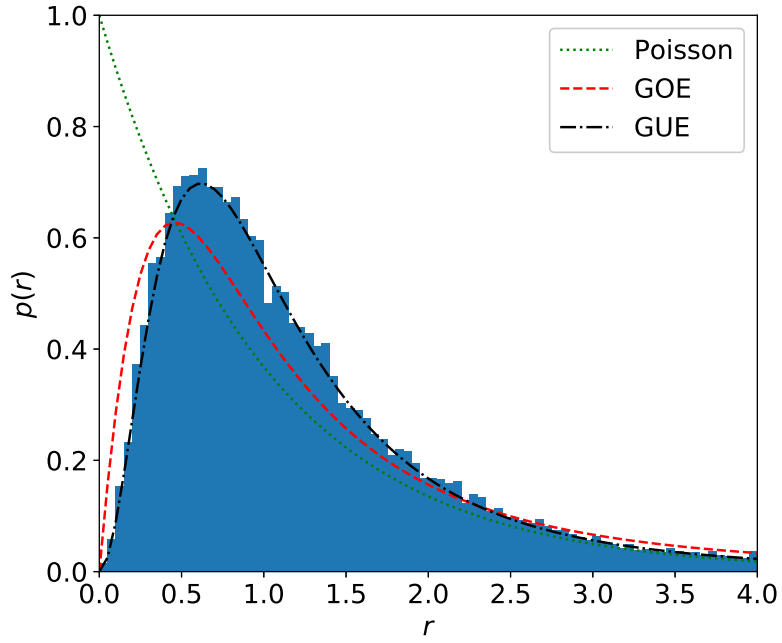

Figure 5.3: The histogram of the ratio of consecutive level spacings. It is computed from 32768 all energy eigenvalues of the Hamiltonian [Eq. (5.7)] with parameters $\lambda = 0.5, h_{yz} = 0.5, h_{zy} = -0.25, h_{zz} = 1.0, h_x = -1.05, h_z = 0.5$, and length $L = 15$.

Nevertheless, the decay can still look exponential along rays $j = vt$ in space-time, $C(j = vt, t) = 1 - f\, e^{\lambda(v)t}$, defining velocity-dependent Lyapunov exponents (VDLEs) which look like $\lambda(v) \sim -c(v - v_B)^{\alpha}$ near v_B [78]. The VDLEs provide more information about the operator spreading than the butterfly velocities alone.

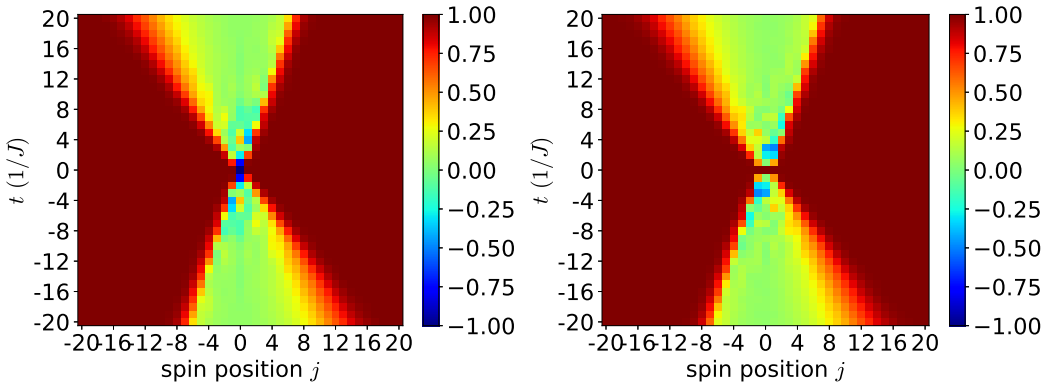

Figure 5.4: OTOCs $C_{xz}(j,t)$ (left panel) and $C_{xx}(j,t)$ (right panel) in the Hamiltonian H [Eq. (5.7)] with parameters $\lambda = 0.5, h_{yz} = 0.5, h_{zy} = -0.25, h_{zz} = 1.0, h_x = -1.05, h_z = 0.5$, and length $L = 41$.

First, as shown in FIG. (5.4), we observe asymmetric butterfly velocities in rela-

tively large systems with $L = 41$ spins. In our numerical calculations, we use the time-evolving block decimation (TEBD) algorithm after mapping matrix product operators to matrix product states [134–136], which is able to efficiently simulate the evolution of operators in the Heisenberg picture. The OTOCs shown in FIG. (5.4) clearly demonstrate asymmetric butterfly velocities.

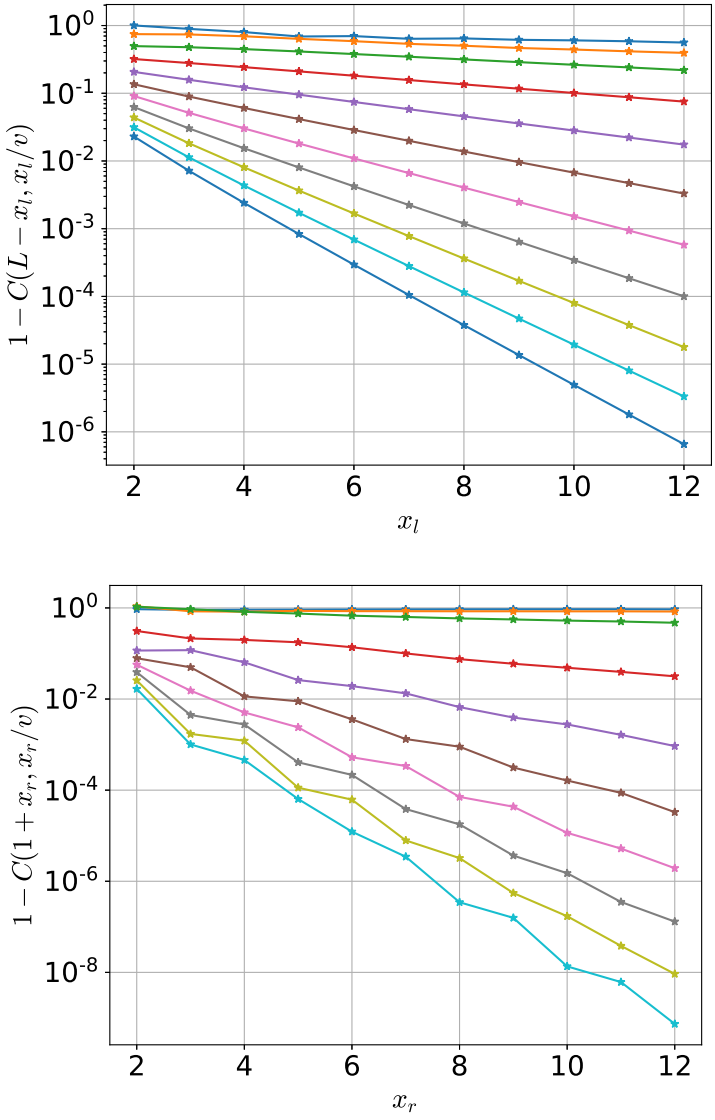

Figure 5.5: OTOCs in the Hamiltonian H [Eq. (5.7)] with parameters $\lambda = 0.5, h_{yz} = 0.5, h_{zy} = -0.25, h_{zz} = 1.0, h_x = -1.05, h_z = 0.5$, and length $L = 14$. The upper (lower) panel shows the left (right) propagating OTOCs along rays at different velocities. Exponential decay can be observed which is consistent with the negative VDLEs for large v.

Second, we estimate the asymmetric butterfly velocities from the extracted VDLEs

$\lambda(v) \sim -c(v - v_B)^\alpha$. Because of the limited computational resources for exact diagonalization, the right and left butterfly velocities are measured by setting the initial local operator at the boundary $j = 1$ and $j = L$, respectively. In FIG. (5.5), the OTOCs exponentially decay along the rays with different speed

$$C(1 + x_r, x_r/v) = \langle \sigma_1^x(x_r/v)\sigma_{1+x_r}^z \sigma_1^x(x_r/v)\sigma_{1+x_r}^z \rangle_{\beta=0}, \tag{5.9}$$

$$C(L - x_l, x_l/v) = \langle \sigma_L^x(x_l/v)\sigma_{L-x_l}^z \sigma_L^x(x_l/v)\sigma_{L-x_l}^z \rangle_{\beta=0}. \tag{5.10}$$

For a given velocity v, $\lambda(v)/v$ is the slope of logarithm of the left and right propagating OTOCs versus the distance x. After extracting the VDLEs $\lambda(v)$ from the OTOCs, here we give a rough estimation of the butterfly velocities via fitting the curve $\lambda(v) \sim -c(v - v_B)^\alpha$. In FIG. (5.6), we obtain the results $v_B^r \sim 0.29J$ and $v_B^l \sim 0.66J$.

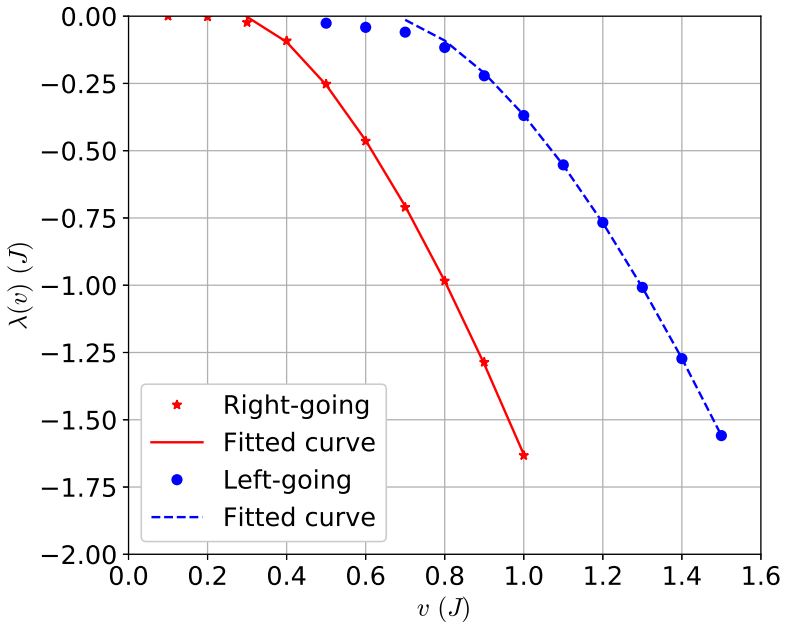

Figure 5.6: VDLEs fitted from the left and right propagating OTOCs in FIG. (5.5) with the slope equaling $\lambda(v)/v$. The parameters c, v_B, α can be fitted via the least square method. Here the results of fitting the last 7 points are $v_B^r \sim 0.29J, \alpha^r \sim 1.52$, and $v_B^l \sim 0.66J, \alpha^l \sim 1.61$.

Asymmetric butterfly velocities from right/left weights

Now we turn to the analysis of asymmetric butterfly velocities directly measured from right and left weights of the spacial spreading operators.

To define the right/left weight, note that every operator in a spin 1/2 system with length L can be written in the complete orthogonal basis of 4^L Pauli strings $S =$

$\otimes_{j=1}^{L} S_j$, i.e. $O(t) = \sum_S a_S(t)S$, where $S_j = I, \sigma^x, \sigma^y$ or σ^z. Unitary evolution preserves the norm of operators, so $\sum_S |a_S(t)|^2 = 1$ holds for a normalized operator. The information of operator spreading is contained in the coefficients $a_S(t)$. In order to describe the spatial spreading, the right weight is defined by

$$\rho_r(j,t) = \sum_{S:S_j \neq I, S_{j'>j}=I} |a_S(t)|^2, \tag{5.11}$$

where the left weight is defined analogously. Because of the conservation of operator norm $\sum_j \rho_{r(l)}(j,t) = 1$, the weight can be interpreted as an emergent local conserved density for the right/left fronts of the spreading operator.

Recent studies [73–76] showed that the hydrodynamics for the right/left weight can be characterized by a biased diffusion equation in non-integrable systems, which means that the front is ballistically propagating with diffusively broadening width. Thus, when the time-evolved operator spreads, ρ_r moves to the right with velocity v_B^r, and ρ_l moves to the left with velocity v_B^l.

Here in the numerical calculations of exact diagnolization, the right and left weights are obtained by setting the initial local operator at the boundary $j = 1$ and $j = L$, respectively. The right weight $\rho_r(1 + x_r, t)$ of $\sigma_1^x(t)$ is calculated in order to compare the left weight $\rho_l(L - x_l, t)$ of $\sigma_L^x(t)$, where $x_r(x_l)$ is the distance between the right (left) end and the location of initial operator. As shown in FIG. (5.7), the estimated velocities are $v_B^r \sim 0.34J$ and $v_B^l \sim 0.77J$ by fitting the times when the weights reach half of the maximum peak for given distances.

Asymmetric butterfly velocities from the operator entanglement growth

In this subsection, the growth of operator entanglement is investigated to estimate the asymmetric butterfly velocities.

The entanglement of time-evolved operators encodes information about its spatial spreading. Refs. [155, 158] discussed a coarse-grained hydrodynamic description for the entanglement dynamics of a spreading operator under Heisenberg time evolution. Let $\hat{S}(t,x)$ be the operator entanglement across bond x at time t. To leading order, its growth depends on the local entanglement gradient

$$\frac{\partial \hat{S}}{\partial t} = 2s_{eq}\Gamma\Big(\frac{1}{2}\frac{\partial \hat{S}}{\partial x}\Big), \tag{5.12}$$

where s_{eq} is the equilibrium entropy density at infinite temperature, and $\Gamma(s)$ is a non-negative growth function. Let us discuss the properties of the growth function

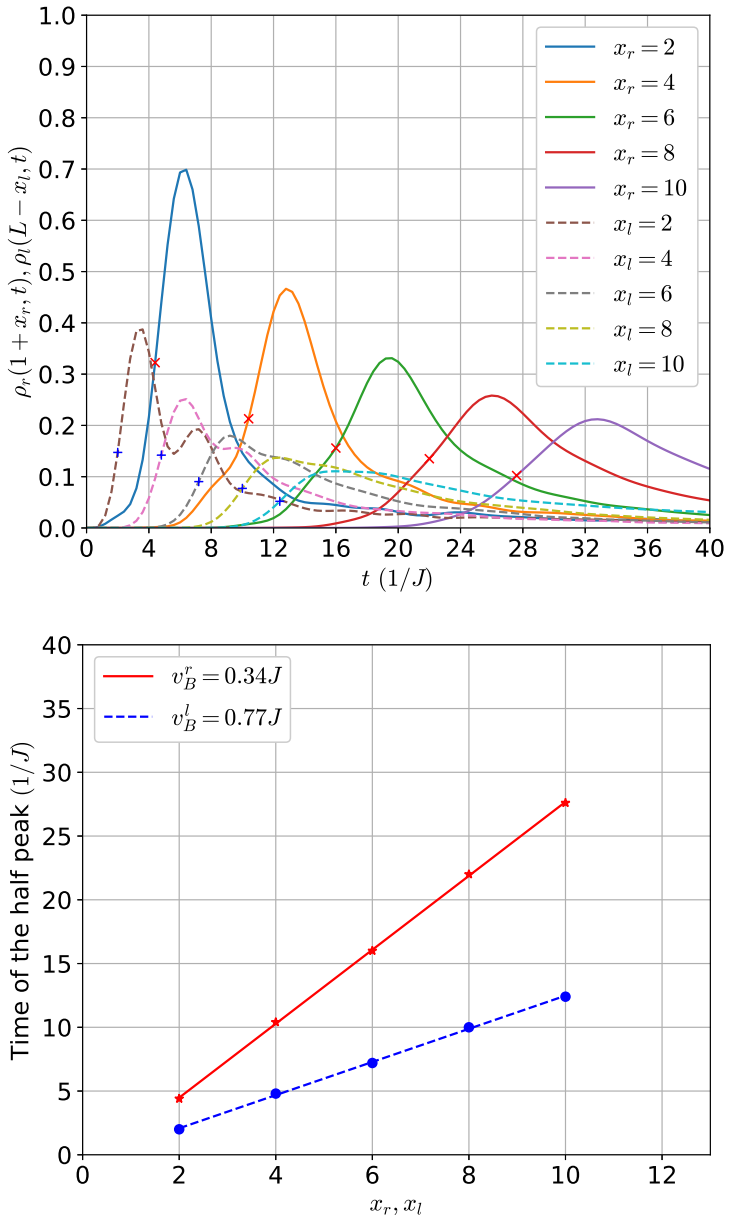

Figure 5.7: Upper panel: the right weights (solid lines) of $\sigma_1^x(t)$ and the left weights (dashed lines) of $\sigma_L^x(t)$. The parameters in the Hamiltonian H [Eq. (5.7)] are $\lambda = 0.5, h_{yz} = 0.5, h_{zy} = -0.25, h_{zz} = 1.0, h_x = -1.05, h_z = 0.5$, and length $L = 14$. The symbols $\times/+$ mark the times when the right/left weights reach half of the maximum peak for given distances. Lower panel: time of the half-peak versus the distance. The solid and dashed lines are the results of linear fitting.

$\Gamma(s)$. First, the growth function equals zero in equilibrium. In thermal equilibrium at infinite temperature, the operator entanglement $\hat{S}(t,x)$ has a pyramid shape $\hat{S}(t,x) = 2s_{eq} \min\{x, L-x\}$ in a one-dimensional system of length L. Thus,

$\Gamma(s_{eq}) = \Gamma(-s_{eq}) = 0$ is satisfied. Second, the butterfly velocities are given by the derivatives $v_B^r = -s_{eq}\Gamma'(s_{eq})$ and $v_B^l = s_{eq}\Gamma'(-s_{eq})$. Thus, this function $\Gamma(s)$ provides yet another way of obtaining butterfly velocities, and it follows that any $\Gamma(s)$ with asymmetries at its endpoints will have asymmetric butterfly speeds. FIG. (5.8) shows the growth of operator entanglement across different spatial cuts in time, showing the system approaching the late time equilibrium pyramidal shape.

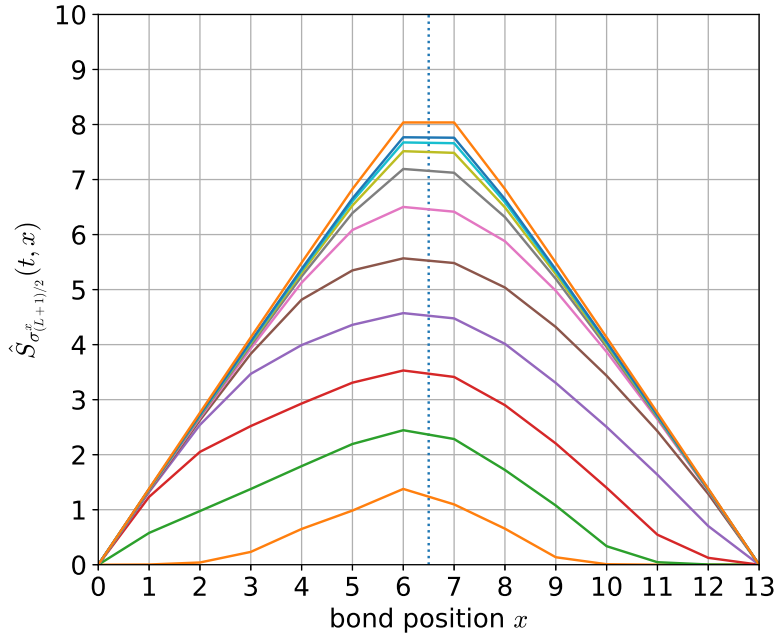

Figure 5.8: Operator entanglement of the time-evolved Pauli operator $\sigma^x_{(L+1)/2}(t)$ in the non-integrable Hamiltonian H [Eq. (5.7)] with parameters $\lambda = 0.5, h_{yz} = 0.5, h_{zy} = -0.25, h_{zz} = 1.0, h_x = -1.05, h_z = 0.5$, and length $L = 13$. The times are $t = 4, 8, \ldots, 36, 40$ and 400 with unit $1/J$. The dotted line is the center of the system.

The statements above are obtained from a minimal curve picture of Ref. [158], i.e. the entanglement $\hat{S}(t,x)$ is the minimum of the sum of the initial entanglement $\hat{S}(0,y)$ and the integral of a velocity-dependent line tension $\mathcal{E}(v)$. The minimal curve is a straight line with constant velocity $v = (x-y)/t$, so that $\hat{S}(t,x) = \min_y \left(ts_{eq}\mathcal{E}(\frac{x-y}{t}) + \hat{S}(0,y)\right)$. Then one can get that the growth function is $\Gamma(s) = \min_v \left(\mathcal{E}(v) - v\, s/s_{eq}\right)$, where s is between $-s_{eq}$ and s_{eq}. Applying the inverse Legendre transformation, the line tension can be expressed as $\mathcal{E}(v) = \max_v \left(\Gamma(s) + v\, s/s_{eq}\right)$. The line tension captures the leading-order hydrodynamics of operator spreading, and the left/right butterfly speeds can be obtained from the intersections of the line tension and the velocity

$$\mathcal{E}(v_B^r) = v_B^r, \quad \mathcal{E}(-v_B^l) = v_B^l. \tag{5.13}$$

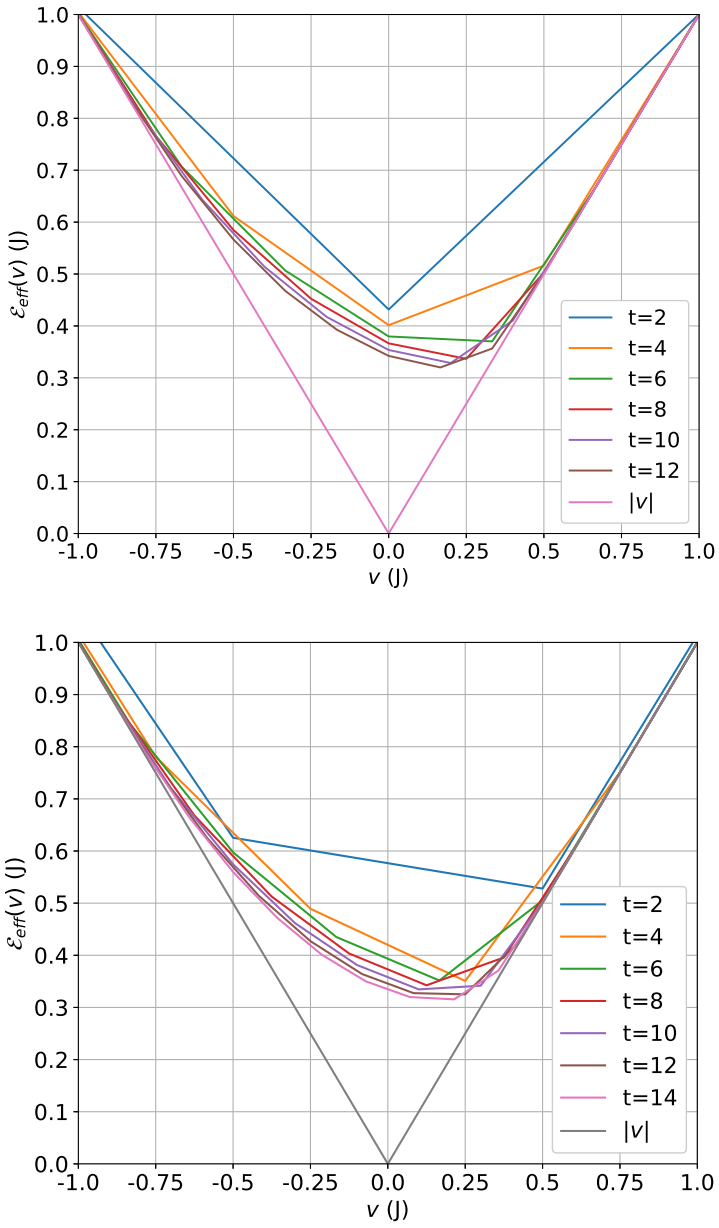

Figure 5.9: Effective line tension $\mathcal{E}_{eff}(v)$ of the Hamiltonian H [Eq. (5.7)] with parameters $\lambda = 0.5, h_{yz} = 0.5, h_{zy} = -0.25, h_{zz} = 1.0, h_x = -1.05, h_z = 0.5$, and length $L = 12$ (upper panel) and $L = 13$ (lower panel). Here $(x + y)/2$ is located at the center of the chain to minimize boundary effects, the velocity is $v = (x - y)/t$, and the unit of time is $1/J$.

Thus, the butterfly velocities can be estimated if one knows the growth function or the line tension. According to Reference [158], the line tension can be estimated via an effective one $\mathcal{E}_{eff}(v) = 1/(s_{eq}t) * S_U(vt/2, -vt/2, t)$ obtained from the entanglement $S_U(x, y, t)$ of the time evolution operator $U(t) = \exp(-iHt)$, where $U(t)$ acting on L spins is treated as a state on $2L$ spins. Looking at the intersections in FIG.

(5.9) indicates $v_B^r \sim 0.5J, v_B^l \sim 0.9J$. This method gives a very rough estimation. We expect that when the system size is large enough, there is a single speed characterizing information propagation in every direction which agrees across different methods of estimation.

5.3 Conclusion and Discussion

In summary, we have constructed 2-local integrable and non-integrable Hamiltonians with asymmetric ballistic information spreading. Exact solutions of the butterfly velocities are obtained in the integrable models. The asymmetric butterfly velocities are estimated from different quantities characterizing operator spreading including out-of-time-ordered correlations, right/left weight of time-evolved operators, and operator entanglement.

Given the constructions and studies in this paper, several open questions would be interesting to explore in the future work. Here, we have focused on the information spreading at infinite temperature. How does the asymmetric spreading change at finite temperature? Additionally, it is worth studying how asymmetries encoded in various quantities are intertwined with each other. For example, does the transport of conserved quantities (like energy) inherit the same signatures of asymmetry as the spreading of local operators? Is it possible to disentangle them? Finally, probing the asymmetry of information propagation may also be interesting to explore in many-body localized systems or disordered systems with Griffiths effects, where the butterfly velocities are zero and the light cones are logarithmic or sub-ballistic.

Appendix A

LINEAR RESPONSE FOR NON-EIGENSTATES

We compute analytically the linear response of a particular class of non-eigenstates using the phenomenological description of the MBL system in terms of the "l-bits" [31]. The analytical result supports our numerical observations in Fig. 2.5 in the main text.

The Hamiltonian in the "l-bits" basis reads

$$H = \sum_i h_i \tau_i^z + \sum_{ij} J_{ij} \tau_i^z \tau_j^z + \cdots, \tag{A.1}$$

where J_{ij} decays exponentially with the distance between i and j. For simplicity and w.l.o.g., we will ignore three- or more-body terms in the Hamiltonian.

We are going to compute the expectation value of $[\tau_1^x(t), \tau_{j_0}^x]$ on product states of "l-bits" in the Y direction. Note that the expectation value on product states in the Z direction is clearly zero, reflecting the absence of transport in eigenstates of the Hamiltonian. By using product states in the Y direction, i.e. the initial state is a direct product of τ_j^y's random eigenstate, we hope to access the off-diagonal elements of the commutator, although our result shows that the linear response of such states still falls short of achieving the unbounded light cone.

The time evolution of τ_1^x is given by

$$\begin{aligned} e^{iHt}\tau_1^x e^{-iHt} &= e^{ith_1\tau_1^z} e^{it\sum_j J_{1j}\tau_1^z\tau_j^z} \tau_1^x e^{-it\sum_j J_{1j}\tau_1^z\tau_j^z} e^{-ith_1\tau_1^z} \\ &= e^{ith_1\tau_1^z} \times \prod_j \left(\cos(tJ_{1j}) + i\sin(tJ_{1j})\tau_1^z\tau_j^z\right) \times \tau_1^x \\ &\times \prod_j \left(\cos(tJ_{1j}) - i\sin(tJ_{1j})\tau_1^z\tau_j^z\right) \times e^{-ith_1\tau_1^z}. \end{aligned} \tag{A.2}$$

Conjugating τ_1^x with $\prod_j(\cos(tJ_{1j}) + i\sin(tJ_{1j})\tau_1^z\tau_j^z)$ generates the following terms:

$$\tau_1^x,\ \tau_1^y\tau_j^z,\ \tau_1^x\tau_j^z\tau_k^z,\ \tau_1^y\tau_j^z\tau_k^z\tau_l^z, \ldots. \tag{A.3}$$

Conjugating these terms with $e^{ith_1\tau_1^z} = (\cos(th_1) + i\sin(th_1)\tau_1^z)$ generates

$$\tau_1^{x'},\ \tau_1^{y'}\tau_j^z,\ \tau_1^{x'}\tau_j^z\tau_k^z,\ \tau_1^{y'}\tau_j^z\tau_k^z\tau_l^z, \ldots, \tag{A.4}$$

where $\tau_1^{x\prime}$ is the result of rotating τ_1^x by $(\cos(th_1) + i\sin(th_1)\tau_1^z)$ and $\tau_1^{y\prime}$ is the result of rotating τ_1^y by $(\cos(th_1) + i\sin(th_1)\tau_1^z)$.

The commutator of these terms with $\tau_{j_0}^x$ involves terms

$$\tau_1^{y\prime}\tau_{j_0}^y,\ \tau_1^{x\prime}\tau_{j_0}^y\tau_k^z,\ \tau_1^{y\prime}\tau_{j_0}^y\tau_k^z\tau_l^z,\ldots. \tag{A.5}$$

The expectation value of these terms on product states in the Y direction is nonzero only for the first term. The bare expectation value (up to ± 1) is $\cos(2th_1)$. The norm of this term is $\tan(2tJ_{1j_0})\prod_k \cos(2tJ_{1k})$. Putting together, the expectation value of the commutator on product state of the "l-bits" in the Y direction is $\cos(2th_1)\tan(2tJ_{1j_0})\prod_k \cos(2tJ_{1k})$.

When $tJ_{1j_0} \ll 1$, the second factor is proportional to tJ_{1j_0} and hence the expectation value decays exponentially with increasing j_0. One might want to think of this as the outside of the light cone. However, the expectation value on the boundary of the supposed light cone $j_c \sim \log t$ also decays with j_c, because $\cos(2tJ_{1k}) < 1$ when $k < j_c$ and $\cos(2tJ_{1k}) \sim 1$ when $k > j_c$. Therefore, the supposed light cone "faints out" with distance. This is exactly the behavior we see in Fig. 5 (lower panels) that there seems to be a logarithmically growing light cone, but it disappears with time. Because of this exponential decay of expectation values at light cone boundaries, the expectation value for any j and t can be bounded by an exponentially decaying function of j, indicating that there is in fact a localized light cone. If we calculate the maximum achievable expectation value for any j, it decays exponentially, similar to that shown in the upper right panel of Fig. 2.5.

Appendix B

PROOF OF A LOWER BOUND

Here, we prove a lower bound $\sqrt{\epsilon a v_{LR}/\Gamma}$ for the width $d(\Gamma)$ of the partially recovered light cone revealed by the corrected OTOC in the channel of phase damping or phase depolarizing. The main ideas in the proof are comparing the difference between the adjoint propagator in the dissipative channel and the unitary one without dissipation, and employing the adjoint propagator of spatially truncated adjoint Liouvillians.

Lemma 6. *Suppose $\mathcal{L}_1^\dagger(t)$ and $\mathcal{L}_0^\dagger(t)$ are the adjoint Liouvillian super-operators describing Markovian dynamics of the same open quantum system with $\|\mathcal{L}_1^\dagger(t) - \mathcal{L}_0^\dagger(t)\| \leq f(t)$, then the difference of adjoint propagators satisfies*

$$\|\mathcal{V}_1^\dagger(t,0) - \mathcal{V}_0^\dagger(t,0)\| \leq \int_0^t d\tau f(\tau), \tag{B.1}$$

where $\mathcal{V}_k^\dagger(t,s) = \mathcal{T}_{\rightarrow} e^{\int_s^t \mathcal{L}_k^\dagger(\tau)d\tau}(t \geq s, k = 0, 1)$, and $\mathcal{T}_{\rightarrow}$ or $\mathcal{T}_{\leftarrow}$ is the time-ordering operator which orders products of time-dependent operators such that their time arguments increase in the direction indicated by the arrow.

Proof.

$$\begin{aligned}
&\|\mathcal{V}_1^\dagger(t,0) - \mathcal{V}_0^\dagger(t,0)\| = \|\mathcal{V}_0^\dagger(0,0)\mathcal{V}_1^\dagger(t,0) - \mathcal{V}_0^\dagger(t,0)\mathcal{V}_1^\dagger(t,t)\| \\
&= \left\| \int_0^t ds \frac{\partial}{\partial s} \left(\mathcal{V}_0^\dagger(s,0)\mathcal{V}_1^\dagger(t,s) \right) \right\| \\
&\leq \int_0^t ds \|\mathcal{V}_0^\dagger(s,0)(\mathcal{L}_0^\dagger(s) - \mathcal{L}_1^\dagger(s))\mathcal{V}_1^\dagger(t,s)\| \\
&\leq \int_0^t ds \|\mathcal{V}_0^\dagger(s,0)\| \cdot \|\mathcal{L}_1^\dagger(s) - \mathcal{L}_0^\dagger(s)\| \cdot \|\mathcal{V}_1^\dagger(t,s)\| \\
&\leq \int_0^t ds \|\mathcal{L}_1^\dagger(s) - \mathcal{L}_0^\dagger(s)\| \leq \int_0^t ds f(s).
\end{aligned}$$

In the derivation, one uses the fact that the adjoint propagators $\mathcal{V}_k^\dagger(t,s)$ are norm-nonincreasing [130, 137, 139]. □

Here, we need to pay attention to the difference between the propagator $\mathcal{V}(t,s) = \mathcal{T}_{\leftarrow} e^{\int_s^t \mathcal{L}(\tau)d\tau}(t \geq s)$ and its adjoint $\mathcal{V}^\dagger(t,s) = \mathcal{T}_{\rightarrow} e^{\int_s^t \mathcal{L}^\dagger(\tau)d\tau}(t \geq s)$. $\mathcal{V}(t,s)$ acts on

the density matrix and is trace-preserving. $\mathcal{V}^\dagger(t,s)$ acts on the observables and the identity is one of its fixed points. For unitary evolution, $\mathcal{V}^\dagger(t,s)$ and $\mathcal{V}(t,s)$ are the inverse of each other and both norm-preserving. When dissipation exists, only $\mathcal{V}^\dagger(t,s)$ is norm-nonincreasing for arbitrary observables, i.e. $\|\mathcal{V}^\dagger(t,s)\cdot O\| \le \|O\|$ $(\forall O = O^\dagger)$.

Lemma 7. *In a one-dimensional system, $\mathcal{L}_H^\dagger = \sum_i \mathcal{L}_{H_i}^\dagger$ is the sum of local adjoint Liouvillian super-operators, and $\mathcal{L}_D^\dagger = \Gamma \sum_k \mathcal{L}_{D,k}^\dagger$ is the sum of adjoint dissipative super-operators acting on each site, where $\|\mathcal{L}_{D,k}^\dagger\| \le 1$ and Γ is the dissipation rate. During the evolution, the operator difference between the dissipative and unitary channels is upper bounded by*

$$\|\mathcal{V}_1^\dagger(t,0)\cdot B - \mathcal{V}_0^\dagger(t,0)\cdot B\| \le \Gamma O(t^2) + \delta \tag{B.2}$$

in the limit of small Γ and large t, where $\mathcal{V}_1^\dagger(t,s) = \mathcal{T}_{\rightarrow} e^{\int_s^t (\mathcal{L}_H^\dagger(\tau)+\mathcal{L}_D^\dagger(\tau))d\tau}(t \ge s)$, $\mathcal{V}_0^\dagger(t,s) = \mathcal{T}_{\rightarrow} e^{\int_s^t \mathcal{L}_H^\dagger(\tau)d\tau}(t \ge s)$, B is a local observable at site 0, and δ is an arbitrarily small constant.

Proof. For an open quantum system described by short-range Liouvillians, the Lieb-Robinson bound

$$\|\,[\mathcal{V}^\dagger(t)\cdot B, A]\,\| \le c\,\|B\|\cdot\|A\|\; e^{-(d_{AB}-v_{LR}t)/\xi} \tag{B.3}$$

implies the existence of an upper limit to the speed of quantum information propagation. The outside signal is exponentially small in the distance from the boundary of the effective light cone. Based on the Lieb-Robinson bound, Ref. [139] obtained the quasi-locality of Markovian quantum dynamics: up to exponentially small error, the evolution of a local observable can be approximately obtained by applying the propagator of a spatially truncated version of the adjoint Liouvillian, provided that the range of the truncated propagator is larger than the support of the time-evolved observable. The truncated propagators we select are

$$\tilde{\mathcal{V}}_0^\dagger(t,0) = \mathcal{T}_{\rightarrow} e^{\int_0^t d\tau \sum_{i:H_i\subset\Lambda(\tau)} \mathcal{L}_{H_i}^\dagger(\tau)},\ \tilde{\mathcal{V}}_1^\dagger(t,0) = \mathcal{T}_{\rightarrow} e^{\int_0^t d\tau \left(\sum_{i:H_i\subset\Lambda(\tau)} \mathcal{L}_{H_i}^\dagger(\tau)+\sum_{k=-d(\tau)/a}^{d(\tau)/a} \mathcal{L}_{D,k}(\tau)\right)},$$

where $d(t) = v_{LR}t + \xi\log(c''/\delta)$ for some large constant c'', a is the distance between two nearest neighboring sites, and $H_i \subset \Lambda(t)$ means the local term H_i is located in the regime $\Lambda(t) = (-d(t), d(t))$. Let $B_k(t) = \mathcal{V}_k^\dagger(t,0)\cdot B$ and $\tilde{B}_k(t) = \tilde{\mathcal{V}}_k^\dagger(t,0)\cdot B$.

Applying the triangle inequality, one obtains

$$\begin{aligned}\|B_1(t) - B_0(t)\| \leq & \|\tilde{B}_1(t) - \tilde{B}_0(t)\| + \\ & \|B_1(t) - \tilde{B}_1(t)\| + \|\tilde{B}_0(t) - B_0(t)\|.\end{aligned}$$

On the right-hand side, the first term is upper bounded by $\|B\| \int_0^t d\tau \Gamma(\xi/a + v_{LR}\tau/a) = \|B\| \Gamma t(v_{LR}t/2 + \xi)/a$ (**Lemma 1**). The second and third terms both are less than or equal to $c' \ \|B\| \ e^{(v_{LR}t - d(t))/\xi} = c' \ \|B\| \ \delta/c''$ [139]. Thus we get $\|\mathcal{V}_1^\dagger(t,0) \cdot B - \mathcal{V}_0^\dagger(t,0) \cdot B\| \leq \|B\|(v_{LR}\Gamma t^2/2 + \xi\Gamma t + 2c'\delta/c'')/a$. Therefore, $\|\mathcal{V}_1^\dagger(t,0) \cdot B - \mathcal{V}_0^\dagger(t,0) \cdot B\| \leq \Gamma O(t^2) + \delta$ in the limit of small Γ and large t. □

In the chaotic Ising chain with dissipations acting on each site, the light cone within the time range $t \leq \sqrt{\frac{\epsilon a}{v_{LR}\Gamma}}$ can be revealed by $\|[\mathcal{V}_1^\dagger(t,0) \cdot B, A]\|$, $\|[\mathcal{V}_1^\dagger(t,0) \cdot B, A]\|/\|\mathcal{V}_1^\dagger(t,0) \cdot B\|$, $\|[\mathcal{V}_1^\dagger(t,0) \cdot B, A]\|_F$ and $\|[\mathcal{V}_1^\dagger(t,0) \cdot B, A]\|_F/\|\mathcal{V}_1^\dagger(t,0) \cdot B\|_F$, where v_{LR} is the Lieb-Robinson velocity, a is the distance between two nearest neighboring sites, ϵ is a small number (for example, $\epsilon \sim 0.1$), the dissipation rate Γ is sufficiently small ($\Gamma \ll \epsilon a v_{LR}/\xi^2$), $\|O\|$ is the operator norm and $\|O\|_F = \lim_{N\to\infty} \sqrt{\mathrm{tr}(OO^\dagger)/2^N}$ is the normalized Frobenius norm of operators in the thermodynamic limit. The width of the light cone is at least $\sqrt{\frac{\epsilon a v_{LR}}{\Gamma}}$.

Proof. According to **Lemma 2**, the t^2 term plays a dominant role in the inequality for sufficiently small dissipation rate $\Gamma \ll \epsilon a v_{LR}/\xi^2$. If $t \leq \sqrt{\frac{\epsilon a}{v_{LR}\Gamma}}$, then one obtains $\|B_1(t) - B_0(t)\| \leq \epsilon\|B\|$ when comparing the operators $B_1(t) = \mathcal{V}_1^\dagger(t,0) \cdot B$ in the dissipative channel and $B_0(t) = \mathcal{V}_0^\dagger(t,0) \cdot B$ in the unitary channel. Applying the triangle inequality, one obtains

$$\begin{aligned}(1-\epsilon)\|B\| \leq \|B_1(t)\| &\leq (1+\epsilon)\|B\|, \\ \|[B_0(t),A]\| - \epsilon\|C_A\|\|B\| \leq \|[B_1(t),A]\| &\leq \|[B_0(t),A]\| + \epsilon\|C_A\|\|B\|, \\ (1+\epsilon)^{-1}\Big(\frac{\|[B_0(t),A]\|}{\|B\|} - \epsilon\|C_A\|\Big) \leq \frac{\|[B_1(t),A]\|}{\|B_1(t)\|} &\leq \\ (1-\epsilon)^{-1}\Big(&\frac{\|[B_0(t),A]\|}{\|B\|} + \epsilon\|C_A\|\Big),\end{aligned}$$

where the super-operator C_A is defined as $C_A \cdot O = [O, A]$. The normalized Frobenius norm is less than or equal to the operator norm, i.e. $\|O\|_F \leq \|O\|$, so we get

$$\begin{aligned}\|B_1(t) - B_0(t)\|_F \leq \|B_1(t) - B_0(t)\| &\leq \epsilon\|B\| \\ \|[B_0(t),A]\|_F - \epsilon\|C_A\|\|B\| \leq \|[B_1(t),A]\|_F &\leq \|[B_0(t),A]\|_F + \epsilon\|C_A\|\|B\|, \\ \frac{\|[B_0(t),A]\|_F - \epsilon\|C_A\|\|B\|}{\|B\|_F + \epsilon\|B\|} \leq \frac{\|[B_1(t),A]\|_F}{\|B_1(t)\|_F} &\leq \frac{\|[B_0(t),A]\|_F + \epsilon\|C_A\|\|B\|}{\|B\|_F - \epsilon\|B\|}.\end{aligned}$$

In the unitary channel, both $\|[B_0(t), A]\|$ and $\|[B_0(t), A]\|_F$ are able to detect the ballistic light cone. Because ϵ is a small number, it is also small that the difference of the corresponding quantities between the dissipative and unitary channel. Thus, $\|[B_1(t), A]\|$, $\|[B_1(t), A]\|/\|B_1(t)\|$, $\|[B_1(t), A]\|_F$ and $\|[B_1(t), A]\|_F/\|B_1(t)\|_F$ are both able to detect the light cone in the time range $t \leq \sqrt{\frac{\epsilon a}{v_{LR}\Gamma}}$. The width of the light cone is at least $\sqrt{\frac{\epsilon a v_{LR}}{\Gamma}}$ for sufficiently small dissipation rate $\Gamma \ll \epsilon a v_{LR}/\xi^2$. □

Corollary 2. *For sufficiently small dissipation rate $\Gamma \ll \epsilon a v_{LR}/\xi^2$, the lower bound $\sqrt{\frac{\epsilon a v_{LR}}{\Gamma}}$ works for the width of the light cone revealed by the corrected OTOC in the chaotic Ising chain with dissipation of phase damping or phase depolarizing.*

Proof. In the channel of phase damping or phase depolarizing, the adjoint propagator $\mathcal{V}_b^\dagger(t)$ is exactly equal to the propagator $\mathcal{V}_f(t)$, then

$$2\left(1 - \frac{F(t, A, B)}{F(t, I, B)}\right) = \frac{\| [\mathcal{V}_b^\dagger(t) \cdot B, A] \|_F^2}{\|\mathcal{V}_b^\dagger(t) \cdot B\|_F^2}. \tag{B.4}$$

Based on **Proposition 1**, the lower bound $\sqrt{\frac{\epsilon a v_{LR}}{\Gamma}}$ works for the width of the light cone revealed by the corrected OTOC in the channel of phase damping or phase depolarizing. □

Appendix C

ANALYTIC SOLUTION OF TIME-EVOLVED OPERATORS AND OTOCS IN THE FREE MODEL

The Jordan-Wigner mapping allows spin operators to be written in terms of free Majorana fermions as follows: : $\sigma_j^x = i\gamma_{2j}\gamma_{2j+1}$, $\sigma_j^z = (\prod_{k=-\infty}^{j-1} i\gamma_{2k}\gamma_{2k+1})\gamma_{2j}$ and $\sigma_j^y = (\prod_{k=-\infty}^{j-1} i\gamma_{2k}\gamma_{2k+1})\gamma_{2j+1}$. Then the Hamiltonian [Eq. (5.2)] is

$$H_\lambda = (1-\lambda)\frac{-J}{2}\sum_j \Big[h_{yz}(-i\gamma_{2j}\gamma_{2j+2}) + h_{zy}(i\gamma_{2j+1}\gamma_{2j+3})\Big] + \lambda\frac{-J}{2}\sum_j \Big[h_{zz}(i\gamma_{2j+1}\gamma_{2j+2}) + h_x(i\gamma_{2j}\gamma_{2j+1})\Big]. \tag{C.1}$$

Below, we obtain analytic solutions for time-evolved operator for this Hamiltonian [Eq. (5.2)] within the Heisenberg picture. Denoting $\gamma_0(t) = \sum_n f_n(t)\gamma_n$ and $\gamma_1(t) = \sum_m h_m(t)\gamma_m$, the time-evolved operator is $\sigma_0^x(t) = i\gamma_0(t)\gamma_1(t) = i\sum_{n<m} F_{n,m}(t)\gamma_n\gamma_m$, where $F_{n,m}(t) = f_n(t)h_m(t) - f_m(t)h_n(t)$, and the out-of-time-ordered correlations are

$$C_{xz}(j,t) = 1 - 2\sum_{n\le 2j, m\ge 2j+1} |F_{n,m}(t)|^2, \tag{C.2}$$

$$C_{xx}(j,t) = 1 - 2\Big[\sum_{n<2j}\left(|F_{n,2j}(t)|^2 + |F_{n,2j+1}(t)|^2\right) + \sum_{m>2j+1}\left(|F_{2j,m}(t)|^2 + |F_{2j+1,m}(t)|^2\right)\Big]. \tag{C.3}$$

Next, we get the analytic solution of time-evolved operators $\gamma_0(t) = \sum_n f_n(t)\gamma_n$ and $\gamma_1(t) = \sum_m h_m(t)\gamma_m$ in the integrable Hamiltonian [Eq. (5.2)]. Plugging the candidate solution into the Heisenberg equation, it is straightforward to get the differential equations for the coefficients $f_n(t)$

$$\begin{cases} \frac{df_{2n}(t)}{dt} & = -\lambda J h_{zz} f_{2n-1}(t) + \lambda J h_x f_{2n+1}(t) \\ & \quad +(1-\lambda)J h_{yz}[-f_{2n+2}(t) + f_{2n-2}(t)], \\ \frac{df_{2n+1}(t)}{dt} & = -\lambda J h_x f_{2n}(t) + \lambda J h_{zz} f_{2n+2}(t) \\ & \quad +(1-\lambda)J h_{zy}[-f_{2n-1}(t) + f_{2n+3}(t)], \end{cases}$$

where the initial condition is $f_n(0) = \delta_{n,0}$. After applying the Fourier transformation $f_{2n}(t) = \frac{1}{2\pi}\int_{-\pi}^{\pi} dq\, e^{-inq} A(q,t)$, $f_{2n+1}(t) = \frac{1}{2\pi}\int_{-\pi}^{\pi} dq\, e^{-inq} B(q,t)$, we get

$$\begin{cases} \frac{\partial A(q,t)}{\partial t} &= \lambda J[h_x - h_{zz}e^{iq}]B(q,t) + (1-\lambda)2iJh_{yz}\sin(q)A(q,t), \\ \frac{\partial B(q,t)}{\partial t} &= \lambda J[-h_x + h_{zz}e^{-iq}]A(q,t) - (1-\lambda)2iJh_{zy}\sin(q)B(q,t). \end{cases} \tag{C.4}$$

Then, the analytic solution is

$$\begin{cases} f_{2n}(t) &= \frac{1}{2\pi}\int_{-\pi}^{\pi} dq\, e^{-inq}\frac{\epsilon_{\lambda,1}e^{i\epsilon_{\lambda,1}t} - \epsilon_{\lambda,2}e^{i\epsilon_{\lambda,2}t}}{\epsilon_{\lambda,1}-\epsilon_{\lambda,2}}, \\ f_{2n+1}(t) &= \frac{1}{2\pi}\int_{-\pi}^{\pi} dq\, e^{-inq}\lambda J[-h_x + h_{zz}e^{-iq}] \times \frac{(-i)(e^{i\epsilon_{\lambda,1}t} - e^{i\epsilon_{\lambda,2}t})}{\epsilon_{\lambda,1}-\epsilon_{\lambda,2}}, \end{cases} \tag{C.5}$$

where $\epsilon_{\lambda,1(2)}(q) = J\Big[(1-\lambda)(h_{yz}-h_{zy})\sin q + (-)\big((1-\lambda)^2(h_{yz}+h_{zy})^2\sin^2 q + \lambda^2(h_{zz}^2 + h_x^2 - 2h_{zz}h_x\cos q)^{1/2}\big)\Big]$.

Similarly, the coefficients in the exact solution $\gamma_1(t) = \sum_m h_m(t)\gamma_m$ are

$$\begin{cases} h_{2m}(t) &= \frac{1}{2\pi}\int_{-\pi}^{\pi} dq\, e^{-imq}\lambda J[h_x - h_{zz}e^{iq}] \times \frac{(-i)(e^{i\epsilon_{\lambda,1}t} - e^{i\epsilon_{\lambda,2}t})}{\epsilon_{\lambda,1}-\epsilon_{\lambda,2}}, \\ h_{2m+1}(t) &= \frac{1}{2\pi}\int_{-\pi}^{\pi} dq\, e^{-imq}\,\frac{\epsilon_{\lambda,1}e^{i\epsilon_{\lambda,1}t} - \epsilon_{\lambda,2}e^{i\epsilon_{\lambda,2}t}}{\epsilon_{\lambda,1}-\epsilon_{\lambda,2}}. \end{cases} \tag{C.6}$$

BIBLIOGRAPHY

[1] J. M. Deutsch. Thermodynamic entropy of a many-body energy eigenstate. *New J. Phys.*, 12(7):075021, 2010. doi: 10.1088/1367-2630/12/7/075021. URL http://dx.doi.org/10.1088/1367-2630/12/7/075021.

[2] Lea F. Santos, Anatoli Polkovnikov, and Marcos Rigol. Weak and strong typicality in quantum systems. *Phys. Rev. E*, 86:010102, 2012. doi: 10.1103/PhysRevE.86.010102. URL https://link.aps.org/doi/10.1103/PhysRevE.86.010102.

[3] J. M. Deutsch, Haibin Li, and Auditya Sharma. Microscopic origin of thermodynamic entropy in isolated systems. *Phys. Rev. E*, 87:042135, 2013. doi: 10.1103/PhysRevE.87.042135. URL https://link.aps.org/doi/10.1103/PhysRevE.87.042135.

[4] J. M. Deutsch. Quantum statistical mechanics in a closed system. *Phys. Rev. A*, 43:2046–2049, 1991. doi: 10.1103/PhysRevA.43.2046. URL https://journals.aps.org/pra/abstract/10.1103/PhysRevA.43.2046.

[5] Mark Srednicki. Chaos and quantum thermalization. *Phys. Rev. E*, 50:888–901, 1994. doi: 10.1103/PhysRevE.50.888. URL https://journals.aps.org/pre/abstract/10.1103/PhysRevE.50.888.

[6] Marcos Rigol, Vanja Dunjko, and Maxim Olshanii. Thermalization and its mechanism for generic isolated quantum systems. *Nature*, 452(7189):854–858, 2008. doi: 10.1038/nature06838. URL http://dx.doi.org/10.1038/nature06838.

[7] James R. Garrison and Tarun Grover. Does a single eigenstate encode the full Hamiltonian? *Phys. Rev. X*, 8:021026, 2018. doi: 10.1103/PhysRevX.8.021026. URL https://link.aps.org/doi/10.1103/PhysRevX.8.021026.

[8] Anatoly Dymarsky, Nima Lashkari, and Hong Liu. Subsystem eigenstate thermalization hypothesis. *Phys. Rev. E*, 97:012140, 2018. doi: 10.1103/PhysRevE.97.012140. URL https://link.aps.org/doi/10.1103/PhysRevE.97.012140.

[9] Yichen Huang. Universal eigenstate entanglement of chaotic local Hamiltonians. *Nucl. Phys. B*, 938:594 – 604, 2019. doi: https://doi.org/10.1016/j.nuclphysb.2018.09.013. URL http://www.sciencedirect.com/science/article/pii/S0550321318302608.

[10] Hyungwon Kim and David A. Huse. Ballistic spreading of entanglement in a diffusive nonintegrable system. *Phys. Rev. Lett.*, 111:127205, 2013. doi:

10.1103/PhysRevLett.111.127205. URL http://link.aps.org/doi/10.1103/PhysRevLett.111.127205.

[11] P. W. Anderson. Absence of diffusion in certain random lattices. *Phys. Rev.*, 109(5):1492–1505, 1958. doi: 10.1103/PhysRev.109.1492. URL https://journals.aps.org/pr/abstract/10.1103/PhysRev.109.1492.

[12] D. M. Basko, I. L. Aleiner, and B. L. Altshuler. Metal–insulator transition in a weakly interacting many-electron system with localized single-particle states. *Ann. Phys.*, 321(5):1126–1205, 2006. doi: 10.1016/j.aop.2005.11.014. URL https://www.sciencedirect.com/science/article/pii/S0003491605002630.

[13] Vadim Oganesyan and David A. Huse. Localization of interacting fermions at high temperature. *Phys. Rev. B*, 75(15):155111, 2007. doi: 10.1103/PhysRevB.75.155111. URL https://link.aps.org/doi/10.1103/PhysRevB.75.155111.

[14] Rahul Nandkishore, Sarang Gopalakrishnan, and David A. Huse. Spectral features of a many-body-localized system weakly coupled to a bath. *Phys. Rev. B*, 90:064203, 2014. doi: 10.1103/PhysRevB.90.064203. URL http://link.aps.org/doi/10.1103/PhysRevB.90.064203.

[15] Sarang Gopalakrishnan and Rahul Nandkishore. Mean-field theory of nearly many-body localized metals. *Phys. Rev. B*, 90:224203, 2014. doi: 10.1103/PhysRevB.90.224203. URL http://link.aps.org/doi/10.1103/PhysRevB.90.224203.

[16] Sonika Johri, Rahul Nandkishore, and R. N. Bhatt. Many-body localization in imperfectly isolated quantum systems. *Phys. Rev. Lett.*, 114:117401, 2015. doi: 10.1103/PhysRevLett.114.117401. URL http://link.aps.org/doi/10.1103/PhysRevLett.114.117401.

[17] Rahul Nandkishore and Sarang Gopalakrishnan. Many body localized systems weakly coupled to baths. *Annalen der Physik*, 529(7):1600181, 2017. doi: 10.1002/andp.201600181. URL https://doi.org/10.1002/andp.201600181.

[18] R. Nandkishore and D. A. Huse. Many-body localization and thermalization in quantum statistical mechanics. *Annu. Rev. Condens. Matter Phys.*, 6(1):15–38, 2015. doi: 10.1146/annurev-conmatphys-031214-014726. URL https://www.annualreviews.org/doi/abs/10.1146/annurev-conmatphys-031214-014726.

[19] E. Altman and R. Vosk. Universal dynamics and renormalization in many-body-localized systems. *Annu. Rev. Condens. Matter Phys.*, 6 (1):383–409, 2015. doi: 10.1146/annurev-conmatphys-031214-014701. URL http://www.annualreviews.org/doi/abs/10.1146/annurev-conmatphys-031214-014701.

[20] Romain Vasseur and Joel E Moore. Nonequilibrium quantum dynamics and transport: from integrability to many-body localization. *J. Stat. Mech.*, 2016(6):064010, 2016. doi: 10.1088/1742-5468/2016/06/064010. URL https://iopscience.iop.org/article/10.1088/1742-5468/2016/06/064010.

[21] J. Z. Imbrie. On many-body localization for quantum spin chains. *J. Stat. Phys.*, 163(5):998–1048, 2016. doi: 10.1007/s10955-016-1508-x. URL https://link.springer.com/article/10.1007/s10955-016-1508-x.

[22] J. Z. Imbrie. Diagonalization and many-body localization for a disordered quantum spin chain. *Phys. Rev. Lett.*, 117:027201, 2016. doi: 10.1103/PhysRevLett.117.027201. URL http://link.aps.org/doi/10.1103/PhysRevLett.117.027201.

[23] Fabien Alet and Nicolas Laflorencie. Many-body localization: An introduction and selected topics. *C.R. Phys.*, 19(6):498 – 525, 2018. doi: https://doi.org/10.1016/j.crhy.2018.03.003. URL http://www.sciencedirect.com/science/article/pii/S163107051830032X.

[24] Dmitry A. Abanin, Ehud Altman, Immanuel Bloch, and Maksym Serbyn. Colloquium: Many-body localization, thermalization, and entanglement. *Rev. Mod. Phys.*, 91:021001, 2019. doi: 10.1103/RevModPhys.91.021001. URL https://link.aps.org/doi/10.1103/RevModPhys.91.021001.

[25] G. De Chiara, S. Montangero, P. Calabrese, and R. Fazio. Entanglement entropy dynamics of Heisenberg chains. *J. Stat. Mech.*, 2006(03):P03001, 2006. doi: 10.1088/1742-5468/2006/03/P03001. URL https://iopscience.iop.org/article/10.1088/1742-5468/2006/03/P03001.

[26] M. Znidaric, T. Prosen, and P. Prelovsek. Many-body localization in the Heisenberg XXZ magnet in a random field. *Phys. Rev. B*, 77(6):064426, 2008. doi: 10.1103/PhysRevB.77.064426. URL http://link.aps.org/doi/10.1103/PhysRevB.77.064426.

[27] J. H. Bardarson, F. Pollmann, and J. E. Moore. Unbounded growth of entanglement in models of many-body localization. *Phys. Rev. Lett.*, 109 (1):017202, 2012. doi: 10.1103/PhysRevLett.109.017202. URL http://link.aps.org/doi/10.1103/PhysRevLett.109.017202.

[28] Maksym Serbyn, Z. Papić, and Dmitry A. Abanin. Universal slow growth of entanglement in interacting strongly disordered systems. *Phys. Rev. Lett.*, 110:260601, 2013. doi: 10.1103/PhysRevLett.110.260601. URL http://journals.aps.org/prl/abstract/10.1103/PhysRevLett.110.260601.

[29] A. Nanduri, H. Kim, and D. A. Huse. Entanglement spreading in a many-body localized system. *Phys. Rev. B*, 90:064201, 2014. doi: 10.1103/PhysRevB.90.064201. URL http://link.aps.org/doi/10.1103/PhysRevB.90.064201.

[30] Maksym Serbyn, Z. Papić, and D. A. Abanin. Quantum quenches in the many-body localized phase. *Phys. Rev. B*, 90:174302, 2014. doi: 10.1103/PhysRevB.90.174302. URL http://journals.aps.org/prb/abstract/10.1103/PhysRevB.90.174302.

[31] D. A. Huse, R. Nandkishore, and V. Oganesyan. Phenomenology of fully many-body-localized systems. *Phys. Rev. B*, 90(17):174202, 2014. doi: 10.1103/PhysRevB.90.174202. URL http://link.aps.org/doi/10.1103/PhysRevB.90.174202.

[32] Brian Swingle. A simple model of many-body localization. *arXiv:1307.0507*, 2013. URL https://arxiv.org/abs/1307.0507.

[33] Yichen Huang. Entanglement dynamics in critical random quantum Ising chain with perturbations. *Ann. Phys. (N. Y.)*, 380:224 – 227, 2017. doi: 10.1016/j.aop.2017.02.018. URL http://www.sciencedirect.com/science/article/pii/S0003491617300763.

[34] A. I. Larkin and Yu. N. Ovchinnikov. Quasiclassical method in the theory of superconductivity. *Sov. J. Exp. Theor. Phys.*, 28(6):1200, 1969. URL http://www.jetp.ac.ru/cgi-bin/e/index/e/28/6/p1200?a=list.

[35] Alexei Kitaev. Hidden correlations in the Hawking radiation and thermal noise. In *talk given at the Fundamental Physics Prize Symposium*, 2014. URL http://online.kitp.ucsb.edu/online/joint98/kitaev/.

[36] Alexei Kitaev. A simple model of quantum holography. In *talk given at KITP Program: Entanglement in Strongly-Correlated Quantum Matter*, 2015. URL http://online.kitp.ucsb.edu/online/entangled15/kitaev/.

[37] Stephen H. Shenker and Douglas Stanford. Black holes and the butterfly effect. *J. High Energ. Phys.*, 3:67, 2014. doi: 10.1007/JHEP03(2014)067. URL http://dx.doi.org/10.1007/JHEP03(2014)067.

[38] Stephen H. Shenker and Douglas Stanford. Multiple shocks. *J. High Energ. Phys.*, 12:46, 2014. doi: 10.1007/JHEP12(2014)046. URL http://dx.doi.org/10.1007/JHEP12(2014)046.

[39] Stephen H. Shenker and Douglas Stanford. Stringy effects in scrambling. *J. High Energ. Phys.*, 5:132, 2015. doi: 10.1007/JHEP05(2015)132. URL https://link.springer.com/article/10.1007/JHEP05(2015)132.

[40] Daniel A. Roberts and Douglas Stanford. Diagnosing chaos using four-point functions in two-dimensional conformal field theory. *Phys. Rev. Lett.*, 115:131603, 2015. doi: 10.1103/PhysRevLett.115.131603. URL http://journals.aps.org/prl/abstract/10.1103/PhysRevLett.115.131603.

[41] Daniel A. Roberts, Douglas Stanford, and Leonard Susskind. Localized shocks. *J. High Energ. Phys.*, 3:51, 2015. doi: 10.1007/JHEP03(2015)051. URL http://dx.doi.org/10.1007/JHEP03(2015)051.

[42] Daniel A. Roberts and Brian Swingle. Lieb-Robinson bound and the butterfly effect in quantum field theories. *Phys. Rev. Lett.*, 117:091602, 2016. doi: 10.1103/PhysRevLett.117.091602. URL http://journals.aps.org/prl/abstract/10.1103/PhysRevLett.117.091602.

[43] Pavan Hosur, Xiao-Liang Qi, Daniel A. Roberts, and Beni Yoshida. Chaos in quantum channels. *J. High Energ. Phys.*, 2:4, 2016. doi: 10.1007/JHEP02(2016)004. URL http://dx.doi.org/10.1007/JHEP02(2016)004.

[44] Juan Maldacena, Stephen H. Shenker, and Douglas Stanford. A bound on chaos. *J. High Energ. Phys.*, 8:106, 2016. doi: 10.1007/JHEP08(2016)106. URL http://dx.doi.org/10.1007/JHEP08(2016)106.

[45] Joseph Polchinski and Vladimir Rosenhaus. The spectrum in the Sachdev-Ye-Kitaev model. *J. High Energ. Phys.*, 4:1, 2016. doi: 10.1007/JHEP04(2016)001. URL https://doi.org/10.1007/JHEP04(2016)001.

[46] Juan Maldacena and Douglas Stanford. Remarks on the Sachdev-Ye-Kitaev model. *Phys. Rev. D*, 94:106002, 2016. doi: 10.1103/PhysRevD.94.106002. URL https://link.aps.org/doi/10.1103/PhysRevD.94.106002.

[47] Yingfei Gu, Xiao-Liang Qi, and Douglas Stanford. Local criticality, diffusion and chaos in generalized Sachdev-Ye-Kitaev models. *J. High Energ. Phys.*, 5:125, 2017. doi: 10.1007/JHEP05(2017)125. URL https://doi.org/10.1007/JHEP05(2017)125.

[48] Efim B. Rozenbaum, Sriram Ganeshan, and Victor Galitski. Lyapunov exponent and out-of-time-ordered correlator's growth rate in a chaotic system. *Phys. Rev. Lett.*, 118:086801, 2017. doi: 10.1103/PhysRevLett.118.086801. URL https://link.aps.org/doi/10.1103/PhysRevLett.118.086801.

[49] Daniel A Roberts and Beni Yoshida. Chaos and complexity by design. *J. High Energ. Phys.*, 4:121, 2017. doi: 10.1007/JHEP04(2017)121. URL https://doi.org/10.1007/JHEP04(2017)121.

[50] Aavishkar A Patel, Debanjan Chowdhury, Subir Sachdev, and Brian Swingle. Quantum butterfly effect in weakly interacting diffusive metals. *Phys. Rev. X*, 7:031047, 2017. doi: 10.1103/PhysRevX.7.031047. URL https://journals.aps.org/prx/abstract/10.1103/PhysRevX.7.031047.

[51] Yichen Huang, Fernando G. S. L. Brandão, and Yong-Liang Zhang. Finite-size scaling of out-of-time-ordered correlators at late times. *Phys. Rev. Lett.*, 123:010601, 2017. doi: 10.1103/PhysRevLett.123.010601. URL https://link.aps.org/doi/10.1103/PhysRevLett.123.010601.

[52] Márk Mezei and Douglas Stanford. On entanglement spreading in chaotic systems. *J. High Energ. Phys.*, 5:65, 2017. doi: 10.1007/JHEP05(2017)065. URL https://doi.org/10.1007/JHEP05(2017)065.

[53] Andrew Lucas. Constraints on hydrodynamics from many-body quantum chaos. *arXiv: 1710.01005*, 2017. URL https://arxiv.org/abs/1710.01005.

[54] G. Menezes and J. Marino. Slow scrambling in sonic black holes. *EPL*, 121(6):60002, 2017. doi: 10.1209/0295-5075/121/60002. URL http://iopscience.iop.org/article/10.1209/0295-5075/121/60002.

[55] Yichen Huang, Yong-Liang Zhang, and Xie Chen. Out-of-time-ordered correlators in many-body localized systems. *Ann. Phys. (Berl.)*, 529(7):1600318, 2017. doi: 10.1002/andp.201600318. URL http://dx.doi.org/10.1002/andp.201600318.

[56] R. Fan, P. Zhang, H. Shen, and H. Zhai. Out-of-time-order correlation for many-body localization. *Sci. Bull.*, 62(10):707–711, 2017. doi: 10.1016/j.scib.2017.04.011. URL https://doi.org/10.1016/j.scib.2017.04.011.

[57] Yu Chen. Quantum logarithmic butterfly in many body localization. *arXiv:1608.02765*, 2016. URL https://arxiv.org/abs/1608.02765.

[58] B. Swingle and D. Chowdhury. Slow scrambling in disordered quantum systems. *Phys. Rev. B*, 95:060201(R), 2017. doi: 10.1103/PhysRevB.95.060201. URL https://journals.aps.org/prb/abstract/10.1103/PhysRevB.95.060201.

[59] R.-Q. He and Z.-Y. Lu. Characterizing many-body localization by out-of-time-ordered correlation. *Phys. Rev. B*, 95:054201, 2017. doi: 10.1103/PhysRevB.95.054201. URL http://journals.aps.org/prb/abstract/10.1103/PhysRevB.95.054201.

[60] Xiao Chen, Tianci Zhou, David A. Huse, and Eduardo Fradkin. Out-of-time-order correlations in many-body localized and thermal phases. *Ann. Phys. (Berl.)*, 529(7):1600332, 2017. doi: 10.1002/andp.201600332. URL http://dx.doi.org/10.1002/andp.201600332.

[61] Kevin Slagle, Zhen Bi, Yi-Zhuang You, and Cenke Xu. Out-of-time-order correlation in marginal many-body localized systems. *Phys. Rev. B*, 95 (16):165136, 2017. doi: 10.1103/PhysRevB.95.165136. URL https://journals.aps.org/prb/abstract/10.1103/PhysRevB.95.165136.

[62] Yevgeny Bar Lev David J. Luitz. Information propagation in isolated quantum systems. *Phys. Rev. B*, 96:020406, 2017. doi: 10.1103/PhysRevB.96.020406. URL https://journals.aps.org/prb/abstract/10.1103/PhysRevB.96.020406.

[63] Cheng-Ju Lin and Olexei I. Motrunich. Out-of-time-ordered correlators in a quantum Ising chain. *Phys. Rev. B*, 97(14):144304, 2018. doi: 10.1103/PhysRevB.97.144304. URL https://journals.aps.org/prb/abstract/10.1103/PhysRevB.97.144304.

[64] Subir Sachdev and Jinwu Ye. Gapless spin-fluid ground state in a random quantum Heisenberg magnet. *Phys. Rev. Lett.*, 70:3339–3342, 1993. doi: 10.1103/PhysRevLett.70.3339. URL https://link.aps.org/doi/10.1103/PhysRevLett.70.3339.

[65] Yasuhiro Sekino and L Susskind. Fast scramblers. *J. High Energ. Phys.*, 2008 (10):065–065, 2008. doi: 10.1088/1126-6708/2008/10/065. URL http://dx.doi.org/10.1088/1126-6708/2008/10/065.

[66] Nima Lashkari, Douglas Stanford, Matthew Hastings, Tobias Osborne, and Patrick Hayden. Towards the fast scrambling conjecture. *J. High Energ. Phys.*, 2013(4), 2013. doi: 10.1007/jhep04(2013)022. URL http://dx.doi.org/10.1007/JHEP04(2013)022.

[67] E. H. Lieb and D. W. Robinson. The finite group velocity of quantum spin systems. *Commun. Math. Phys.*, 28:251–257, 1972. doi: 10.1007/BF01645779. URL https://link.springer.com/article/10.1007/BF01645779.

[68] M. B. Hastings and T. Koma. Spectral gap and exponential decay of correlations. *Commun. Math. Phys.*, 265(3):781–804, 2006. doi: 10.1007/s00220-006-0030-4. URL http://dx.doi.org/10.1007/s00220-006-0030-4.

[69] Bruno Nachtergaele, Yoshiko Ogata, and Robert Sims. Propagation of correlations in quantum lattice systems. *J. Stat. Phys.*, 124(1):1–13, 2006. doi: 10.1007/s10955-006-9143-6. URL http://link.springer.com/article/10.1007%2Fs10955-006-9143-6.

[70] Aram W. Harrow and Richard A. Low. Random quantum circuits are approximate 2-designs. *Commun. Math. Phys.*, 291(1):257–302, 2009. doi: 10.1007/s00220-009-0873-6. URL https://doi.org/10.1007/s00220-009-0873-6.

[71] Fernando G. S. L. Brandao, Aram W. Harrow, and Michal Horodecki. Local random quantum circuits are approximate polynomial-designs. *Commun. Math. Phys.*, 346(2):397–434, 2016. doi: 10.1007/s00220-016-2706-8. URL https://link.springer.com/article/10.1007%2Fs00220-016-2706-8.

[72] Adam Nahum, Jonathan Ruhman, Sagar Vijay, and Jeongwan Haah. Quantum entanglement growth under random unitary dynamics. *Phy. Rev. X*, 7(3):031016, 2017. doi: 10.1103/PhysRevX.7.031016. URL https://journals.aps.org/prx/abstract/10.1103/PhysRevX.7.031016.

[73] C. W. von Keyserlingk, Tibor Rakovszky, Frank Pollmann, and S. L. Sondhi. Operator hydrodynamics, OTOCs, and entanglement growth in systems without conservation laws. *Phys. Rev. X*, 8(2):021013, 2018. doi: 10.1103/PhysRevX.8.021013. URL https://journals.aps.org/prx/abstract/10.1103/PhysRevX.8.021013.

[74] Adam Nahum, Sagar Vijay, and Jeongwan Haah. Operator spreading in random unitary circuits. *Phys. Rev. X*, 8(2):021014, 2018. doi: 10.1103/PhysRevX.8.021014. URL https://journals.aps.org/prx/abstract/10.1103/PhysRevX.8.021014.

[75] Tibor Rakovszky, Frank Pollmann, and C.W. von Keyserlingk. Diffusive hydrodynamics of out-of-time-ordered correlators with charge conservation. *Phys. Rev. X*, 8:031058, 2018. doi: 10.1103/PhysRevX.8.031058. URL https://journals.aps.org/prx/abstract/10.1103/PhysRevX.8.031058.

[76] Vedika Khemani, Ashvin Vishwanath, and D. A. Huse. Operator spreading and the emergence of dissipation in unitary dynamics with conservation laws. *Phy. Rev. X*, 8:031057, 10 2017. doi: 10.1103/PhysRevX.8.031057. URL https://journals.aps.org/prx/abstract/10.1103/PhysRevX.8.031057.

[77] S. Xu and B. Swingle. Accessing scrambling using matrix product operators. *arXiv: 1802.00801*, 2018. URL https://arxiv.org/abs/1802.00801.

[78] Vedika Khemani, David A. Huse, and Adam Nahum. Velocity-dependent lyapunov exponents in many-body quantum, semi-classical, and classical chaos. *Phys. Rev. B*, 98:144304, 2018. doi: 10.1103/PhysRevB.98.144304. URL https://journals.aps.org/prb/abstract/10.1103/PhysRevB.98.144304.

[79] Luca D'Alessio, Yariv Kafri, Anatoli Polkovnikov, and Marcos Rigol. From quantum chaos and eigenstate thermalization to statistical mechanics and thermodynamics. *Adv. Phys.*, 65(3):239–362, 2016. doi: 10.1080/00018732.2016.1198134. URL https://doi.org/10.1080/00018732.2016.1198134.

[80] Jordan Cotler, Nicholas Hunter-Jones, Junyu Liu, and Beni Yoshida. Chaos, complexity, and random matrices. *J. High Energ. Phys.*, 11:48, 2017. doi: 10.1007/jhep11(2017)048. URL http://dx.doi.org/10.1007/JHEP11(2017)048.

[81] Nicholas Hunter-Jones. Operator growth in random quantum circuits with symmetry. *arXiv: 1812.08219*, 2018. URL https://arxiv.org/abs/1812.08219.

[82] H. Abdul-Rahman, B. Nachtergaele, R. Sims, and G. Stolz. Entanglement dynamics of disordered quantum XY chains. *Lett. Math. Phys.*, 106(5): 649–674, 2016. doi: 10.1007/s11005-016-0835-9. URL https://link.springer.com/article/10.1007/s11005-016-0835-9.

[83] B. Nachtergaele and R. Sims. Lieb-Robinson bounds and the exponential clustering theorem. *Commun. Math. Phys.*, 265(1):119–130, 2006. doi: 10.1007/s00220-006-1556-1. URL http://dx.doi.org/10.1007/s00220-006-1556-1.

[84] I. H. Kim, A. Chandran, and D. A. Abanin. Local integrals of motion and the logarithmic lightcone in many-body localized systems. *arXiv:1412.3073*, 2014. URL https://arxiv.org/abs/1412.3073.

[85] Brian Swingle, Gregory Bentsen, Monika Schleier-Smith, and Patrick Hayden. Measuring the scrambling of quantum information. *Phys. Rev. A*, 94:040302, 2016. doi: 10.1103/PhysRevA.94.040302. URL http://journals.aps.org/pra/abstract/10.1103/PhysRevA.94.040302.

[86] G. Zhu, M. Hafezi, and T. Grover. Measurement of many-body chaos using a quantum clock. *Phys. Rev. A*, 94:062329, 2016. doi: 10.1103/PhysRevA.94.062329. URL https://journals.aps.org/pra/abstract/10.1103/PhysRevA.94.062329.

[87] Norman Y Yao, Fabian Grusdt, Brian Swingle, Mikhail D Lukin, Dan M Stamper-Kurn, Joel E Moore, and Eugene A Demler. Interferometric approach to probing fast scrambling. *arXiv: 1607.01801*, 2016. URL https://arxiv.org/abs/1607.01801.

[88] E. Hamza, R. Sims, and G. Stolz. Dynamical localization in disordered quantum spin systems. *Commun. Math. Phys.*, 315(1):215–239, 2012. doi: 10.1007/s00220-012-1544-6. URL http://dx.doi.org/10.1007/s00220-012-1544-6.

[89] R. Vasseur, S. A. Parameswaran, and J. E. Moore. Quantum revivals and many-body localization. *Phys. Rev. B*, 91:140202, 2015. doi: 10.1103/PhysRevB.91.140202. URL http://link.aps.org/doi/10.1103/PhysRevB.91.140202.

[90] M. Serbyn, M. Knap, S. Gopalakrishnan, Z. Papić, N. Y. Yao, C. R. Laumann, D. A. Abanin, M. D. Lukin, and E. A. Demler. Interferometric probes of many-body localization. *Phys. Rev. Lett.*, 113:147204, 2014. doi: 10.1103/PhysRevLett.113.147204. URL http://link.aps.org/doi/10.1103/PhysRevLett.113.147204.

[91] M. Goihl, M. Friesdorf, A. H. Werner, W. Brown, and J. Eisert. Experimentally accessible witnesses of many-body localisation. *arXiv:1601.02666*, 2016. URL https://arxiv.org/abs/1601.02666.

[92] Arijeet Pal and David A. Huse. Many-body localization phase transition. *Phys. Rev. B*, 82(17):174411, 2010. doi: 10.1103/PhysRevB.82.174411. URL http://link.aps.org/doi/10.1103/PhysRevB.82.174411.

[93] D. J. Luitz, N. Laflorencie, and F. Alet. Many-body localization edge in the random-field Heisenberg chain. *Phys. Rev. B*, 91:081103, 2015. URL http://link.aps.org/doi/10.1103/PhysRevB.91.081103.

[94] M. Serbyn, Z. Papić, and D. A. Abanin. Criterion for many-body localization-delocalization phase transition. *Phys. Rev. X*, 5:041047, 2015. doi: 10.1103/PhysRevX.5.041047. URL http://link.aps.org/doi/10.1103/PhysRevX.5.041047.

[95] M. Serbyn, Z. Papić, and D. A. Abanin. Local conservation laws and the structure of the many-body localized states. *Phys. Rev. Lett.*, 111(12):127201, 2013. doi: 10.1103/PhysRevLett.111.127201. URL http://journals.aps.org/prl/abstract/10.1103/PhysRevLett.111.127201.

[96] M. Schreiber, S. S. Hodgman, P. Bordia, H. P. Lüschen, M. H. Fischer, R. Vosk, E. Altman, U. Schneider, and I. Bloch. Observation of many-body localization of interacting fermions in a quasirandom optical lattice. *Science*, 349(6250):842–845, 2015. doi: 10.1126/science.aaa7432. URL https://science.sciencemag.org/content/349/6250/842.

[97] J.-y. Choi, S. Hild, J. Zeiher, P. Schauß, A. Rubio-Abadal, T. Yefsah, V. Khemani, D. A. Huse, I. Bloch, and C. Gross. Exploring the many-body localization transition in two dimensions. *Science*, 352(6293):1547–1552, 2016. doi: 10.1126/science.aaf8834. URL https://science.sciencemag.org/content/352/6293/1547.

[98] J. Smith, A. Lee, P. Richerme, B. Neyenhuis, P. W. Hess, P. Hauke, M. Heyl, D. A. Huse, and C. Monroe. Many-body localization in a quantum simulator with programmable random disorder. *Nat. Phys.*, 12, 2016. doi: 10.1038/nphys3783. URL https://www.nature.com/articles/nphys3783.

[99] Pranjal Bordia. Coupling identical one-dimensional many-body localized systems. *Phys. Rev. Lett.*, 116:140401, 2016. doi: 10.1103/PhysRevLett.116.140401. URL https://journals.aps.org/prl/abstract/10.1103/PhysRevLett.116.140401.

[100] Yong-Liang Zhang, Yichen Huang, and Xie Chen. Information scrambling in chaotic systems with dissipation. *Phys. Rev. B*, 99:014303, 2019. doi: 10.1103/PhysRevB.99.014303. URL https://link.aps.org/doi/10.1103/PhysRevB.99.014303.

[101] Alexei Kitaev. Averaging over the unitary group. Ph/CS219C (Spring 2016), Caltech, course note.

[102] Yu Chen. Universal logarithmic scrambling in many body localization. *arXiv: 1608.02765*, 2016. URL https://arxiv.org/abs/1608.02765.

[103] Mark Srednicki. The approach to thermal equilibrium in quantized chaotic systems. *J. Phys. A: Math. and Gene.*, 32(7):1163–1175, 1999. doi: 10.1088/0305-4470/32/7/007. URL http://dx.doi.org/10.1088/0305-4470/32/7/007.

[104] J. P. Keating, N. Linden, and H. J. Wells. Spectra and eigenstates of spin chain Hamiltonians. *Commun. Math. Phys.*, 338(1):81–102, 2015. doi: 10.1007/s00220-015-2366-0. URL http://dx.doi.org/10.1007/s00220-015-2366-0.

[105] Fernando G. S. L. Brandão and Marcus Cramer. Equivalence of statistical mechanical ensembles for non-critical quantum systems. *arXiv: 1502.03263*, 2015. URL https://arxiv.org/abs/1502.03263.

[106] Hyungwon Kim, Tatsuhiko N. Ikeda, and David A. Huse. Testing whether all eigenstates obey the eigenstate thermalization hypothesis. *Phys. Rev. E*, 90:052105, Nov 2014. doi: 10.1103/PhysRevE.90.052105. URL https://link.aps.org/doi/10.1103/PhysRevE.90.052105.

[107] I. Arad, T. Kuwahara, and Z. Landau. Connecting global and local energy distributions in quantum spin models on a lattice. *J. Stat. Mech.: Theory Exp*, 2016(3):033301, 2016. doi: 10.1088/1742-5468/2016/03/033301. URL http://stacks.iop.org/1742-5468/2016/i=3/a=033301.

[108] Y. Nakata, P. S. Turner, and M. Murao. Phase-random states: Ensembles of states with fixed amplitudes and uniformly distributed phases in a fixed basis. *Phys. Rev. A*, 86(1):012301, 2012. doi: 10.1103/PhysRevA.86.012301. URL https://link.aps.org/doi/10.1103/PhysRevA.86.012301.

[109] Y. Nakata, C. Hirche, M. Koashi, and A. Winter. Efficient quantum pseudorandomness with nearly time-independent Hamiltonian dynamics. *Phy. Rev. X*, 7(2):021006, 2017. doi: 10.1103/PhysRevX.7.021006. URL https://link.aps.org/doi/10.1103/PhysRevX.7.021006.

[110] M. C. Bañuls, J. I. Cirac, and M. B. Hastings. Strong and weak thermalization of infinite nonintegrable quantum systems. *Phys. Rev. Lett.*, 106:050405, 2011. doi: 10.1103/PhysRevLett.106.050405. URL http://link.aps.org/doi/10.1103/PhysRevLett.106.050405.

[111] Tibor Rakovszky, Frank Pollmann, and C. W. von Keyserlingk. Sub-ballistic growth of Rényi entropies due to diffusion. *Phys. Rev. Lett.*, 122:250602, 2019. doi: 10.1103/PhysRevLett.122.250602. URL https://link.aps.org/doi/10.1103/PhysRevLett.122.250602.

[112] Yichen Huang. Dynamics of Rényi entanglement entropy in local quantum circuits with charge conservation. *arXiv: 1902.00977*, 2019. URL https://arxiv.org/abs/1902.00977.

[113] G. Casati, B. V. Chirikov, F. M. Izrailev, and J. Ford. *Stochastic behavior of a quantum pendulum under a periodic perturbation*, volume 93, page 334. Springer, New York, 1979. URL https://link.springer.com/book/10.1007%2FBFb0021732.

[114] Shmuel Fishman, D. R. Grempel, and R. E. Prange. Chaos, quantum recurrences, and Anderson localization. *Phys. Rev. Lett.*, 49(8):509–512, 1982. doi: 10.1103/PhysRevLett.49.509. URL https://journals.aps.org/prl/abstract/10.1103/PhysRevLett.49.509.

[115] S. Adachi, M. Toda, and K Ikeda. Quantum-classical correspondence in many-dimensional quantum chaos. *Phys. Rev. Lett.*, 61(6):659–661, 1988. doi: 10.1103/PhysRevLett.61.659. URL https://journals.aps.org/prl/abstract/10.1103/PhysRevLett.61.659.

[116] Martin C. Gutzwiller. *Chaos in Classical and Quantum Mechanics*. Springer, N.Y., 1990. URL https://www.springer.com/us/book/9780387971735.

[117] Fritz Haake. *Quantum Signatures of Chaos*. Springer-Varlag, Berlin, 1991. URL https://www.springer.com/us/book/9783662045060.

[118] Wojciech Hubert Zurek and Juan Pablo Paz. Decoherence, chaos, and the second law. *Phys. Rev. Lett.*, 72(16):2508–2511, 1994. doi: 10.1103/PhysRevLett.72.2508. URL https://journals.aps.org/prl/abstract/10.1103/PhysRevLett.72.2508.

[119] H. Ammann, R. Gray, I. Shvarchuck, and N. Christensen. Quantum delta-kicked rotor: Experimental observation of decoherence. *Phys. Rev. Lett.*, 80 (19):4111–4115, 1998. doi: 10.1103/PhysRevLett.80.4111. URL https://journals.aps.org/prl/abstract/10.1103/PhysRevLett.80.4111.

[120] Xue-Yang Song, Chao-Ming Jian, and Leon Balents. Strongly correlated metal built from Sachdev-Ye-Kitaev models. *Phys. Rev. Lett.*, 119:216601, Nov 2017. doi: 10.1103/PhysRevLett.119.216601. URL https://link.aps.org/doi/10.1103/PhysRevLett.119.216601.

[121] D. Ben-Zion and J. McGreevy. Strange metal from local quantum chaos. *Phys. Rev. B*, 97(15):155117, 2018. doi: 10.1103/PhysRevB.97.

155117. URL https://journals.aps.org/prb/abstract/10.1103/PhysRevB.97.155117.

[122] Naoto Tsuji, Philipp Werner, and Masahito Ueda. Exact out-of-time-ordered correlation functions for an interacting lattice fermion model. *Phys. Rev. A*, 95:011601, 2017. doi: 10.1103/PhysRevA.95.011601. URL https://journals.aps.org/pra/abstract/10.1103/PhysRevA.95.011601.

[123] A Bohrdt, CB Mendl, M Endres, and M Knap. Scrambling and thermalization in a diffusive quantum many-body system. *New J. Phys.*, 19:063001, 2017. doi: 10.1088/1367-2630/aa719b. URL http://iopscience.iop.org/article/10.1088/1367-2630/aa719b.

[124] Martin Gärttner, Justin G Bohnet, Arghavan Safavi-Naini, Michael L Wall, John J Bollinger, and Ana Maria Rey. Measuring out-of-time-order correlations and multiple quantum spectra in a trapped ion quantum magnet. *Nat. Phys.*, 13:781, 2017. doi: 10.1038/nphys4119. URL https://www.nature.com/nphys/journal/v13/n8/full/nphys4119.html.

[125] Jun Li, Ruihua Fan, Hengyan Wang, Bingtian Ye, Bei Zeng, Hui Zhai, Xinhua Peng, and Jiangfeng Du. Measuring out-of-time-order correlators on a nuclear magnetic resonance quantum simulator. *Phys. Rev. X*, 7:031011, 2017. doi: 10.1103/PhysRevX.7.031011. URL https://journals.aps.org/prx/abstract/10.1103/PhysRevX.7.031011.

[126] Michele Campisi and John Goold. Thermodynamics of quantum information scrambling. *Phys. Rev. E*, 95:062127, 2017. doi: 10.1103/PhysRevE.95.062127. URL https://journals.aps.org/pre/abstract/10.1103/PhysRevE.95.062127.

[127] Nicole Yunger Halpern. Jarzynski-like equality for the out-of-time-ordered correlator. *Phys. Rev. A*, 95:012120, 2017. doi: 10.1103/PhysRevA.95.012120. URL https://journals.aps.org/pra/abstract/10.1103/PhysRevA.95.012120.

[128] Nicole Yunger Halpern, Brian Swingle, and Justin Dressel. Quasiprobability behind the out-of-time-ordered correlator. *Phys. Rev. A*, 97(4):042105, 2018. doi: 10.1103/PhysRevA.97.042105. URL https://journals.aps.org/pra/abstract/10.1103/PhysRevA.97.042105.

[129] S.V. Syzranov, A.V. Gorshkov, and V. Galitski. Out-of-time-order correlators in finite open systems. *Phy. Rev. B*, 97(16):161114, 2018. doi: 10.1103/PhysRevB.97.161114. URL https://journals.aps.org/prb/abstract/10.1103/PhysRevB.97.161114.

[130] Heinz-Peter Breuer and Francesco Petruccione. *The theory of open quantum systems*. Oxford University Press, Oxford, 2002. URL http://www.oxfordscholarship.com/view/10.1093/acprof:oso/9780199213900.001.0001/acprof-9780199213900.

[131] Bei Zeng, Xie Chen, Duan-Lu Zhou, and Xiao-Gang Wen. Quantum information meets quantum matter–from quantum entanglement to topological phase in many-body systems. *arXiv:1508.02595*, 2015. URL https://arxiv.org/abs/1508.02595.

[132] J.R. Johansson, P.D. Nation, and Franco Nori. Qutip: An open-source python framework for the dynamics of open quantum systems. *Comput. Phys. Commun.*, 183(8):1760 – 1772, 2012. doi: 10.1016/j.cpc.2012.02.021. URL http://www.sciencedirect.com/science/article/pii/S0010465512000835.

[133] J.R. Johansson, P.D. Nation, and Franco Nori. Qutip 2: A python framework for the dynamics of open quantum systems. *Comput. Phys. Commun.*, 184 (4):1234 – 1240, 2013. doi: 10.1016/j.cpc.2012.11.019. URL http://www.sciencedirect.com/science/article/pii/S0010465512003955.

[134] Guifré Vidal. Efficient simulation of one-dimensional quantum many-body systems. *Phys. Rev. Lett.*, 93(4):040502, 2004. doi: 10.1103/PhysRevLett.93.040502. URL https://journals.aps.org/prl/abstract/10.1103/PhysRevLett.93.040502.

[135] Michael Zwolak and Guifré Vidal. Mixed-state dynamics in one-dimensional quantum lattice systems: a time-dependent superoperator renormalization algorithm. *Phys. Rev. Lett.*, 93(20):207205, 2004. doi: 10.1103/PhysRevLett.93.207205. URL https://journals.aps.org/prl/abstract/10.1103/PhysRevLett.93.207205.

[136] Ulrich Schollwöck. The density-matrix renormalization group in the age of matrix product states. *Ann. Phys.*, 326(1):96–192, 2011. doi: 10.1016/j.aop.2010.09.012. URL http://www.sciencedirect.com/science/article/pii/S0003491610001752.

[137] David Poulin. Lieb-Robinson bound and locality for general Markovian quantum dynamics. *Phys. Rev. Lett.*, 104(19):190401, 2010. doi: 10.1103/PhysRevLett.104.190401. URL https://journals.aps.org/prl/abstract/10.1103/PhysRevLett.104.190401.

[138] Bruno Nachtergaele, Anna Vershynina, and Valentin A Zagrebnov. Lieb-Robinson bounds and existence of the thermodynamic limit for a class of irreversible quantum dynamics. *AMS Contemp. Math.*, 552:161–175, 2011. URL https://arxiv.org/abs/1103.1122.

[139] Thomas Barthel and Martin Kliesch. Quasilocality and efficient simulation of Markovian quantum dynamics. *Phys. Rev. Lett.*, 108:230504, 2012. doi: 10.1103/PhysRevLett.108.230504. URL http://link.aps.org/doi/10.1103/PhysRevLett.108.230504.

[140] Benoît Descamps. Asymptotically decreasing Lieb-Robinson velocity for a class of dissipative quantum dynamics. *J. Math. Phys.*, 54(9):092202, 2013. doi: 10.1063/1.4820785. URL https://aip.scitation.org/doi/10.1063/1.4820785.

[141] Martin Kliesch, Christian Gogolin, and Jens Eisert. *Lieb-Robinson Bounds and the Simulation of Time-Evolution of Local Observables in Lattice Systems*, pages 301–318. Springer International Publishing, Cham, Switzerland, 2014. doi: 10.1007/978-3-319-06379-9_17. URL https://doi.org/10.1007/978-3-319-06379-9_17.

[142] Toby S. Cubitt, Angelo Lucia, Spyridon Michalakis, and David Perez-Garcia. Stability of local quantum dissipative systems. *Commun. Math. Phys.*, 337 (3):1275–1315, Aug 2015. doi: 10.1007/s00220-015-2355-3. URL https://doi.org/10.1007/s00220-015-2355-3.

[143] Sarang Gopalakrishnan, David A. Huse, Vedika Khemani, and Romain Vasseur. Hydrodynamics of operator spreading and quasiparticle diffusion in interacting integrable systems. *Phys. Rev. B*, 98:220303, 2018. doi: 10.1103/PhysRevB.98.220303. URL https://link.aps.org/doi/10.1103/PhysRevB.98.220303.

[144] Brian Swingle and Nicole Yunger Halpern. Resilience of scrambling measurements. *Phys. Rev. A*, 97:062113, 2018. doi: 10.1103/PhysRevA.97.062113. URL https://journals.aps.org/pra/abstract/10.1103/PhysRevA.97.062113.

[145] Douglas Stanford. Many-body chaos at weak coupling. *J. High Energ. Phys.*, 10:9, 2016. doi: 10.1007/jhep10(2016)009. URL http://dx.doi.org/10.1007/JHEP10(2016)009.

[146] Yingfei Gu and Xiao-Liang Qi. Fractional statistics and the butterfly effect. *J. High Energ. Phys.*, 8:129, 2016. doi: 10.1007/jhep08(2016)129. URL http://dx.doi.org/10.1007/JHEP08(2016)129.

[147] Debanjan Chowdhury and Brian Swingle. Onset of many-body chaos in the O(N) model. *Phys. Rev. D*, 96:065005, 2017. doi: 10.1103/PhysRevD.96.065005. URL https://link.aps.org/doi/10.1103/PhysRevD.96.065005.

[148] Balázs Dóra and Roderich Moessner. Out-of-time-ordered density correlators in Luttinger liquids. *Phys. Rev. Lett.*, 119:026802, 2017. doi: 10.1103/PhysRevLett.119.026802. URL https://link.aps.org/doi/10.1103/PhysRevLett.119.026802.

[149] Ivan Kukuljan, Sašo Grozdanov, and Tomaž Prosen. Weak quantum chaos. *Phys. Rev. B*, 96:060301, 2017. doi: 10.1103/PhysRevB.96.060301. URL https://link.aps.org/doi/10.1103/PhysRevB.96.060301.

[150] Markus Heyl, Frank Pollmann, and Balázs Dóra. Detecting equilibrium and dynamical quantum phase transitions in Ising chains via out-of-time-ordered correlators. *Phys. Rev. Lett.*, 121:016801, 2018. doi: 10.1103/PhysRevLett.121.016801. URL https://link.aps.org/doi/10.1103/PhysRevLett.121.016801.

[151] Xiao Chen and Tianci Zhou. Operator scrambling and quantum chaos. *arXiv: 1804.08655*, 2018. URL https://arxiv.org/abs/1804.08655.

[152] Winton Brown and Omar Fawzi. Scrambling speed of random quantum circuits. *arXiv: 1210.6644*, 10 2012. URL https://arxiv.org/abs/1210.6644.

[153] Amos Chan, Andrea De Luca, and J. T. Chalker. Solution of a minimal model for many-body quantum chaos. *Phys. Rev. X*, 8:041019, 2018. doi: 10.1103/PhysRevX.8.041019. URL https://link.aps.org/doi/10.1103/PhysRevX.8.041019.

[154] Fangli Liu, James R. Garrison, Dong-Ling Deng, Zhe-Xuan Gong, and Alexey V. Gorshkov. Asymmetric particle transport and light-cone dynamics induced by Anyonic statistics. *Phys. Rev. Lett.*, 121:250404, 2018. doi: 10.1103/PhysRevLett.121.250404. URL https://link.aps.org/doi/10.1103/PhysRevLett.121.250404.

[155] Charles Stahl, Vedika Khemani, and David A. Huse. Asymmetric butterfly velocities in Hamiltonian and circuit models. *arXiv: 1802.05589*, 2018. URL https://arxiv.org/abs/1812.05589.

[156] Yong-Liang Zhang and Vedika Khemani. Asymmetric butterfly velocities in 2-local Hamiltonians. *arXiv: 1909.03988*, 2019. URL https://arxiv.org/abs/1909.03988.

[157] Y. Y. Atas, E. Bogomolny, O. Giraud, and G. Roux. Distribution of the ratio of consecutive level spacings in random matrix ensembles. *Phys. Rev. Lett.*, 110:084101, 2013. doi: 10.1103/PhysRevLett.110.084101. URL https://link.aps.org/doi/10.1103/PhysRevLett.110.084101.

[158] Cheryne Jonay, David A. Huse, and Adam Nahum. Coarse-grained dynamics of operator and state entanglement. *arXiv: 1803.00089*, 2018. URL https://arxiv.org/abs/1803.00089.